

# **Improvement in the Dielectric Properties of Barium Hexaferrite Nanoparticles by Substitution of Zinc and Nickel**



**By**

**Abdul Karim**

**School of Chemical and Materials Engineering (SCME)  
National University of Sciences and Technology (NUST)**

**2018**

# **Improvement in the Dielectric Properties of Barium Hexaferrite Nanoparticles by Substitution of Zinc and Nickel**



Name: Abdul Karim

Reg. No: 00000117537

**This thesis is submitted as a partial fulfillment of the requirements for  
the degree of**

**MS in Nanoscience and Engineering**

**Supervisor Name: Dr. Iftikhar Hussain Gul**

**School of Chemical and Materials Engineering (SCME)  
National University of Sciences and Technology (NUST), H-12  
Islamabad, Pakistan**

**July, 2018**

# Certificate

This is to certify that work in this thesis has been carried out by **Mr. Abdul Karim** and completed under my supervision in Thermal Transport Laboratory, School of Chemical and Materials Engineering, National University of Sciences and Technology, H-12, Islamabad, Pakistan.

Supervisor: \_\_\_\_\_

**Prof. Dr. Iftikhar Hussain Gul**

Thermal Transport Laboratory

Materials Engineering Department

School of Chemicals and Materials Engineering

National University of Sciences and Technology, Islamabad

Submitted through

Principal/Dean,

School of Chemicals and Materials Engineering

National University of Sciences and Technology, Islamabad

## **Dedication**

I want to dedicate this thesis work to my family and fellow friends of SCME for their support and love, leading me to complete my work.

# Acknowledgements

**In the name of Almighty Allah, the most beneficent and most merciful.**

I want to express my sincere thanks to, Principal of the SCME and HOD Materials Engineering for providing me necessary facilities for my the research work. I feel privileged to have the honour to acknowledge my research supervisor Dr. Iftikhar Hussain Gul , who was very affectionate and cooperative during entire research work. Without his kind and sincere efforts it might have not been possible for me to end this work in time.

I offer my special and sincere thanks to my Lab Fellows; Mr. Muhammad Zarrar Khan(PhD-Scholar), Sohaib Akram (MS-Scholar), Arman Liaqat(MS-Scholar), Ahmed Ali(MS-Scholar), Wajid Ali(MS-Scholar) and Mahmood Khan(MS-Scholar), who helped me in completing my research project.

My Sincere regards to our Lab Attendants Mr. Zafar Iqbal, Mr. Khurram, Mr.Nouman and Mr. Shams who were always there to help me and support me to finish my practical work in time.

*Abdul Karim*

# Abstract

There has been a tremendous interest in hexagonal ferrites during the last ten years for a number of marvelous applications. Particularly they find their use in electronic industry for wireless communications such as mobile phones at MW/GHz frequencies, in the absorption of electromagnetic wave, stealth technologies, radar absorbing materials (RAM) and also as composite materials. Due to their expanded use, hexaferrites have become very important magnetic materials being produced commercially. Barium based M-type hexaferrites, BaM, ( $\text{BaFe}_{12}\text{O}_{19}$ ) is one of such materials that is currently used in these applications. In the current work BaM prepared using Zn and Ni dopants to meet the desired target. For this purpose dopants substitution is performed in two series of  $\text{Ba}_{1-x}\text{Zn}_x\text{Fe}_{12}\text{O}_{19}$  ( $x = 0, 0.2, 0.35, 0.5$ ) and  $\text{Ba}_{1-2x}\text{Zn}_x\text{Ni}_x\text{Fe}_{12}\text{O}_{19}$  ( $x = 0, 0.1, 0.175, 0.2$ ) using sol gel method. The aqueous solution, containing metal nitrates were brought in use to prepare barium hexferrite nanoparticles. The prepared samples were calcined at 800 °C for 8 hrs. FTIR, XRD and SEM were used for study of structural properties. XRD pattern confirmed the formation of pure M-type hexagonal phase. Range of the particle size of the powder prepared by this method is from 16 nm to 60 nm. IR peaks observed after calcinations also confirmed the metal-oxygen bond bending & stretching vibrations of the desired product. Electrical properties like dielectric constant, dielectric loss factor, dielectric tangent loss and AC conductivity were also measured which were in close agreement to achieve the target. Dielectric constant for un-doped material was 29 where as it increase gradually after doping with Zinc and Nickel which shows that resistance of the sample has been reduced and its conductivity increases.

# Table of Contents

## Chapter 1: Introduction

Heading No. No.	Title	Page
1.1	Introduction	1
1.2	Brief history of magnetism	1
1.3	Source and origin of magnetism	3
1.4	Types of magnetism	3
1.4.	Dia-magnetic	4
1.4.2	Para-magnetic	5
1.4.3	Ferro-magnetic	6
1.4.4	Ferri-magnetic	7
1.4.5	Anti-ferromagnetic	7
1.4.6	Super-paramagnetic	8
1.5.	Classification of Permanent/Hard Magnets	9
1.6	Ferrites	9
1.6.1	Soft ferrites	10
1.6.2	Hard ferrites	10
1.7	Types of ferrites	12
1.8.	Types of Hexaferrites	12
1.9.	M-type Barium Hexaferrites or BaM	13
1.10.	Properties of Hexaerrites	14
1.11	Synthesis methods for hexagonal ferrites	17
1.12.	Applications of Ferrites	18
1.13.	Objectives of work.	20

## **Chapter 2:**

### **Literature Study**

2.1	Barium based Hexaferrites. (BaM)	21
2.2.	Literature Study	21

## **Chapter 3:**

### **Resources and Approaches**

3.1.	Experimental Details	27
3.1.1.	Materials	27
3.1.2.	Synthesis of Barium hexaferrite without any dopant	27
3.1.3.	Synthesis of BaFe <sub>12</sub> O <sub>19</sub> with (Zn <sup>2+</sup> ) and (Ni <sup>2+</sup> ) dopants	28
3.2.	Sample Preparation	28
3.2.1.	Preparation of SEM Samples	28
3.2.2.	Preparation of Samples for measurement of electrical properties	29
3.2.3.	Preparation of FTIR samples	29
3.3.	Characterization Techniques	29
3.4.	X-Ray Diffraction (XRD) Technique	30
3.5	Scanning Electron Microscopy (SEM)	34
3.6	Fourier Transmission Infrared Spectroscopy (FTIR)	35
3.7	Dielectric Properties	36
3.8	AC Conductivity	37
3.9	AC impedance spectroscopy	37
3.10	Electric Modulus	38

## **Chapter 4:**

### **Results and Discussions**



<b>Heading No.</b>	<b>Title</b>	<b>Page</b>
<b>No.</b>		
4.1	X-ray diffraction analysis	39
4.1.1.	XRD of Barium hexaferrites ( $\text{BaFe}_{12}\text{O}_{19}$ ) NP	39
4.1.2.	Zn substituted hexaferrites ( $\text{Ba}_{1-x}\text{Zn}_x\text{Fe}_{12}\text{O}_{19}$ )	40
4.1.3.	Zn and Ni substituted hexaferrites ( $\text{Ba}_{1-2x}\text{Zn}_x\text{Ni}_x\text{Fe}_{12}\text{O}_{19}$ )	40
4.1.4.	Cell volume and Lattice Parameters	41
4.1.6.	Crystallite size determination	42
4.2	Scanning electron microscopy (Surface Morphology)	43
4.3	Fourier transform infrared spectroscopy	48
4.4.	Electrical Properties	50
4.4.1.	Dielectric properties	50
4.4.1.1.	Dielectric constant ( $\epsilon'$ )	50
4.4.1.2.	Dielectric losses	51
4.4.2.	AC Conductivity ( $\sigma$ )	54
4.4.3.	Comparison graphs of Electrical properties of Samples	56
4.4.4.	AC impedance spectroscopy	60
4.4.5.	Cole–Cole diagram (for Electric Modulus “M”)	64
4.5	Conclusion	68
4.6	Future Recommendations	68
	References	70

# List of Figures

## Chapter 1:

Figure No. No.	Title	Page
1.1	Diamagnetic behaviour	4
1.2	Paramagnetic behaviour	5
1.3	Ferromagnetic behaviour and Ferrimagnetic behaviour	6
1.4	Anti-ferromagnetic behaviour	8
1.5	Super-paramagnetic behaviour	8
1.6	Unit cell of spinel-structure with tetrahedral and octahedral sites	11
1.7	The schematic structural view of $\text{BaFe}_{12}\text{O}_{19}$	15
1.8	Cross sectional view of the M $\text{BaFe}_{12}\text{O}_{19}$	16
1.9	Practical applications of hexaferrites	19

## Chapter 3:

Figure No.	Title	Page No.
3.1	Scattering of incident beams of x-rays at the plane	31
3.2	Formation of a diffracted cone of radiations	32
3.3	Basic principle of SEM	34
3.4	A layout of SEM functioning	35
3.5	FTIR Spectrophotometer and basic principle	36

## Chapter 4:

4.1	XRD of $\text{BaFe}_{12}\text{O}_{19}$ Nanoparticles(NP)	39
4.2	XRD of $\text{Ba}_{1-x}\text{Zn}_x\text{Fe}_{12}\text{O}_{19}$ (NP)	40
4.3	XRD of $\text{Ba}_{1-2x}\text{Zn}_x\text{Ni}_x\text{Fe}_{12}\text{O}_{19}$ (NP)	41
4.4	SEM image of $\text{BaFe}_{12}\text{O}_{19}$ (NP)	44
4.5	SEM image of $\text{Ba}_{0.8}\text{Zn}_{0.2}\text{Fe}_{12}\text{O}_{19}$ (NP)	45
4.6	SEM image of $\text{Ba}_{0.65}\text{Zn}_{0.35}\text{Fe}_{12}\text{O}_{19}$ (NP)	45
4.7	SEM image of $\text{Ba}_{0.5}\text{Zn}_{0.5}\text{Fe}_{12}\text{O}_{19}$ (NP)	46

4.8	SEM image of $Ba_{0.8}Zn_{0.1}Ni_{0.1}Fe_{12}O_{19}$ (NP)	46
4.9	SEM image of $Ba_{0.65}Zn_{0.175}Ni_{0.175}Fe_{12}O_{19}$ (NP)	47
4.10	SEM image of $Ba_{0.6}Zn_{0.2}Ni_{0.2}Fe_{12}O_{19}$ (NP)	47
4.11	FTIR spectroscopy of $Ba_{1-x}Zn_xFe_{12}O_{19}$ (NP)	49
4.12	FTIR spectroscopy of $Ba_{1-2x}Zn_xNi_xFe_{12}O_{19}$ (NP)	49
4.13	Dielectric Constant vs $\ln f$ $Ba_{1-x}Zn_xFe_{12}O_{19}$ (NP)	50
4.14	Dielectric Constant vs $\ln f$ $Ba_{1-2x}Zn_xNi_xFe_{12}O_{19}$ (NP)	51
4.15	Dielectric Loss vs $\ln f$ $Ba_{1-x}Zn_xFe_{12}O_{19}$ (NP)	52
4.16	Dielectric Loss vs $\ln f$ $Ba_{1-2x}Zn_xNi_xFe_{12}O_{19}$ (NP)	52
4.17	Dielectric Tangent Loss vs $\ln f$ $Ba_{1-x}Zn_xFe_{12}O_{19}$ (NP)	53
4.18	Dielectric Tangent Loss vs $\ln f$ $Ba_{1-2x}Zn_xNi_xFe_{12}O_{19}$ (NP)	53
4.19	AC Conductivity vs $\ln f$ $Ba_{1-x}Zn_xFe_{12}O_{19}$ (NP)	54
4.20	AC Conductivity vs $\ln f$ $Ba_{1-2x}Zn_xNi_xFe_{12}O_{19}$ (NP)	54
4.21	Comparison of $(\epsilon')$ at 100Hz of $Ba_{1-x}Zn_xFe_{12}O_{19}$ (NP)	56
4.22	Comparison of $(\epsilon')$ at 100Hz of $Ba_{1-2x}Zn_xNi_xFe_{12}O_{19}$ (NP)	56
4.23	Comparison of $\epsilon''$ at 100Hz of $Ba_{1-x}Zn_xFe_{12}O_{19}$ (NP)	57
4.24	Comparison of $\epsilon''$ at 100Hz of $Ba_{1-2x}Zn_xNi_xFe_{12}O_{19}$ (NP)	57
4.25	Comparison of $\sigma_{ac}$ at 100Hz of $Ba_{1-x}Zn_xFe_{12}O_{19}$ (NP)	58
4.26	Comparison of $\sigma_{ac}$ at 100Hz of $Ba_{1-2x}Zn_xNi_xFe_{12}O_{19}$ (NP)	58
4.27	Comparison of $\sigma_{ac}$ at 5MHz of $Ba_{1-x}Zn_xFe_{12}O_{19}$ (NP)	59
4.28	Comparison of $\sigma_{ac}$ at 5MHz of $Ba_{1-2x}Zn_xNi_xFe_{12}O_{19}$ (NP)	59
4.29	Impedance(Z) vs $\ln f$ $Ba_{1-x}Zn_xFe_{12}O_{19}$ (NP)	60
4.30	Impedance(Z) vs $\ln f$ $Ba_{1-2x}Zn_xNi_xFe_{12}O_{19}$ (NP)	61
4.31	Impedance ( $Z'$ ) vs $\ln f$ $Ba_{1-x}Zn_xFe_{12}O_{19}$ (NP)	61
4.32	Impedance ( $Z''$ ) vs $\ln f$ $Ba_{1-x}Zn_xFe_{12}O_{19}$ (NP)	62
4.33	Impedance ( $Z'$ ) vs $\ln f$ $Ba_{1-2x}Zn_xNi_xFe_{12}O_{19}$ (NP)	62
4.34	Impedance ( $Z''$ ) vs $\ln f$ $Ba_{1-2x}Zn_xNi_xFe_{12}O_{19}$ (NP)	63
4.35	Cole Cole Plot of $Z'$ vs $Z''$ for $Ba_{1-x}Zn_xFe_{12}O_{19}$ (NP)	63
4.36	Cole Cole Plot of $Z'$ vs $Z''$ for $Ba_{1-2x}Zn_xNi_xFe_{12}O_{19}$ (NP)	64
4.37	Electric Modulus ( $M'$ ) vs $\ln f$ $Ba_{1-x}Zn_xFe_{12}O_{19}$ (NP)	65
4.38	Electric Modulus ( $M'$ ) vs $\ln f$ $Ba_{1-2x}Zn_xNi_xFe_{12}O_{19}$ (NP)	65
4.39	Electric Modulus ( $M''$ ) vs $\ln f$ $Ba_{1-x}Zn_xFe_{12}O_{19}$ (NP)	66

4.40	Electric Modulus ( $M''$ ) vs $\ln f$ $Ba_{1-2x}Zn_xNi_xFe_{12}O_{19}$ (NP)	66
4.41	Cole Cole Plot( $M'$ vs $M''$ ) $Ba_{1-x}Zn_xFe_{12}O_{19}$ (NP)	67
4.42	Cole Cole Plot( $M'$ vs $M''$ ) $Ba_{1-2x}Zn_xNi_xFe_{12}O_{19}$ (NP)	67

# List of Tables

## Chapter 1:

Table 1.1. Materials classification based on the amplitude of their magnetic susceptibility and some other properties. Page No.9

Table 1.2. Physical properties of the main hexaferrites at ambient temperature. Page No.15

## Chapter 4:

Table 4.1. Calculated values of the crystallite sized, bulk density, X-ray density and porosity for  $Ba_{1-x}Zn_xFe_{12}O_{19}$  (NP) for ( $x = 0, 0.2, 0.35, 0.5$ ). Page No.42

Table 4.2. . Calculated values of the crystallite sized, bulk density, X-ray density and porosity for  $Ba_{1-2x}Zn_xNi_xFe_{12}O_{19}$  (NP) for ( $x = 0, 0.1, 0.175, 0.2$ ). Page No.43

Table 4.3 Dielectric constant & loss, Tangent loss and ac conductivity at 100 Hz. Page No.55

Table 4.4 Dielectric constant & loss, Tangent loss and ac conductivity at 5M Hz. Page No.55

# Chapter1: Introduction

## 1.1 Introduction

Study of Nanotechnology deals with the understanding and control of matter on nanoscale, which is about 1 to 100 nano-meters. Such dimension improves its properties for novel applications. The property of nanomaterials usually preferred because of the complete homogenization, low sintering temperature and small particle size is obtained through this method depends on their sizes, shapes and morphology. So the researchers are developing nanomaterials with different methods to control its size, shape and morphology.

The larger surface area and quantum size effect can change the electrical, magnetic and mechanical properties of such nanomaterials. The most important electronic and magnetic materials is spinal ferrites, for more than a century due to their structure and properties. Spinal ferrites has its applications in permanent magnets, recording tapes, magnetic devices, switching devices, colour imaging, flexible recording media and hard disc recording media. There are many methods to obtain nano ferrites such as Co-precipitation [1], Solvothermal [2], Sol-Gel [3], Hydrothermal [4] etc.

Further these methods are classified into two types; Solid State methods and Wet chemical methods. Whereas wet chemical method is usually preferred because of the complete homogenization, low sintering temperature and small particle size is obtained through this method[5].

## 1.2 Brief history of Magnetism

The term “magnetism” was derived from the word “magnesia”, which is an island of Aegean Sea where the certain types of stones were found back in 470BC which attracts iron and were named as lodestones. The history of magnetism is very old but its understanding began in twentieth century. Chinese employed magnets in various navigation applications such as compass in the 12th century. A famous

physicist William Gilbert manufactured some artificial magnets and proved that the compass will always point towards north-south because earth itself has a magnetic property[6].

In 1750, John Michel showed that the magnetic poles will always obey the inverse square law which was later proved by Charles Coulomb. The first electromagnet was manufactured in 1825 when the fact was discovered that magnetic field is produced by an electric current. Faraday, Becquerel and Bergmann later discussed the effect of magnetism on liquids and gases and found out some of them has a noticeable extent. The concept of magnetism is based on the dipole and magnetic field. The magnetic field is infect volume of space where change in energy occurs that can be detected and calculated. Whereas magnetic poles describes the location of where the magnetic field is detected to be entering and leaving within the magnetic material. Magnetic poles do not exist in isolation rather they occur in two opposite poles (North and South Pole) which are separated by a distance and forming a dipole. The North-Pole describes that the magnetic field is leaving the dipole and South-Pole describes that the magnetic field is entering the dipole. By cutting the magnet bar into pieces; two or more dipoles or magnets can be created [7].

The response of the material when it is subjected into magnetic field is called magnetism. Some materials response attracted behaviour, some response repelled behaviour and some response unaffected behaviour when they are subjected to applied magnetic field. The magnetic response disappeared after a critical temperature which was studied by Curie; he examined that magnetic materials response no magnetic behaviour after a certain temperature which is termed as Curie temperature. Every material has its own Curie temperature for which it shows no magnetic response [8].

### **1.3 Source and origin of Magnetism**

Anything which has weight and occupied space is called matter and atom is its fundamental unit. The atoms is consisting of protons, neutrons and electrons. The electrons revolve around the nucleus with constant motion and revolve round its own axis also.

Whereas the nucleus of atom contains protons and neutrons in it. Hence magnetism arises from two types of motion of electrons in an atom. One is the motion of electron around the nucleus of an atom which is similar with rotation of planets around the sun in our solar system. The second is the spin of electrons round its own axis which is similar with Earth's rotation round its own axis. The protons are positively charged particles and neutron has no electrical charge, whereas charge on electrons is negative which takes part in producing magnetic field. When an electrical charge is in motion then a magnetic field is produced. Pauli Exclusion Principle shows that for large fraction of elements the magnetic moment of electrons will cancel each other. Magnetic moment can be defined as the quantity of magnet which determines the torque it will experience when an external field is applied. Pauli Exclusion Principle states that only two electrons of opposite spin can be occupied in each electronic orbit. A certain number of transition metals do not cancel magnetic moment i.e. iron, nickel and cobalt; such elements are the examples of magnetic materials. Magnetic moment arises in such transition metals from the spin of electrons. But there are also certain numbers of elements which do not cancel orbital motion of electrons and show magnetic behaviour; such elements are rare earth metals i.e. europium, neodymium, samarium and cerium. Besides of these rare earth metals and transition metals, magnetism is also observed in a variety of chemical compounds which contain these elements. Metal oxides are the examples of such chemical compounds in which oxygen is bonded with metals [9].

### **1.4 Types of Magnetism**

If a magnetic field is applied around the material then it shows various kinds of behaviours depending upon the factors like the net magnetic moments of atoms or the atomic and molecular level of structures. As we know that magnetic moment is associated with the orbital and spin motion of electrons, which can be alter by the applied external field. With applied external field, some materials align themselves



parallel to it while some materials align themselves opposite to it. Electrons are usually found in pairs in an atom which spin in opposite directions, that's how magnetic field is cancelled. Those materials that have unpaired electrons show some net magnetic field. Based on these characteristics, the magnetic behaviour can be classified as, [10].

- 1) Dia-magnetic
- 2) Para-magnetic
- 3) Ferro-magnetic
- 4) Ferri-magnetic
- 5) Anti-ferromagnetic
- 6) Super-paramagnetic

### 1.4.1 Diamagnetic

It results net magnetic field to zero in an atom when electrons are in orbital motion in an externally applied magnetic field. Such materials show slight magnetic moment properties in an applied magnetic field, after the removal to externally applied magnetic field the magnetic properties of material do not retain. Only in the presence of externally applied field Diamagnetic behaviour appears, when the field is applied electron orbits get realigned and show some magnetic behaviour. In this case, applied field is opposed by the field produced by the orbital motion of electron as represented in Fig: 1.1, by the negative susceptibility. Such materials have very weak and negative susceptibility to applied magnetic fields. The examples of such materials are wood, copper, gold, bismuth, silver and plastic etc[11].

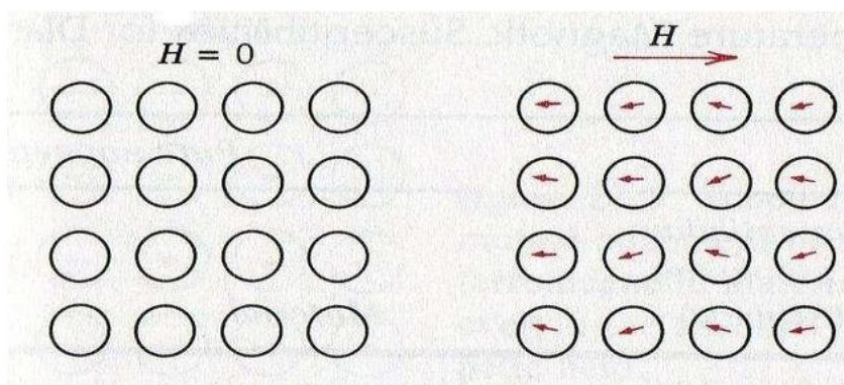


Fig: 1.1: Diamagnetic behaviour [12]

### 1.4.2 Paramagnetic

It results by the both orbital and spin motion of electrons in the magnetic field. The incomplete cancellation of spin and orbital magnetic moment of electrons leads to it in a permanent dipole moment in the absence of external magnetic field, such behaviour is called paramagnetic behaviour.

Most of the dipole moments align in the direction of the applied magnetic field and thus acquire a net magnetization when the external magnetic field is applied. After the removal of external magnetic field the dipole moments realign themselves as they were before the applied magnetic field as shown in Fig: 1.2. Paramagnetic behaviour is infect the result of the applied external field, on applying the field the unpaired electrons in electron orbits get realigned and show some magnetic behaviour. These materials show slight attraction to strong magnet. These materials have small and positive susceptibility to applied magnetic fields. The examples of paramagnetic materials are platinum, oxygen, manganese, aluminium, lithium and strontium etc. Such materials are called paramagnetic and such behaviour is called paramagnetic behaviour.[13]

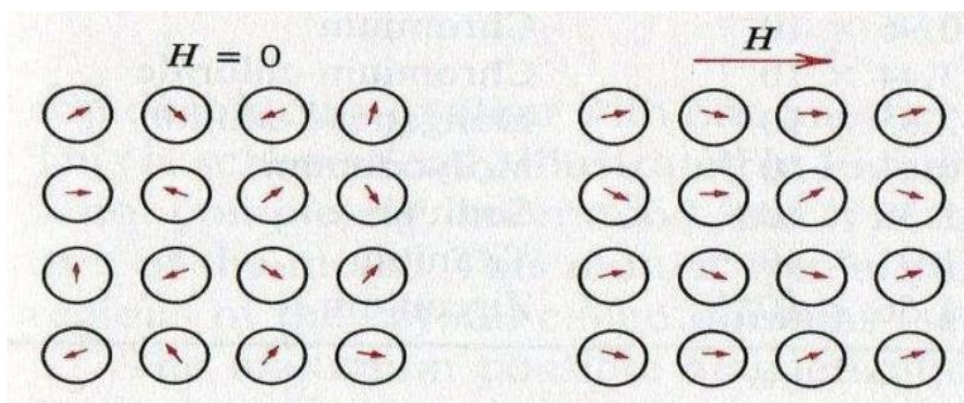


Fig: 1.2: Paramagnetic behaviour[12]

### 1.4.3 Ferromagnetic

It also results by the both orbital and spin motion of electrons in the magnetic fields. Due to the incomplete cancellation of spin and orbital motion of electron in the absence of external magnetic field some unpaired electrons shows good response of magnetic behaviour and have a net magnetic moment. And by applying external magnetic field all the dipole moments align in that direction of this applied magnetic field and thus acquire a net magnetization which shows a strong response to the applied magnetic field. In other words most of the dipoles are aligned and possess a net magnetic field before applying the magnetic field and after applying the external magnetic field all the dipoles align along the direction of externally applied magnetic field and hence show a strong response of magnetic behaviour and even on removing the external magnetic field the dipoles retain its alignment and hence retain its magnetic behaviour until a critical temperature which is called Curie temperature. When the material loses its magnetic property at a certain temperature then that temperature is called Curie temperature. Very large and positive susceptibility is shown by Such materials to an external magnetic field. The examples of such materials are cobalt, iron and nickel etc. Such materials are called ferromagnetic and such behaviour is called ferromagnetic behaviour [10]. The ferromagnetic behaviour is shown in Fig: 1.3

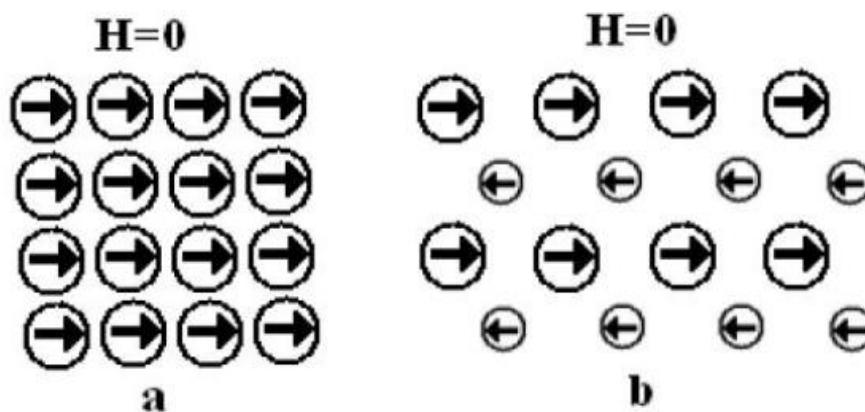


Fig: 1.3: Ferromagnetic behaviour and Ferrimagnetic [12]

#### **1.4.4 Ferrimagnetic**

It also results by the both orbital and spin motion of electrons in the magnetic field. But unlike the ferromagnetic, some of the dipoles align in the direction and some of the dipoles align in the opposite direction in the presence of externally applied field, however the opposing dipoles are unequal in magnitude and show a net magnetic moment which is lower than the ferromagnetic material. The most common example of ferrimagnetic material is ferrous ferrite. In ferrous ferrite,  $\text{Fe}^{+3}$  ions occupy tetrahedral B site which is coordinated to 4 oxygen anions whereas  $\text{Fe}^{+3}$  and  $\text{Fe}^{+2}$  ions occupy octahedral A site which is coordinated to 6 oxygen anions. So the  $\text{Fe}^{+3}$  which is present at both sites has opposite type of magnetizations which cancel each other. And hence the single  $\text{Fe}^{+2}$  ions results in the net magnetization as shown in Fig: 1.3[10].

#### **1.4.5 Anti-ferromagnetic**

It results by the antiparallel arrangement which occurs between the spin of electrons of the neighbouring atoms. A crystal consists of two lattices under antiferromagnetic behaviour for which one is magnetized in one direction and the other is magnetized in another direction. Anti-ferromagnetic behaviour was first observed in MnO in 1938. The magnetic moment of neighbouring atoms cancels each other and the material show no net magnetization in the absence of externally applied field and some of the dipoles align in that direction of applied magnetic field and show small net magnetization in the presence of external field. And this magnetization will increase with increasing temperature until a critical temperature is achieved which is called Neel temperature. This behaviour exists at low temperature and diminishes above the Neel temperature. The examples of Anti-ferromagnetic materials are MnO, NiO, Cr, FeO ferromagnetic and such behaviour is called anti ferromagnetic behaviour is shown in and CoO etc. Such materials are called anti-ferromagnetic behaviour. The antiferromagnetic behaviour is shown in Fig: 1.4[14].

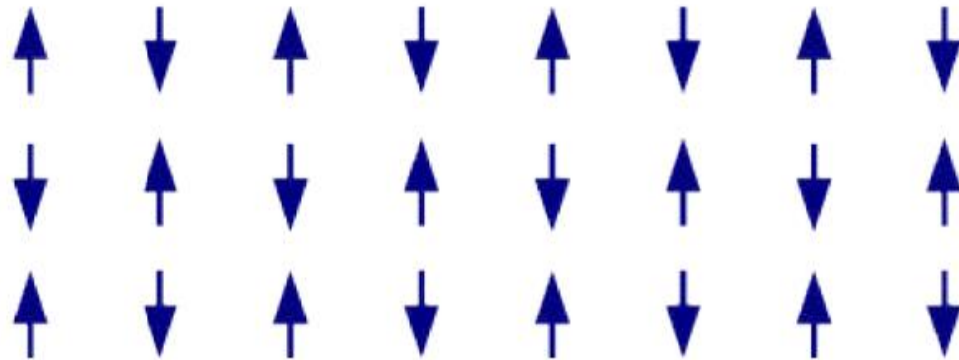


Fig: 1.4: Anti-ferromagnetic behaviour[12]

### 1.4.6 Super-paramagnetic

It is a phenomenon in which the materials exhibit a paramagnetic behaviour under the Curie temperature or ferri-magnetic behaviour is converted into paramagnetic behaviour is called Curie temperature. In such materials, the neighbouring atoms to align magnetic susceptibility of converted paramagnetic behaviour is much larger than that of paramagnets. The super-paramagnetic behaviour is shown in Fig.1.5

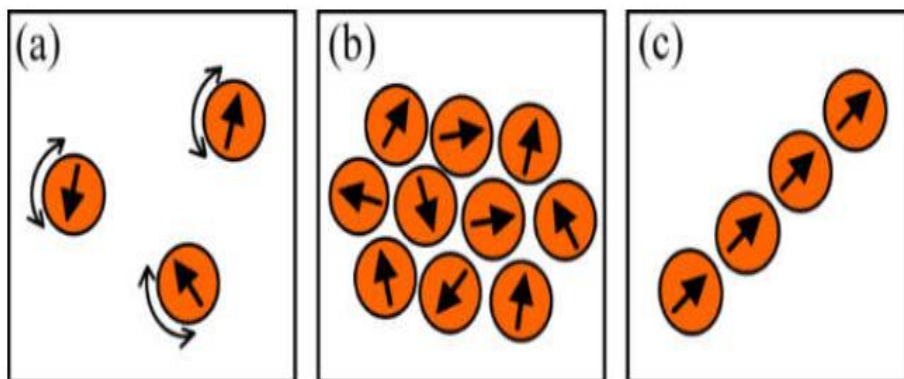
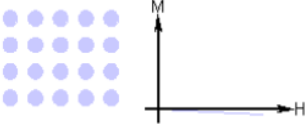
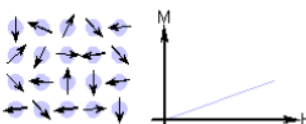
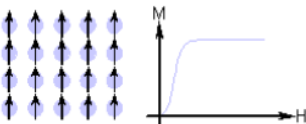
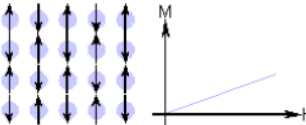
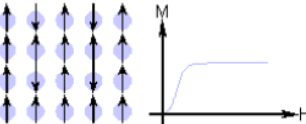


Fig: 1.5: Super-paramagnetic behaviour [12]

## 1.5. Classification of Permanent/Hard on the basis of some properties:

**Table 1.1. Materials classification on the basis of amplitude of their magnetic susceptibility and some other properties [15]**

Type of magnetism	Magnetic susceptibility, $\chi$	Atomic / Magnetic Behavior	Temperature dependence	Examples and comments
Diamagnetic	Negative and small, Au: $-2.74 \times 10^{-6}$ Cu: $-0.77 \times 10^{-6}$		Temperature independent	The shells of the atoms are closed as in the case of covalent solids such as Ge, Si, and metals such as Au, Cu, Ag, etc.
Paramagnetic	Positive and small, $\beta$ -Sn: $0.19 \times 10^{-6}$ Pt: $21.04 \times 10^{-6}$ Mn: $66.10 \times 10^{-6}$ $10^{-5} - 10^{-4}$		Temperature independent	Atoms have randomly oriented magnetic moments as in alkali and transition metals
	Positive and small		Follows Curie or Curie-Weiss law: $\chi = \frac{C}{T - \theta}$	Atoms constituting the material have a permanent magnetic moment as in ferromagnets (Fe), antiferromagnets (Cr), ferrimagnets ( $\text{Fe}_2\text{O}_3$ ) at high temperatures
Ferromagnetic	Positive and large, function of applied field, microstructure dependent Fe: $\sim 100,000$		Ferromagnetic below Curie temperature and paramagnetic above it	Atoms have parallel aligned magnetic moments, possesses large permanent magnetization even without external magnetic field as in some transition metals and rare earths such as Fe, Co, Ni, Gd, Dy
Antiferromagnetic	Positive and small, Cr: $3.6 \times 10^{-6}$		Antiferromagnetic below the Néel temperature and paramagnetic above it	Atoms have mixed parallel and anti-parallel aligned magnetic moments. Primarily oxides and salts of transition metals such as MnO, NiO, $\text{MnF}_2$ .
Ferrimagnetic	Positive and large, function of applied field, microstructure dependent, Ba ferrite: $\sim 3$		Ferrimagnetic below the Curie temperature and paramagnetic above it	Atoms have anti-parallel aligned magnetic moments, possesses large magnetization even without external magnetic field

First three categories are beyond the scope of our discussion so, only Ferrites will be discussed in detail here:

## 1.6. Ferrites

Ferrites are considered to be the most important ferrimagnetic materials because of the presence of the ferrimagnetic oxides in it. Due to these oxides, ferrites are called insulating materials. The principle component of ferrite is iron oxide. These materials are magnetic in nature and are used in various applications such as permanent magnets and cores of transformer etc. Production of eddy current is

restricted in ferrites due their high electrical resistivity. Due to this property they are widely used in high frequency applications. Ferrites are classified by two categories: structure and hysteresis losses. According to hysteresis losses, ferrites are of two types: soft ferrite and hard ferrite[16,17].

### **1.6.1 Soft Ferrite**

Soft ferrites are considered hard and brittle because they have low remanence, less saturation magnetization, low magnetostriction, less permeability, very low coercivity and low Curie temperature ( $T_c$ ). These materials take less time to demagnetize as they have low value of energy dissipation in magnetization. They have very high values of resistivity and they appear to be black or grey. They prevent the energy losses in transformer cores and inductors etc. The examples of such ferrite are nickel-zinc ferrite and manganese-zinc ferrite[16,17].

### **1.6.2 Hard Ferrite**

Hard ferrites have high coercivity, high remanence, high saturation magnetization, high magnetostriction, high permeability and high Curie temperature ( $T_c$ ). These materials take long time to demagnetize. These materials are also known as ceramic magnets. They are very cheap in cost because of the easily availability of the raw materials to make them. Due to their low cost they are widely used house hold appliances. The examples of hard ferrites are cobalt ferrite and strontium ferrite[16,17].

## **1.7. Types of Ferrite**

According of structure, there are three types of ferrites which are as under: [18]

- Spinel ferrite
  
- Garnet ferrite
  
- Hexagonal ferrite

### 1.7.1 Spinel Ferrite

$MFe_2O_4$  is the general formula of spinel ferrite, where M represents divalent cations. Some examples of divalent cations are nickel ( $Ni^{+2}$ ), copper ( $Cu^{+2}$ ), zinc ( $Zn^{+2}$ ) and cobalt ( $Co^{+2}$ ) etc. Their structure is simple as compared to the other classes of ferrites. Close packed face centred cubic (FCC) structure is possessed by spinel structure. There are 32 Oxygen ions in its unit cell. There are two types of space sites in the ferrites which are referred as Tetrahedral sites (A) and Octahedral sites (B) as shown in Fig.1.6. The (A) site is surrounded by 4 oxygen atoms. There are 64 tetrahedral sites in spinal ferrite out of which cations occupy 8 tetrahedral sites. The (B) site is surrounded by 6 oxygen atoms. There are 32 octahedral sites in spinal ferrite structure out of which 16 octahedral sites are occupied by anions [20,21].

**1.7.1.1 Types of Spinel Ferrite** There are two types of spinel ferrites depending on the structure are , (a) Normal (b) Inverse

Metal ions occupy the (A) sites in crystal structure of normal-spinel ferrite, In inverse-spinel ferrite, divalent metal ions occupy the (B) sites. Trivalent metal ions occupy both the (A) and (B) sites while divalent metal ions occupy the (B) sites in crystal structure of spinal ferrite [22].

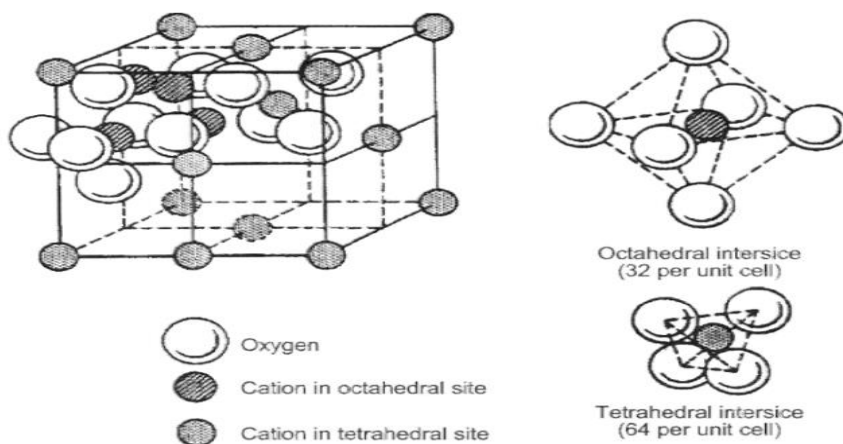


Fig.1.6: Unit cell of spinel structure (with A, Tetrahedral and B, Octahedral sites)[12].



### 1.7.2 Garnet Ferrite

These ferrites were discovered by Giller and Gilleo in 1957. The general formula of such ferrite is  $M_3Fe_5O_{12}$ , where M is the rare-earth trivalent ions. Some rare earth trivalent ions are Gd, Dy and Y etc. They have cubic structures and are magnetically hard materials [19].

### 1.7.3 Hexagonal Ferrite

The general formula of hexagonal ferrite is  $MFe_{12}O_{19}$ , where M can be barium, lead, strontium or combination of these. In its structure there are 3 sites tetrahedral, octahedral and trigonal in which metal ions are occupied. Due to their high value of coercivity they are widely used in loud speakers, microwave applications, magnetic recording devices and as fridge magnets. Barium hexaferrite is best known example of hexaferrite [23,24].

## 1.8.Types of Hexaferrites

Hexagonal ferrites are subdivided into following six types on the basis of their chemical composition and crystal structure [25].

- 1) **M-type** ( $AFe_{12}O_{19}$ ) e-g  $BaFe_{12}O_{19}$  (**BaM**) &  $SrFe_{12}O_{19}$  (**SrM**)
- 2) **W-type** ( $AMe_2Fe_{16}O_{27}$ ), e-g ( $BaMe_2Fe_{16}O_{27}$ ) &  $BaCo_2Fe_{16}O_{27}$ ,
- 3) **X-type** ( $A_2Me_2Fe_{28}O_{46}$ ), e-g  $Ba_2Co_2Fe_{28}O_{46}$ , or  $Co_2X$ .
- 4) **Y-type** ( $A_2Me_2Fe_{12}O_{22}$ ) e-g  $Ba_2Co_2Fe_{12}O_{22}$ , or  $Co_2Y$ .
- 5) **Z-type** ( $A_3Me_2Fe_{24}O_{41}$ ) e-g  $Ba_3Co_2Fe_{24}O_{41}$ , or  $Co_2Z$ .
- 6) **U-type** ( $A_4Me_2Fe_{36}O_{60}$ ) e-g  $Ba_4Co_2Fe_{36}O_{60}$ , or  $Co_2U$

In M type hexaferrites ions like Ba, Sr or Pb are represented by 'A' divalent metal ions are represented by 'Me' like Mg or Zn.

Our research work deals with the synthesis and characterization of M-type hexaferrites so only M-type hexaferrites will be discussed here in details.

## 1.9. M-type Barium Hexaferrites or BaM

General formula for M type hexa ferrite is  $A \cdot 6\text{Fe}_2\text{O}_3$ . Divalent ion is represented by 'A'.  $\text{Ba}^{2+}$ ,  $\text{Sr}^{2+}$  or  $\text{Pb}^{2+}$  are some of its examples. Lattice constants are  $a = 5.89 \text{ \AA}$  and  $c = 23.19 \text{ \AA}$  for  $\text{Ba} \cdot \text{Fe}_{12}\text{O}_{19}$ .

Barium hexaferrite was known to researchers from many years. It has melting point of  $1390^\circ\text{C}$  which was initially affirmed in 1936 [26]. The compound is isomorphous in nature because of which firstly its structure was not affirmed as a hexagonal magnetoplumbite. It was concentrated on and portrayed concerning its magnetic nature by Philips [27] in mid 1950s. Ferroxdure was the first name given to this compound [28]. The BaM compound has lower saturation magnetization than the other existing alloy magnets, it has high electrical resistivity.

Along the c-axis BaM possess high magnetic uniaxial anisotropy [29]. The molecular mass of its molecule is 1112 g. The highest value of density reported in literature is  $5.295 \text{ g cm}^{-3}$  [30].

5.9 GPa is its hardness along in the c-axis as [31], and measured value as 6.0 GPa [32]. Since the discovery of M-type ferrites at the early years of 1950s [26-28].

These materials have continually been used as,

permanent magnets,

magnetic recording media,

plastroferrites, microwave devices and injection-molded pieces.

The research efforts on international level started due to their widespread use in almost every field. The interest is because of their economical cost, excellent chemical stability, corrosion resistant nature and relatively high value of coercivity.

### **1.9.1. The structure of the hexagonal ferrites**

Hexaferrites consist of highly complex structure which is very closely related with one other [33]. Actually it consists of three ferrite compounds in the form of molecular combinations which are 'S' type, 'M' type and 'Y' type. Due to smaller size of barium ion as compared to the oxygen ion, it occupies the lattice in its immediate place. This  $Ba^{2+}$  can be replaced further by another divalent metal ions, for example, Pb or Sr to keep up the structure without significant distortion, if it is of adequate size.

Miller indices are needed for the explanation of a hexagonal shape crystal. C-axis is the major axis and its length is called "c" lattice parameter. Only single other parameter, "a" is needed for the description of hexagonal shape of crystal. A schematic structure of barium hexaferrite is given here in figure 1.3.

### **1.10. Properties of Hexaferrites**

As shown in figure 1.3, that hexaferrites or hexagonal ferrites, have an even more complex crystal structure. Hexaferrites are of various types depending on their composition; however, all of them have similarities in their crystalline structure. Main source of magnetic moment in hexaferrite structures are Fe cations and can be found on any one of the three sites, may be found on *tetra*, *octa*, or *hexahedral sites*. Some of the Physical, Magnetic, Microwave and Dielectric properties of Hexaferrites are as follow.

#### **1.10.1. Physical properties**

Hexaferrites vary greatly with respect to their physical properties. Hexaferrites have excellent intrinsic hard properties due to which they are mostly used for making permanent magnets. A high temperature, 900+ °C, is required for the formation of ferrites for microelectronics. Some of the physical properties of some the major hexaferrites are summarized in Table( 1.2).

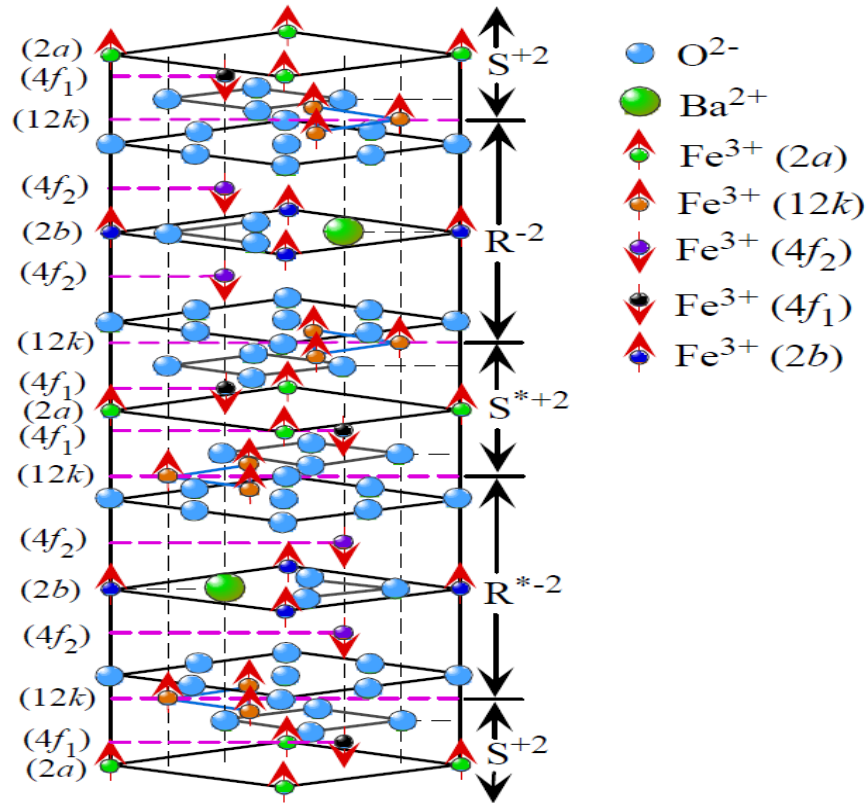


**Figure 1.7-** The schematic structural representation of  $\text{BaFe}_{12}\text{O}_{19}$ .  $4f_1$  are tetrahedral,  $2a$ ,  $12k$ , and  $4f_2$  are octahedral, and  $2b$  are hexahedral sites [34].

**Table 1.2. Physical properties of the main hexaferrites at ambient temperature [32]**

Ferrite	Formula	Molecular mass (g)	$\rho$ ( $\text{g cm}^{-3}$ )	$c$ ( $\text{\AA}$ )	Magnetisation at room temp
BaM	$\text{BaFe}_{12}\text{O}_{19}$	1112	5.28	23.18	uniaxial
SrM	$\text{SrFe}_{12}\text{O}_{19}$	1062	5.11	23.03	uniaxial
$\text{Co}_2\text{Y}$	$\text{Ba}_2\text{Co}_2\text{Fe}_{12}\text{O}_{22}$	1410	5.40	43.56	in plane
$\text{Co}_2\text{Z}$	$\text{Ba}_3\text{Co}_2\text{Fe}_{24}\text{O}_{41}$	2522	5.35	52.30	in plane
$\text{Co}_2\text{W}$	$\text{BaCo}_2\text{Fe}_{16}\text{O}_{27}$	1577	5.31	32.84	in cone
$\text{Co}_2\text{X}$	$\text{Ba}_2\text{Co}_2\text{Fe}_{28}\text{O}_{46}$	2688	5.29	84.11	in cone
$\text{Co}_2\text{U}$	$\text{Ba}_4\text{Co}_2\text{Fe}_{36}\text{O}_{60}$	3624	5.31	38.16 <sup>a</sup>	in plane

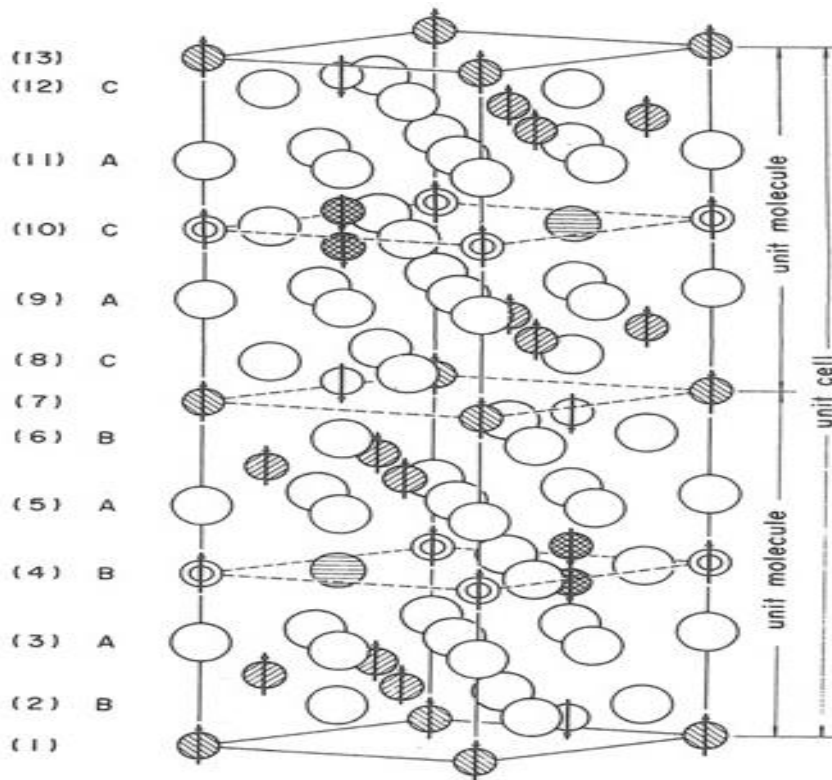


Figure 1.8 Cross sectional view of  $\text{BaFe}_{12}\text{O}_{19}$  [8]

### 1.10.2. Magnetic Properties:

Size of the crystal lattice is varied in large metal ions like Ba or Sr. This forms the basis which results into the magnetocrystalline anisotropy (MCA). Preferred axis of magnetization shown by most of the common hexagonal ferrites is along the c-axis due to which it shows a different XRD pattern with respect to other randomly oriented ferrite samples.

Other substituent metal ions alter the magnetic properties of hexaferrites to a great extent. Anisotropy and magnetization of BaM is enhanced by doping of  $\text{Al}^{3+}$ ,  $\text{Ga}^{3+}$  or  $\text{Cr}^{3+}$ .

### 1.10.3. Dielectric Properties

Main properties are permittivity (dielectric constant), resistivity, ac conductivity, dielectric loss, dielectric tangent loss, Impedance and electric Modulus which are considered as dielectric properties. These properties provide information about

the establishing electric field in the material. Electron hopping is the dominant and prominent conduction mechanism in ferrites between  $\text{Fe}^{2+}$  and  $\text{Fe}^{3+}$  [35].

### **1.11 Synthesis methods for hexagonal ferrites**

For the synthesis of nanoparticles; there are various methods and each one has some advantages and disadvantages too. The various methods of synthesis possess different magnetic, structural and electrical properties. The various methods are shown below,[36-38].

- Co-precipitation Method
- Sol-Gel Method
- Micro-Emulsion Method
- Sono-Chemical Method
- Hydro-Thermal Method
- Solvo-Thermal Method

In **Co-precipitation method** The reaction process for the synthesis of oxides is divided into two categories; one that make oxides directly and the other that make a precursor which require further processing i.e. drying and calcinations. A base solution of ammonium hydroxide solution or sodium hydroxide is additionally used to form the metal hydroxides. The resulting chlorides are washed away and the hydroxide is washed and filtered followed by calcinations to obtain the final product. Co-precipitation is a very useful technique to obtain the fine nanoparticles. The product obtained from this method is pure and homogeneous in chemistry. After adding sodium hydroxide formation of the oxide nanoparticles depends on the control of pH value. The particle sizes of the nanomaterials depend on the pH of the starting precursors. Molarity of the chemicals also controls the particle size of the nanomaterial. [39-41]

In **sol-gel method**, a gel is formed which provide high degree of homogeneity and the atomic diffusion is reduced during the solid-state calcinations. This technique provide better control on products and costly. The materials which are made through this technique have wide applications in optics, electronics and energy etc [42-43].

In **micro-emulsion method**, a surfactant is dissolved in an organic solvent which form aggregates of spheroidal shape which are named as “reverse micelles”. These micelles are in fact ‘water in oil’ micro-emulsions where the tiny drops of water are surrounded by the molecules of surfactant and thus forming a water pool. The water pools of such micelles acts as micro reactors in which the particle size is controlled by the size of these pools. Precipitation in micro-emulsions is very useful for the preparation of ultra-fine ferrite nanoparticles for the controlled size and morphology [44-45].

In **sono-chemical method**, the starting materials are chemically reacted under ultrasonic waves which are 20kHz plus in frequency range. Fabrication of nanostructured materials in various organic and inorganic reactions. This method has advantages of the reduction of the growth of crystal, the morphological control and uniformity of mixing [46-47].

The **hydro-thermal/solvo-thermal method** is used because of its simplicity, low cost, and remarkable morphology of the prepared nanoferrites. The hydro-thermal/solvo-thermal method is used to synthesize the crystalline structures (single crystals and films etc) under high vapor-pressure from the aqueous solution. By controlling the growth of particles and the solution re-crystallization results in the production of various morphological crystals i.e. nano-spheres, nanorods, nano-crystals, nano-cubes, hollow spheres, nano-rod bunches and urchin-like crystals [48-50].

## **1.12. Applications of Ferrites**

Ferrites are important magnetic materials due to their high resistive values. They have many applications at high frequencies. They are cheap and have high DC

electrical resistivity, high coercivity, good magnetic properties, low eddy current losses, mechanical stiffness. They have wide selection of materials and are also chemically stable over wide range of temperature. Because of such properties, Ferrites are widely used in the following applications:

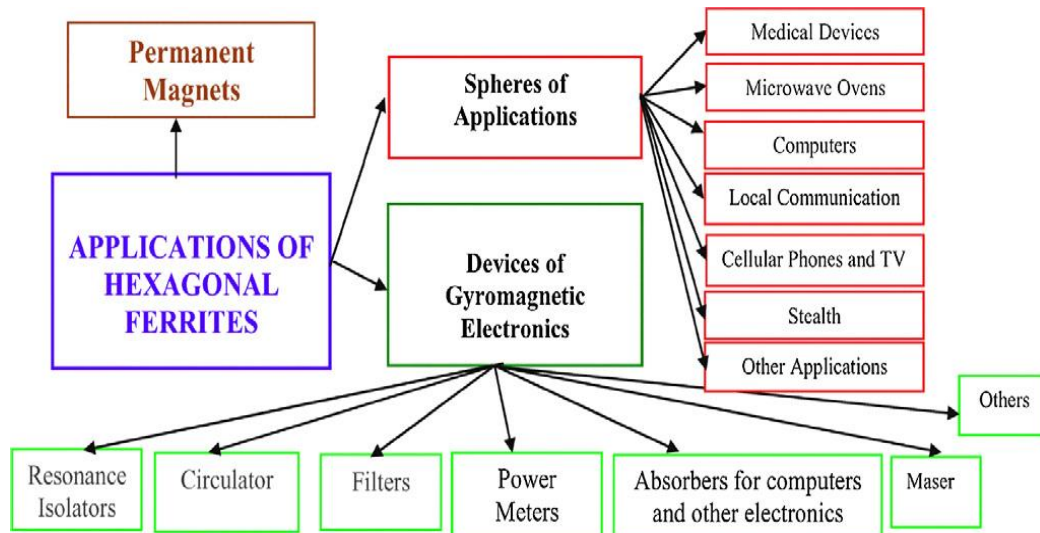


Figure 1.9- Practical applications of hexaferrites [51].

### 1.12.1. Electrical Microwave devices

Because of expanding interest in wireless and portable devices, instrumentation, radar detection, satellites and GPS, remote sensors, security and military defence and aviation applications utilization of hexagonal ferrites is increasing day by day [52-53].

### 1.12.2. Data storage and recording

Ba and Sr ferrites are attractive materials for magnetic recording. If nano particles of these materials are coted on recording media then recording capacity can be remarkably increased [54].

### 1.12.3. Plastroferrites

These are the composite materials in which a magnetic powder ceramic ferrite is used after incorporation into thermoplastic matrix or a resin. They can be stamped



and can also be cut in differently shaped as per applications. Plastroferrites are found in most common use in refrigerator door magnets [55].

#### **1.12.4. Permanent magnets**

Permanent magnets are prepared using hard ferrites and are used in most of the applications utilizing permanent magnets. Hexaferrites are 90% of total permanent magnets manufactured worldwide every year. Mostly these are used in tiny motors like windscreen wiper motor and in number of sensors applications [56].

#### **1.12.5 Other miscellaneous applications**

Hexaferrites are widely used in applications like industry, as magnetic separators for extracting metals, DC motors magnetic tools, robotics, , lifting apparatus, magnetic bearings, brakes and clutches, measuring equipment and used in medical tools like NMR and MRI. Magnetic nanoparticles are used in drug delivery [57-58].

### **1.13. Objectives of work.**

The present work has the following objectives.

- Synthesis of barium hexaferrite nanoparticles using an inexpensive and simple sol gel method.
- Synthesis of compositions series of Ba hexaferrite with Zn and then both Zn and Ni for the studying of changes on its dielectric and magnetic properties.

# Chapter 2: Literature Study

## 2.1. Barium based Hexaferrites. (BaM)

Various researches have been carried to develop hexaferrites using number of methods and their properties. Extensive work on the other hand, has been done to find the effect of various dopants for Ba and Fe in M-type barium hexaferrites (BaM).

Work that is being done in the past few years on hexaferrites with reference to different processing methods and different dopant ions is given below.

## 2.2. Literature Study

**M.A.Ahmed et al in 2010** studied the series of composition  $Ba_{1-y}La_yZn_{0.5}Mg_{0.5}CoFe_{16}O_{27}$  for the values of y from 0 to 0.07, prepared using solid state reaction method. Characterized by XRD spectroscopy and SEM. Constant volume was confirmed by increasing value of 'a' lattice parameter and reduction in lattice parameter 'c'. AC and dc conductivity over temperature range was observed. DC conductivity range from  $4.85 \times 10^{-6}$  to  $3.82 \times 10^{-6} \Omega^{-1} \text{cm}^{-1}$ . The highest values of dielectric, curie temperature, porosity, effective magnetic moment and ac conductivity was observed at  $y=0.05$  [59].

**Muhammad Javed Iqbal et al in 2011** studied compositions of  $BaCoZnFe_{16-2y}Al_yCe_yO_{27}$  with the values of  $y=0,0.2,0.4,0.6,0.8$  and 1 prepared with co-precipitation method. Characterized by XRD, SEM and VSM. Shape of nanoparticles was observed to be varied with substitution of Al and Ce. Permiability was studied by vector network analyser, over the range of 0.5 to 10 GHz. Maximum value of saturation magnetisation was observed at values of  $y=0.2$  and 0.4. Sample is found to be useful for high frequency application and electromagnetic interference [60].

**A. Haq and M. Anis-ur-Rehman in 2012** studied  $Ba_{1-x}Pb_xFe_{12}O_{19}$  for the values of  $x=0,0.2,0.4,0.6,0.8$  and 1. Using co-precipitation method with NaOH pH

was kept 13, molar ratio of Fe and Ba in solution was kept 12. Characterisation was carried out by XRD and SEM. Particle size was observed to be increased with Pb substitution and hexagonal structure was confirmed by SEM micrographs. By VSM hysteresis loop was studied and decrease in coercivity was observed with increase in Pb substitution. While magnetic induction and remanence increased with Pb substitution [61].

**S.M.El-Sayed et al in 2013** studied structural parameters of composition  $\text{BaAl}_x\text{Fe}_{12-x}\text{O}_{19}$  for values of x from 0 to 3.5. Synthesis was carried out by solid state method. Characterise by different techniques and its VSM and XRD spectroscopy shows its magnetic and crystalline behaviour. Values of dielectric and dielectric loss increase with increase of Al substitution in barium ferrite. The IR transmission spectrum was studied over the wave number range of 5000 to 200  $\text{cm}^{-1}$ . Saturation magnetisation and magnetron number reduces with increase in Al substitution [62].

**Jie LI et al in 2013** studied M type Barium ferrite with substitution of La and Co. Synthesis by solid state method, sintered at 1173 K for 6 hours in air and characterized by XRD spectroscopy, SEM and VSM. Influence on the properties of sample by substitution was observed,  $\text{Ba}(\text{LaCo})_x\text{Fe}_{12-2x}\text{O}_{19}$  for the values of x from 0 to 0.5 shows significant rise in saturation magnetization and coercivity. Saturation magnetisation reaches to 65.15  $\text{Am}^2/\text{kg}$  and coercivity reaches to 4165 Oe. SEM analysis shows that substitution of dopants affect the shape of ferrite [63].

**Hasan M. Khan et al in 2014** studied the properties of composition of  $\text{Ca}_{0.5}\text{Ba}_{0.5-x}\text{Tb}_x\text{Zn}_y\text{Fe}_{12-y}\text{O}_{19}$  for the values of x=0 to 0.1 and y=0 to 0.1. Samples were prepared by sol gel method and characterized by XRD, SEM, VSM and FTIR spectroscopy. M type structure of ferrite was confirmed by XRD analysis. Lattice parameter were found to be rise with Tb and Zn doping. Coercivity of sample was enhanced remarkably from 1277 to 2025 Oe. Increase in magnetic anisotropy and fine particle size enhance the recording capability of medium used with these nano particles [64].

**O.M.Hemeda et al in 2015** studied  $Zn_{1-x}Ni_xFe_2O_4$  for  $x=0, 0.2, 0.4, 0.6, 0.8,$  and 1. These compositions were synthesised by combustion technique. Characterization were carried out by XRD and single phase spinel cubic structure was confirmed by XRD. By increase in the frequency from 1k Hz to 10k Hz ac resistivity was observed to be reduced. As hopping of charges increase at high frequency that cause rise in conductivity which results in reduction of resistivity. Using SEM surface morphology and grain size was studied. High resolution TEM confirm crystalline structure with same lattice constant for all samples. Magnetic entropy was studied and maximum change is observed near curie temperature [65].

**S.Chakrabarty et al in 2015** studied that nanocrystalline Zn [ferrites](#) were synthesized using soft chemical way. Its structural and electrical properties were studied after doping with Ni. Growth of single phase nanocrystalline Ni doped Zn ferrites were confirmed by XRD. Change in optical band gap due to doped Ni ions was studied by FTIR and UV visible spectroscopy. Lattice parameter decrease from 8.448 Å to 8.280 Å due to Ni doping. Ac and dc conductivity of Ni doped samples were studied that shows anomalous behavior. Sample having Ni mol fraction from 0.2 to 0.6 show variation from normal to inverse spinal structure [66].

**S. Ozah & N.S. Bhattacharyya in 2014** studied nanocomposite that absorbs microwaves in X-band having composition of  $BaAl_xFe_{12-x}O_{19}$ . This material has hexagonal structure substituted with aluminium possess average nanoparticle size of 26nm. It is found in this work that substitution of  $Al^{+3}$  increase the absorption property of barium hexa ferrite. Material with different compositions possess reflection loss from 27.56 to 40.06 dB [67].

**Virender Pratap Singh et al in 2014** studied synthesis of  $BaGd_xFe_{12-x}O_{19}$  by sol-gel method with different compositions for different values of  $x$  that are  $x= 0, 0.1, 0.2, 0.3$ . The nanocomposite was found good for microwave application and magnetic properties. Its hexagonal structure was confirmed by X-ray diffraction studies and size of the was found to be lie in the range of 84 to 90nm. This material was found good for antenna applications [68].

**S.Chakrabarty et al in 2015** studied that nanocrystalline Zn ferrites were synthesized using soft chemical way. Its structural and electrical properties were studied after doping with Ni. Growth of single phase nanocrystalline Ni doped Zn ferrites were confirmed by XRD. Change in optical band gap due to doped Ni ions was studied by FTIR and UV visible spectroscopy. Lattice parameter decrease from 8.448 Å to 8.280 Å due to Ni doping. Ac and dc conductivity of Ni doped samples were studied that shows anomalous behavior. Sample having Ni mol fraction from 0.2 to 0.6 show variation from normal to inverse spinal structure [69].

**Rutvi J.Pandya et al in 2015** investigate  $\text{Ni}_{0.5}\text{Zn}_{0.5}\text{Fe}_2\text{O}_4$  and  $\text{Ba}_{0.6}\text{Sr}_{0.4}\text{TiO}_3$  for electrical and structural properties by XRD. Cubic spinal structure was observed for these sample series. Permittivity, tangent loss and AC conductivities were studied over the range of frequencies upto 1 MHz. Dielectric values and conductivity become frequency independent at high values. At low frequencies these values remain very high but become low with constant value or high frequency. Electron hopping model explain well the conduction phenomenon [70].

**S. Noushin Ezzati et al in 2015** studied Barium Strontium ferrite synthesis by sol gel method and doped with Ni and Mn with composition of  $(\text{Ba}_{0.25}\text{Sr}_{0.75}\text{Fe}_{11}(\text{Ni}_{0.5}\text{Mn}_{0.5})\text{O}_{19})$ , and characterised by XRD, FTIR and FESEM. Particle size with average value of 45nm was reported & M type hexagonal structure was confirmed by FTIR analysis. By vector network analyser its absorption in X-band ( 8 to 12 GHz) was tested. [71]

**Samira Mandizadeha et al in 2015** studied synthesis of barium hexa ferrite by sol gel mechanism by using ferric nitrate and barium nitrate and characterise it with maleic acid as capping agent.They studied its magnetic properties by VSM and study barium hexa ferrite with different polymers.The effect of quantity of maleic acid and type of polymer used on the properties and morphology of barium hexaferrite was studied by X ray energy dispersive spectroscopy and scanning electron microscopy. It was verified that characteristics and morphology of sample was affected by all these varying parameters [72].

**C.Choodamania et al in 2016** investigate  $Mg_{1-x}Zn_xFe_2O_4$  series for the values of,  $x=0, 0.25, 0.50, 0.75$  and  $1$ ) by preparing it with auto combustion method and then dried powder was calcinated for 2 hours on  $700^\circ C$  and sintered for 3 hours at  $1050^\circ C$ . Electric and magnetic properties and their morphology was studied by characterising it by XRD , impedance spectroscopy, SEM and VSM. Crystallite size was observed to be in the range of 47 to 80 nm. Polyhedral structure with homogeneous grain was confirmed via SEM analysis. AC conductivity, Dielectric loss, and Dielectric constant was found to be lowest at  $x=0.5$ . Saturation magnetization and coercivity was significantly affected by zinc concentration in sample [73].

**A.Poorbafrani & E.Kiani in 2016** studied the microwavw absorption property of  $Co_{0.6}Zn_{0.4}Fe_2O_4$  nanocomposite with paraffine and characterise the sample using XRD and field emission electron microscopy , VSM and alternating gradient force magnetometer. Magnetization saturation and coercivity were improved with suitable stoichiometric ratios of composite. Permittivity and permeability with measurement of reflection loss were determined over the Range of 1 to 18 GHz frequency. At 20 wt% of paraffin shows maximum microwave attenuation capability [74].

**Preeti Gairola et al in 2016** studied enhancement in EMI shielding effect of barium hexaferrite by incorporating it with expanded graphite and polyaniline. Microwave absorption of composite was found to be lie in X-band that is from 8.2-12.4 GHz. Shielding effectiveness was studied to increase upto 37.1 dB, that depends on dielectric loss of material.[75]

**Alireza Shayan et al in 2017** studied the substitution of Aluminium in barium hexa ferrite which brings changes in its grains and show a reasonable decrease in it. They prepared series of  $BaFe_{12-x}Al_xO_{19}$  with ( $x = 0, 0.5, 1.0, 1.5, 2.0$ ) and observe the variation in the magnetic properties of sample and studies the change in hexagonal shape changes to rod like shape. At the frequency of 15.7 GHz for the value of  $x=2$  the sample show maximum reflection loss having magnitude of- 43 dB [76].

**Faseeh ur Raheem et al 2017** studied X type hexagonal ferrite of composition  $\text{Sr}_2\text{NiCoFe}_{28}\text{O}_{46}$  synthesis by micro emulsion method and using information from XRD crystallites size was found to lie in range from 29 to 41nm. A C conductivity rise with frequency and when Yb is introduced as dopant, its ac conductivity reduced as it enhance resistivity. Yb addition optimize coercivity and remanence while saturation magnetization decreased.[77]

**Anum Zafar et al in 2017** studied M type barium hexaferrites by doping with nano-sized europium show better electric and magnetic response. They synthesized using hydrothermal process and characterised the single phase M-type structure by XRD and FTIR. Electrical properties were recorded in the frequency range from 40 to 100MHz. Conductive properties were enhanced at low frequency and saturation magnetisation was increased from 30.49 to 54.27 emu/g, while coercivity increased from 3.03 to 8.73kOe. [78]

**Karamveer Chahal et al in 2017** investigate the synthesis of  $\text{Ba}_{1-x}\text{Pr}_x\text{Co}_x\text{Fe}_{12-x}\text{O}_{19}$  by sol gel method and using XRD ,TGA ,FTIR ,TEM and VSM confirm the M-type hexagonal structure. They attain average crystallite size in the range of  $38\pm 5\text{nm}$ . By VSM they showed increase in coercivity, retentivity and saturation magnetization. FTIR peaks were observed in the range of  $430$  to  $470\text{ cm}^{-1}$  and  $550$  to  $610\text{ cm}^{-1}$  that confirms the formation of tetrahedral and octahedral cluster and also provide an evidence Fe-O bonds stretching vibrations in this range.[79]

# Chapter 3: Resources and Approaches

## 3.1. Experimental Details

### 3.1.1. Materials

Barium Nitrate monohydrate  $\text{Ba}(\text{NO}_3)_2 \cdot \text{H}_2\text{O}$ .

Pure analytical iron (III) nitrate nonahydrate  $\text{Fe}(\text{NO}_3)_3 \cdot 9\text{H}_2\text{O}$ .

Zinc Nitrate hexahydrate  $\text{Zn}(\text{NO}_3)_2 \cdot 6\text{H}_2\text{O}$ .

Nickle Nitrate hexahydrate  $\text{Ni}(\text{NO}_3)_2 \cdot 6\text{H}_2\text{O}$

and citric acid  $\text{C}_6\text{H}_8\text{O}_7$  were used. Initial reagents to synthesize all the samples is deionized water. All the chemicals used for sample preparations in this study were of purity  $\geq 99\%$  and were used without any further purification.

### 3.1.2. Synthesis of Barium hexaferrite ( $\text{BaFe}_{12}\text{O}_{19}$ ) without any dopant

$\text{BaFe}_{12}\text{O}_{19}$  sample was prepared by sol-gel method which is also known as auto combustion method. Solution of  $\text{Fe}(\text{NO}_3)_3 \cdot 9\text{H}_2\text{O}$  and  $\text{Ba}(\text{NO}_3)_2 \cdot \text{H}_2\text{O}$  were prepared according to their stoichiometric ratios. Iron nitrate nonahydrate and Barium nitrate in the molar ratio 100 ml of 0.1 M,  $\text{Ba}(\text{NO}_3)_2 \cdot \text{H}_2\text{O}$  and 100 ml of 1.1M  $\text{Fe}(\text{NO}_3)_3 \cdot 9\text{H}_2\text{O}$  were prepared in separate beakers and dissolved in deionized water with constant stirring using magnetic stirrer for 15 minutes for their complete dissolution and to get clear solution in water. Both solutions were then mixed in a larger beaker. Citric acid of 1.2M having same amount of 100ml was added to the solution with constant magnetic stirrer. After this step ammonia solution is added drop by drop to this mixture until its pH rise to 7.

System is kept under continuous magnetic stirrer and now heating of  $350^\circ\text{C}$  temperature is powered ON, the same condition of stirring. Finally the solution changes to a gel form and catches fire inside the beaker and changes to the powder form.

Finally dark brown coloured powder was obtained. Using mortar and pestle it is further grinded and kept in muffle furnace at  $800^\circ\text{C}$  for 8 hours for calcination purpose.



### **3.1.3. Synthesis of BaFe<sub>12</sub>O<sub>19</sub> with Zinc (Zn<sup>2+</sup>) and Nickel (Ni<sup>2+</sup>) dopants**

Two different series of barium hexaferrite with zinc and then with both zinc and nickel were prepared. First series is Ba<sub>1-x</sub>Zn<sub>x</sub>Fe<sub>12</sub>O<sub>19</sub> for x = 0, 0.2, 0.35, 0.5, were prepared. Second series of Ba<sub>1-2x</sub>Zn<sub>x</sub>Ni<sub>x</sub>Fe<sub>12</sub>O<sub>19</sub> for x = 0, 0.1, 0.175, 0.2, were also prepared. Samples were prepared by the same method followed in first step i-e sol gel method. For preparing first series sample of x=0.2. Iron nitrate and Barium nitrate were prepared in aqueous solutions by similar way but molarity of Barium Nitrate solution and Zinc Nitrate were kept 0.08M and 0.02M respectively that was collectively kept 0.1M. Rest of two samples were prepared similar manner. All the process steps are identical as expressed in section 3.1.2.

For preparation of second series with both Zinc and Nickel, sample of x=0.1 was prepared with solution of Barium nitrate 0.08M, Zinc Nitrate 0.01M and Nickel Nitrate 0.01M were used and all other steps for rest of all samples were followed in similar way and molarities were adjusted accordingly. Same process of grinding and calcination was followed.

## **3.2. Sample Preparation**

Samples were prepared using different methods for the measurement of SEM, FTIR, Electric and magnetic properties. Procedures used for the preparation of different samples are discussed as under:

### **3.2.1. Preparation of SEM Samples**

SEM is used for the study of surface morphology and for getting 3D images of surface. A very small amount of powdered material was dispersed in water using ultrasonicator for about one hour and then drop of the mixture dripped onto a clean substrate. On substrate surface powder particles are dried and dispersed for further processed of analysis by SEM.

### **3.2.2. Preparation of Samples for measurement of electrical properties**

For measurement of electrical properties of samples, pellet of each sample was prepared using pellet die set and Hydraulic press. Each sample was finely grinded before sample preparation. Pellets were prepared using 1 gram of each. Pellets prepared were measured using vernier caliper and found almost same thickness and diameter (2 mm thickness and about 10 mm diameter) for all pellets. By using hydraulic press a load of 3 tonnes for 5 minutes was applied on each pellet. The prepared pellets were kept at 200°C to be sintered for 2 hrs and used for measuring electrical properties (Dielectric constant & Dielectric loss).

### **3.2.3. Preparation of FTIR samples**

KBr pellet method was for sample preparation because alkali salts gives no absorption in IR spectrum. Potassium salt (KBr) was placed in oven at 100 °C for one hour for removal of moisture. Small amount of sample and KBr was taken and ground to fine powder and pellet was prepared using pellet die set and Hydraulic press. Mixture of ground KBr and sample was added into the die and it was then placed into the press and with a pumping movement, moved the hydraulic pump handle downward until it shows 3 tonnes on the scale. Waited for 45 seconds, pressure was released and die was taken out. Finally, a thin sample pellet having thickness in the range of 2-3 mm and dia of ~13 mm was obtained.

### **3.3. Characterization Techniques**

There are many characterization techniques which are used to study the properties of any material. But in this work the following characterization techniques are used to study the properties of ferrites.

#### a) X-Ray Diffraction

- i. Phase formation
- ii. Crystallite Size
- iii. X-ray Density
- iv. Porosity

- b) Scanning Electron Microscope
  - i. Surface morphology
  - ii. Structural observation
- c) Fourier Transformed Infrared Spectroscopy
- d) Impedance Analyzer
  - i. Dielectric properties
  - ii. AC Conductivity
  - iii. AC Impedance Spectroscopy

### **3.4 X-Ray Diffraction technique**

X-Rays diffraction technique was discovered by W.C. Rontgen in 1895. It is very useful technique to study the structural properties of crystal. In crystal there is the huge difference between the slit size and the huge variation in the light wave, the light rays are not suitable for structural properties. On the other hand x-rays wavelength is approx: equal to the slit size of crystal, that's why this method was discovered. It provide us information about structures, phases, crystals orientation and parameters like average crystallite size, structural strain, degree of crystallinity and crystal defects. There are different methods to determine crystal structure like Laue method, rotating crystal and powder diffraction method. Size of the crystal can be determined by the powder diffraction method by two different techniques [80]:

1. Debye Scherrer Method
2. Diffractometer Method

The target material can be of various type of target materials like Copper and Molybdenum etc. in this research we used Cu -  $\lambda = 1.54$  nm as XRD source.

#### **3.4.1 Working principle of XRD**

The X-Ray beam hit the sample and crystal planes which acts as mirror reflect that beam and the angle of their reflection equals to the angle of incidence which in other terms known as constructive interference. This interference in each set of atoms cause the interference of x-rays within the crystal. The phenomenon of interference can be defined by Braggs Law which is given by:

$$n\lambda = 2 d \sin\theta$$

This is called Bragg's equation where 'n' is interference order, 'θ' is angle of incidence, 'd' is interlayer distance and 'λ' is wavelength of incident X-rays. Bragg's law says that the radiations are reflected from the path difference of  $2d\sin\theta$  which are subjected to equally spaced planes at a distance of 'd' and 'θ' is measured from plane. The constructive interference can be formed as shown in Fig.3.1. For the above mentioned equation reflection can only occur when  $\lambda < 2d$  which is the reason why visible light cannot be used. There are three techniques which are commonly used for XRD characterization [81].

1. Laue Method
2. Rotating Crystal Method
3. Powder diffraction method

As the prepared sample is composed of nanopowder we use powder diffraction method. This method is best suitable when single crystals are not available of acceptable sizes. For this method, the prepared sample powder is grinded finely to a small size and then place in a circular plate of aluminum or glass. The X-Rays are hit on prepared powder which is randomly oriented with respect to the x-rays. In powder method, the forming of a diffracted cone of radiation is shown in Fig 3.2. For a particular reflection, some of the nanoparticles are aligned in such a way that their (hkl) planes form the perfect Bragg's angle.

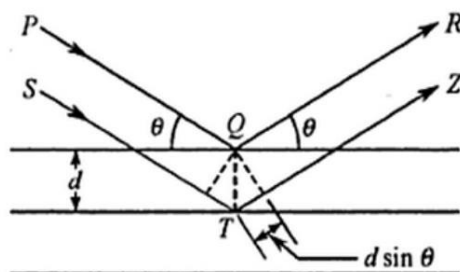


Fig 3.1: Scattering of incident beams of x-rays at the plane of atoms in crystal

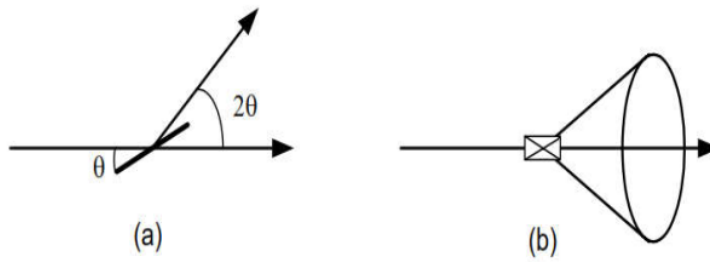


Fig 3.2: Formation of a diffracted cone of radiations in powder method

### 3.4.2 Lattice Constant:

It is a parameter which shows the length of one of the edge of the unit cell of crystal lattice. It is also termed as lattice parameters. It refers that the distance between lattice points is constant. It is calculated by the equation given below:

$$a = \frac{\lambda \sqrt{h^2 + k^2 + l^2}}{2 \sin \theta}$$

Where ‘a’ and ‘λ’ are lattice constant and the wavelength of X-rays respectively, (hkl) are the miller indices and “θ” is the diffraction angle [82].

### 3.4.3 Crystallite Size:

The crystallite size has great impact on the structural properties of the material. The diffraction patterns which are obtained through experimentation are verified and compared to JCPDS cards for phase confirmation and identification. The peak broadening effect in XRD relates to small and large crystallite size. The average crystallite size was calculated by Debye-Scherrer formula which shows that peak width is inversely proportional to crystallite size as shown below:

$$d = \frac{0.9 \lambda}{\beta \cos \theta}$$

Where “ $\lambda$ ” is the wavelength of the X-rays, “ $\theta$ ” is the diffraction angle and “ $\beta$ ” is FWHM value of respective peaks [83].

#### 3.4.4 X-Ray Density:

The X-Ray density is calculated by:

$$\rho_x = \frac{Z M}{N_A a^3}$$

Where “M” is Molecular weight of sample, “NA” is Avogadro's Number ( $6.022 \times 10^{23}$ ) and “a” is lattice constant and “Z” is formula unit of cell. For spinel ferrite the cell has 8 formula units. This equation shows the direct proportionality of x-ray density with molecular weight and inverse proportionality of x-ray density with lattice.

#### 3.4.5 Bulk Density

It is the intrinsic property of the material and is also termed as measured density. It is calculated by conventional density formula

$$\rho_m = \frac{m}{\pi r^2 h}$$

Where “m” is mass of the sample, “r” is radius of the pellets and “h” is thickness of the pellets of the samples.

To calculate the bulk density, the powder samples were pressed in a circular pellet using hydraulic press machine [84].

#### 3.4.6 Porosity Fraction:

The porosity fraction is calculated from the X-Ray and bulk density data and is determined by the formula given below:

$$Porosity (\%) = \left(1 - \frac{\rho_m}{\rho_x}\right) \times 100$$

Where  $\rho_x$  is the X-Ray density and  $\rho_m$  is the bulk density of the sample.

### 3.5 Scanning Electron Microscope

It is one of the key techniques to provide imaging of sample surface. It uses electron imaging techniques which uses high energy beam of electrons for imaging. The high energy electron beam interacts with the surface of the sample and gives valuable information about

- Surface morphology
- Composition of the sample
- Phase mapping

After the interaction of electron beams with surface of sample, it generate various types of signals which are; auger electron, secondary electron, back scattered electron, transmitted electron, x-rays and cathodoluminescence.

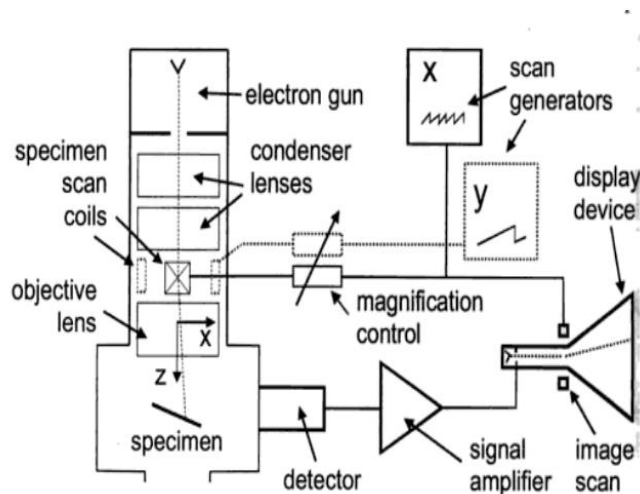


Fig3.3: Basic principle of SEM [85]

#### 3.5.1 Working principle of SEM:

In the scanning electron microscope, the high energy beam of electrons is focused to the surface of sample by using some pairs of magnetic lens. In the last lens, beam is deflected in the x and y direction to scan the rectangular area of the sample surface in order to control the brightness of the resulting image. The vacuum is produced in the chamber to prevent from defocusing of electron beam and contamination of dust particles. When the electrons interact with the surface of sample, it emits various types of electrons from the surface. Different types of detectors are used to collect these various types of electrons. For every type of

electron there is a different detector. The most common detector for SEM is used for secondary electrons [86].

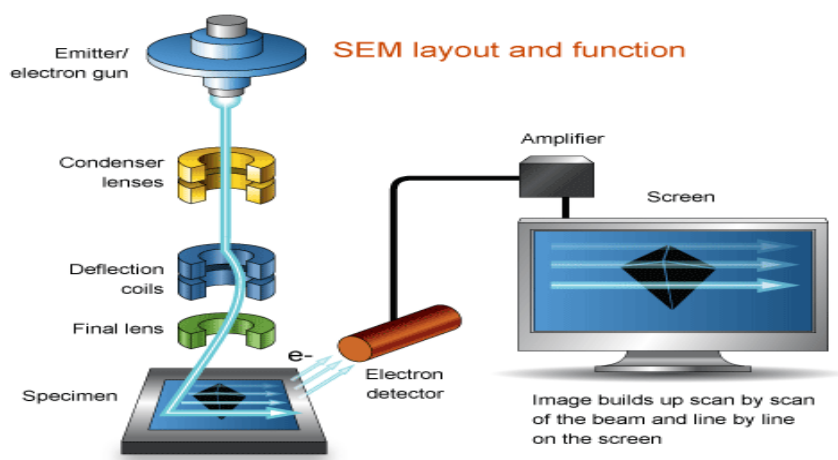


Figure 3.4 A layout of SEM functioning [87]

### 3.6 Fourier Transform Infrared Spectroscopy

FT-IR is a technique used to get the infrared spectrum of absorption or emission of solid, liquid or gas. The materials are characterized through a specific spectrum which involves different types of radiations like U.V/Visible/NIR or even IR. The light is passed in a specific wavelength region and the intensity of the signal transmitted is measured. The intensity of the signal shows how much energy part of the spectrum is emitted after the interaction.

#### 3.6.1 Working principle of FT-IR

There is a mirror configuration between the source and the detector. The mirrors are used for the selection of the wavelength by simply moving the mirrors. The light is emitted from the source which is focused along a wavelength by moving mirrors and the transmitted light is measured by the detector. The intensity of the transmitted light shows the attached functional groups to the sample. The processing requires a complete algorithm known as the Fourier Transform Spectroscopy. The equipment of FT-IR and its basic principle is shown in Fig.3.4.



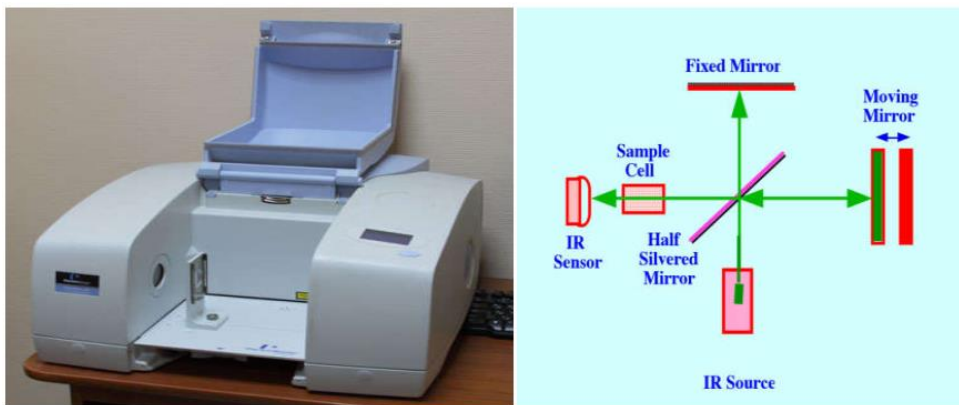


Fig.3.5 shows the equipment of FT-IR and its basic principle. (Adopted from: Analytical Spectroscopy by Raymond P. W. Scott)

### 3.7 Dielectric properties

The dielectric parameters were measured using LCR Meter Bridge. Capacitance and d-factor was measured of the pellets and then dielectric constant was calculated by the equation

$$\epsilon' = \frac{C t}{\epsilon_0 A}$$

Where “C” is capacitance, “t” is thickness of the pellets, “A” is surface area of the pellets and “ $\epsilon_0$ ” is permittivity of free space.

Dielectric constant is a property of the material that expresses the force between two point charges. It is the factor by which the electric field is decreased between the charges relative to vacuum. Maxwell-Wagner model explain the dielectric parameters and Koop’s theory also explain them well [88].

Dielectric loss (imaginary part of dielectric) corresponds to energy dissipation losses. It was calculated by the equation

$$\epsilon'' = \epsilon' \tan \delta$$

The dielectric loss tangent shows energy dissipation as heat. It is the ratio of dielectric constant and dielectric loss as shown by the equation

$$\tan \delta = \epsilon'' / \epsilon'$$

### 3.8 AC Conductivity

AC conductivity was measured at room temperature over a frequency range of 100Hz to 5 MHz frequency. It shows the conductive behavior and the hopping mechanism of the material. It was calculated from the dielectric parameters by the following equation:

$$\sigma_{AC} = \omega \epsilon_0 \epsilon' \tan \delta$$

Where “ $\epsilon_0$ ” is permittivity of free space, “ $\epsilon'$ ” is dielectric constant and ‘ $\tan \delta$ ’ is dielectric loss tangent. SI unit of AC conductivity is S/m.

### 3.9. AC impedance spectroscopy

The AC impedance parameters of the samples were measured at room temperature. Resistance (R) and reactance (X) were measured over the frequency range of range of 100 Hz to 5 MHz. The impedance is a complex quantity where resistance (R) and reactance (X) shows the real and imaginary parts of impedance in the circuit by the relation:

$$Z = R + jX$$

The impedance -Cole plot shows the resistive behavior of the material. The SI unit of impedance is ‘ $\Omega$ ’ where resistance (R) and reactance (X) shows the real and imaginary parts of impedance in the circuit by the relation:

$$Z' = R = |Z| \cos \theta_z$$

$$Z'' = X = |Z| \sin \theta_z$$

The impedance shows the resistive behavior of the material. The SI unit of impedance is ‘ $\Omega$ ’. The Cole-Cole plot based on real and imaginary parts of impedance shows contribution of resistance in the material [89].

### 3.10. Electric Modulus

The real and imaginary parts of the electrical modulus  $M'$  and  $M''$  respectively can be calculated as follows

$$M' = \frac{\varepsilon'}{(\varepsilon'^2 + \varepsilon''^2)}$$

$$M'' = \frac{\varepsilon''}{(\varepsilon'^2 + \varepsilon''^2)}$$

In above expressions  $\varepsilon'$  and  $\varepsilon''$  is the real and imaginary part of dielectric constant, respectively. The Cole-Cole plot based on real and imaginary parts of electric modulus is also plotted [89].

# Chapter:4 Results and Discussion

## 4.1 X-Ray Diffraction Technique

X Ray diffraction technique has been used to carry out phase confirmation and completion of chemical reaction along with X-ray densities and lattice parameters using powder sample. Two different substitutions in Barium hexaferrites were examined by XRD. First series is  $Ba_{1-x}Zn_xFe_{12}O_{19}$  for  $x = 0, 0.2, 0.35, 0.5$ , and second series of  $Ba_{1-2x}Zn_xNi_xFe_{12}O_{19}$  for  $x = 0, 0.1, 0.175, 0.2$ , both samples were analyzed by XRD for phase confirmation of hexagonal ferrites.

### 4.1.1. XRD of Barium hexaferrites ( $BaFe_{12}O_{19}$ )

Sharpness of the peaks depicts that material is basically crystalline in nature. Characterized diffraction peaks relating to the pure Barium hexaferrite, i.e. (006), (110),(008),(112), (107), (114),(200), (203), (205), (206), (10 11), (209), (217), (20 11), (20 12), (220), (2014), (228), (317) and (403) are seen in the samples heated at 800 °C (figure 4.1 ). The peaks shown here coordinate precisely with the standard pattern for Barium hexaferrite (Reference card no. ICDD-00-039-1433) as shown in figure 4.1.

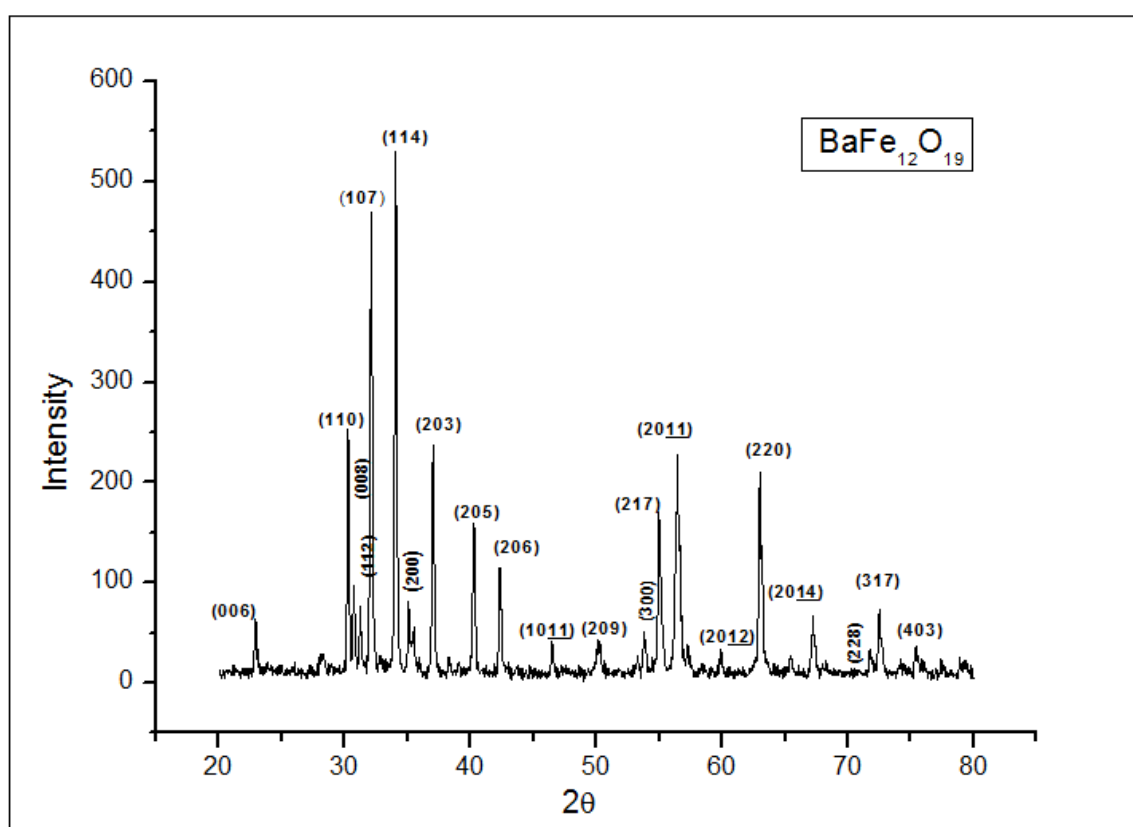


Fig 4.1 : XRD of Barium hexaferrite Nanoparticles ( $BaFe_{12}O_{19}$ )

#### 4.1.2. Zn substituted hexaferrites ( $\text{Ba}_{1-x}\text{Zn}_x\text{Fe}_{12}\text{O}_{19}$ )

The XRD pattern of all three compositions of Zn substituted Barium hexaferrites having compositions of  $x = 0, 0.2, 0.35, 0.5$ , were synthesized by sol gel method as shown in figure 4.2 to 4.4. Miller indices  $h, k$  and  $l$  corresponding to the XRD peaks for the compound synthesised are comparable exactly with the standard one of barium hexaferrite [ICDD-00-039-1433] indicating the single hexagonal phase structure of these samples. This powder samples with substitutions of Zn shows that the doped cations did not change the values of lattice parameters and they replace the barium atoms in prepared sample and did not affect hexagonal structure and geometry.

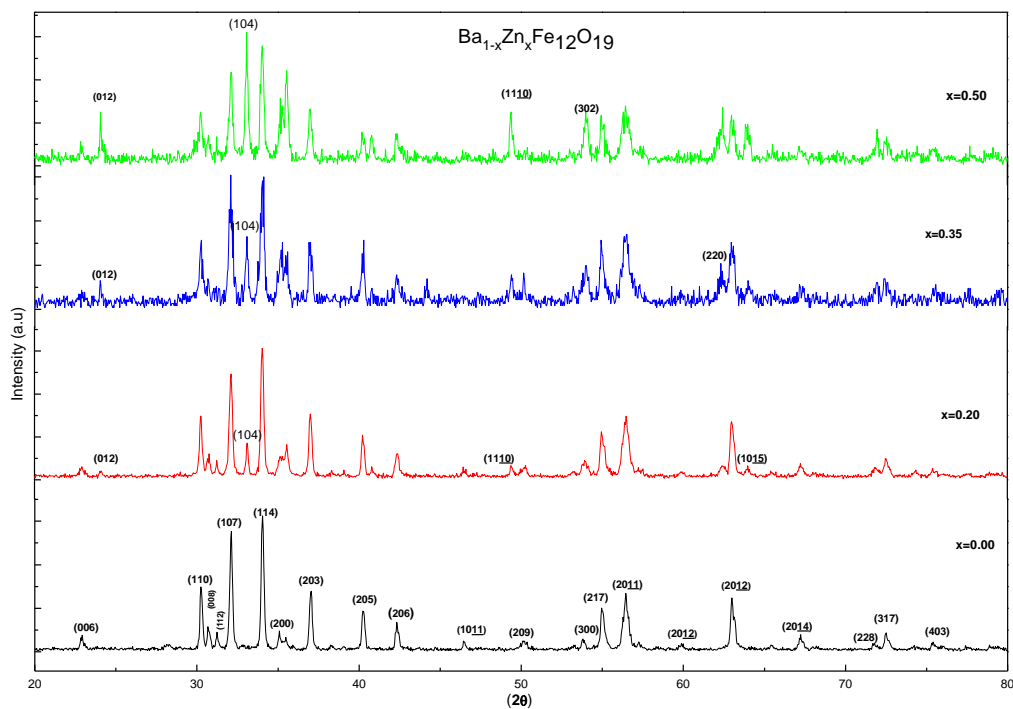


Fig 4.2 : XRD of  $\text{Ba}_{1-x}\text{Zn}_x\text{Fe}_{12}\text{O}_{19}$  Nanoparticles.

#### 4.1.3. Zn and Ni substituted hexaferrites ( $\text{Ba}_{1-2x}\text{Zn}_x\text{Ni}_x\text{Fe}_{12}\text{O}_{19}$ )

The XRD pattern of all three compositions of Zn and Ni substituted Barium hexaferrites having compositions of  $x = 0, 0.1, 0.175, 0.2$ , were synthesized by sol gel method as shown in figure 4.5 to 4.7. Miller indices corresponding to the XRD peaks for the synthesized compound are exactly matching with the standard barium hexaferrite [ICDD-00-039-1433] showing its single hexagonal phase of

structure of these samples. The results from XRD shows that the doped cations replaced the barium cations without affecting the structure and geometry of the standard sample. Some of the new peaks appear as shown in figure 4.2 which confirms the presence of substitution in sample.

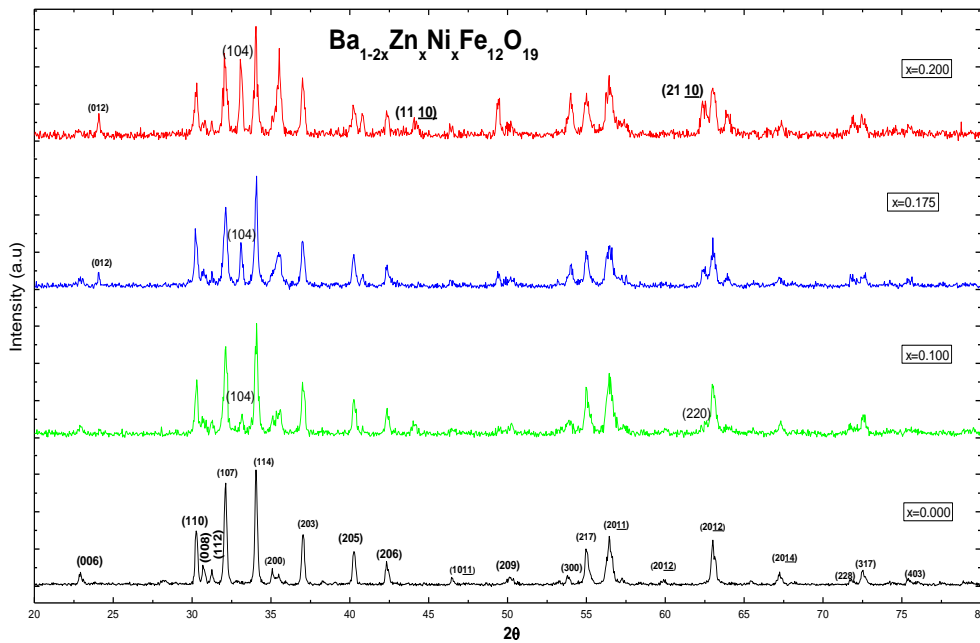


Fig 4.3: XRD of  $\text{Ba}_{1-2x}\text{Zn}_x\text{Ni}_x\text{Fe}_{12}\text{O}_{19}$  Nanoparticles.

#### 4.1.4. Cell volume and Lattice Parameters

The index XRD information for all of the specimens is utilized to ascertain lattice constants  $a$  &  $c$ , crystallite size  $D$ , cell volume  $V_{\text{cell}}$ , and X-ray density  $d_x$  and bulk density for all the samples table 4.1 are calculated, utilizing the mathematical statements discussed in chapter 3, separately [90].

The lattice parameters  $a$  &  $c$  for hexagonal ferrites have been calculated in the range of,  $a = 5.8913140 \text{ \AA}$  and  $c = 23.2510500 \text{ \AA}$ . These are calculated for different compositions of this sample through eqs. (3.1) and (3.2) using the values of  $hkl$  and  $d$ -spacing. These values are comparable with the literature values of

$a = 5.880 \text{ \AA}$  and  $c = 23.153 \text{ \AA}$  for the barium hexaferrite as reported by Narang et al [114]. It is clear from table 4.1 that by increasing the Zn contents and then both Zn and Ni, cell volume decrease and bulk density increase slightly. This can be deduced because the ionic radius of  $\text{Zn}^{2+}$  ( $0.84 \text{ \AA}$ ) is while the ionic radius of  $\text{Ni}^{2+}$  ( $0.74 \text{ \AA}$ ) both smaller than that and  $\text{Ba}^{2+}$  ( $1.30 \text{ \AA}$ ). [91,92]

#### 4.1.6. Crystallite size determination

Scherer formula is used to determined the crystallite sizes ( $D$ ) of all the synthesized samples. The calculated crystallite size remain with in the range of 29-60 nm for all the samples. This is because of the fact that in the material Zn and Ni ions are doped continuously at the barium sites [93].

**Table 4.1. . Calculated values of the crystallite size  $D$ , bulk density  $d_b$ , X-ray density  $d_x$ , and porosity for  $\text{Ba}_{1-x}\text{Zn}_x\text{Fe}_{12}\text{O}_{19}$  (NP) ( $x = 0, 0.2, 0.35, 0.5$ ).**

<b>Composition</b>	X= 0	X= 0.2	X= 0.35	X= 0.5
$\text{Ba}_{1-x}\text{Zn}_x\text{Fe}_{12}\text{O}_{19}$				
Crystallite size, D (nm)	48	48	29	60
Bulk density, ( $d_m$ ) $\text{g/cm}^3$	2.97	2.85	2.82	2.80
X-ray density, ( $d_x$ ) $\text{g/cm}^3$	5.271	5.270	5.267	5.262
Porosity %	43.65	45.92	46.54	46.78

**Table 4.2. Calculated values of the crystallite size  $D$ , bulk density  $d_b$ , X-ray density  $d_x$ , and porosity for  $Ba_{1-2x}Zn_xNi_xFe_{12}O_{19}$  ( $x = 0, 0.1, 0.175, 0.2$ ).**

<b>Composition</b>	X=0	X=0.1	X= 0.175	X= 0.2
$Ba_{1-2x}Zn_xNi_xFe_{12}O_{19}$				
Crystalline size, D (n m)	48	40	48	60
Measured density, ( $d_m$ ) $g/cm^3$	2.97	2.79	2.77	2.70
X-ray density, ( $d_x$ ) $g/cm^3$	5.271	5.268	5.263	5.259
Porosity %	43.65	47.03	47.38	48.65

#### **4.2. SEM Analysis (Surface Morphology)**

SEM technique is used for microstructure analysis of ferrites. It provides useful information about phase formation, grain/ crystallite size & composition of sample. It is also useful to interpret about porosity of the samples material. Preparation of samples were carried out using distilled water and sonicated for 2 hours each sample before analysis. Surface morphology for all samples with various compositions was analyzed by SEM being operated at 20 KV. SEM images for different compositions is shown figures 4.4 to 4.10. The minimum and maximum particle size obtained by SEM for each sample ranges from 16.00 nm to 60.00 nm respectively.

The (SEM) scanning electron microscopic image for the un-doped barium hexaferrite in pure form ( $BaFe_{12}O_{19}$ ) can be seen in figure 4.8. The surface of the un-doped sample looks too denser showing some degree of agglomeration in the particles. The porous nature is confirmed by presence of voids on its surface. This observation depicts that the during calcination process pores are induced in the



synthesized samples that results in low values of bulk densities. The surface morphology of the samples doped with Zn are appeared in figures 4.4 to 4.7. Specimens having the dopant content with the values of  $x = 0.20$ ,  $x = 0.35$  and  $x=0.50$  and the samples doped with both Zn and Ni are appeared in figures 4.8 to 4.10, having the dopant content with the values of  $x = 0.100$ ,  $x = 0.175$  and  $x=0.200$  are selected from the substituted sample series. The blended specimens surface shows very much characterized crystalline nanoparticles however some of them have shaped into little agglomerates. The individual nanoparticles might, however, have a tendency to combine together because of calcination of the samples at high temperature of  $800^{\circ}\text{C}$ . The molecule size of the doped specimens is smaller than the un-doped material. In each of the synthesized series, particle size is varying over the series with the increase of dopant content as shown in figures 4.4 to 4.10. The confirmation of all the observation by the XRD data is given in table 4.1 & 4.2.

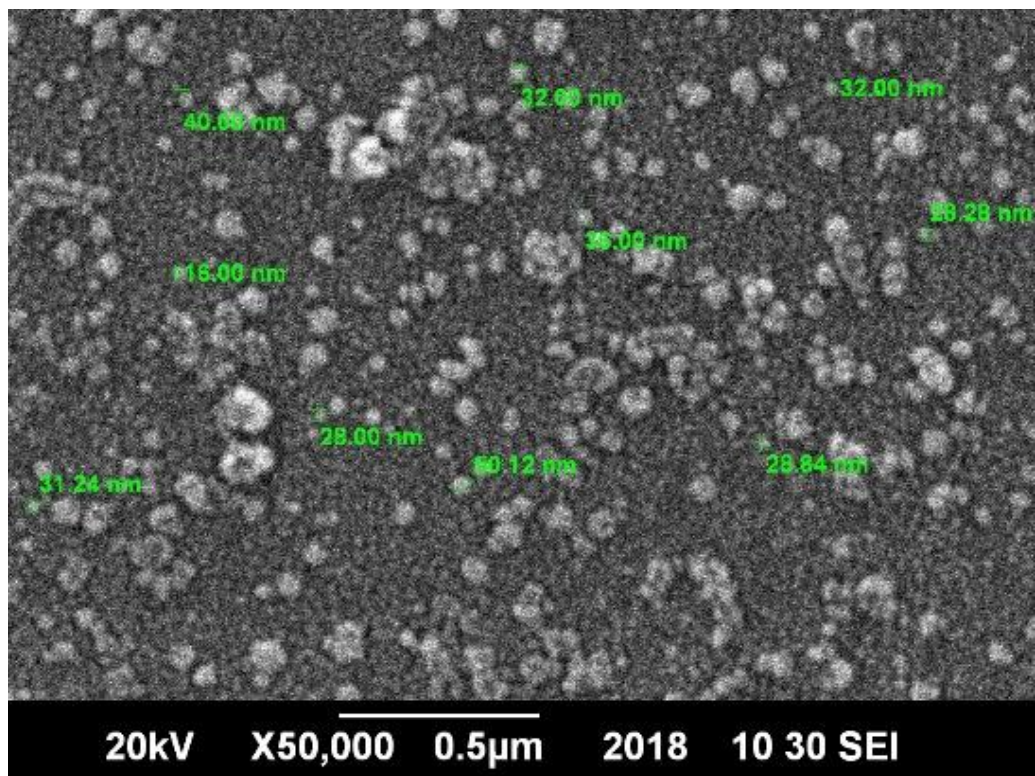


Fig.4.4. SEM image of Barium hexaferrite Nanoparticles ( $\text{BaFe}_{12}\text{O}_{19}$ )

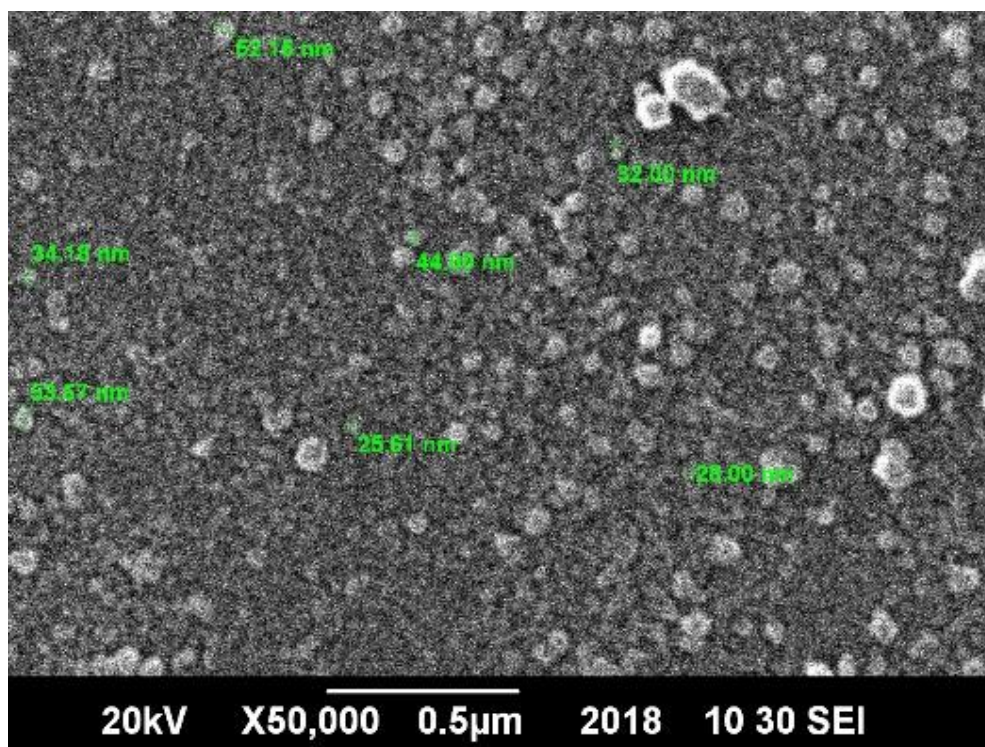


Fig.4.5. SEM image of  $\text{Ba}_{0.8}\text{Zn}_{0.2}\text{Fe}_{12}\text{O}_{19}$  (NP)

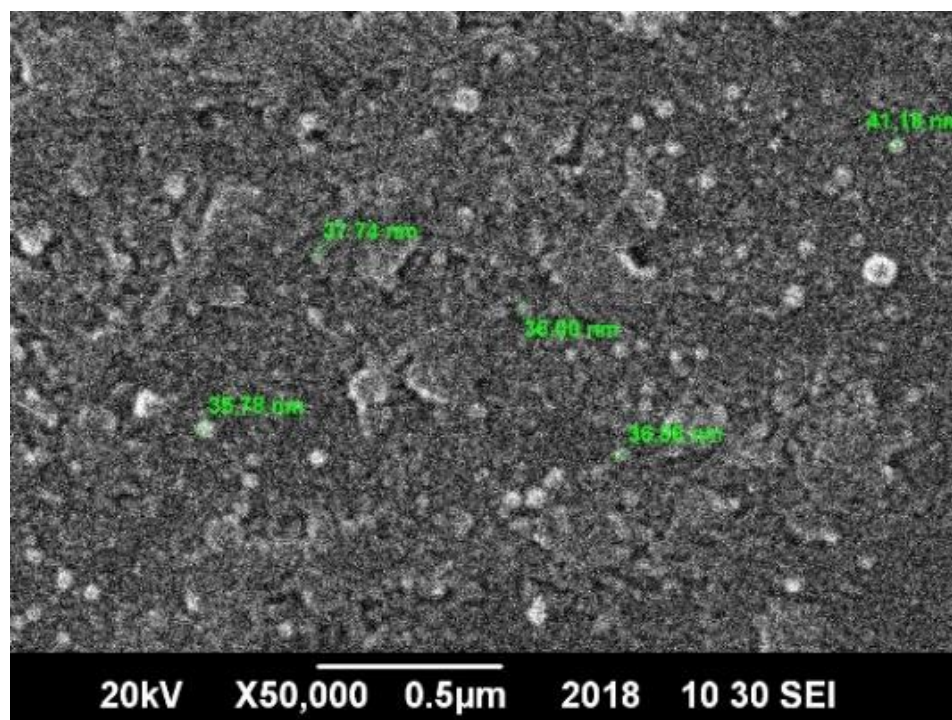


Fig.4.6 SEM image of  $\text{Ba}_{0.65}\text{Zn}_{0.35}\text{Fe}_{12}\text{O}_{19}$  (NP)

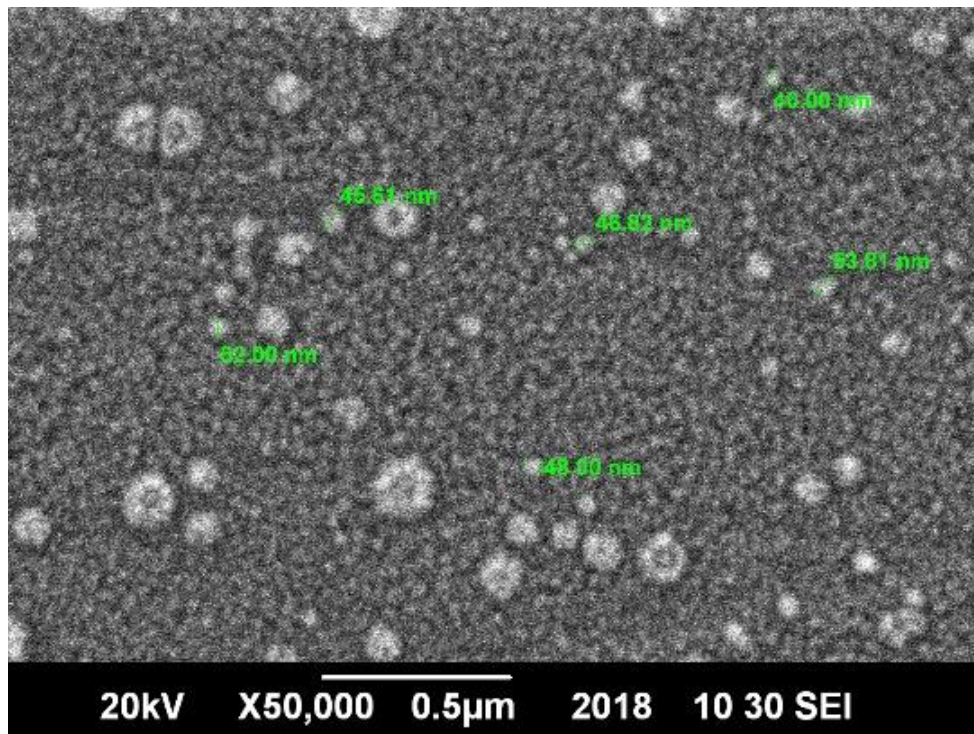


Fig.4.7 SEM image of  $\text{Ba}_{0.5}\text{Zn}_{0.5}\text{Fe}_{12}\text{O}_{19}$  (NP)

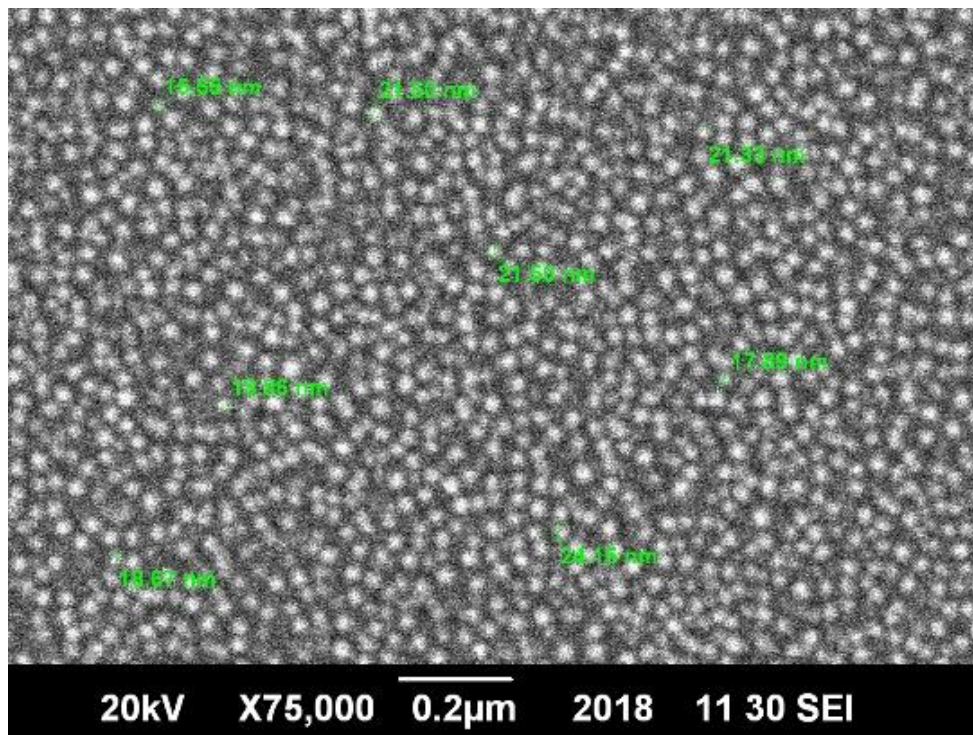


Fig.4.8. SEM image of  $\text{Ba}_{0.8}\text{Zn}_{0.1}\text{Ni}_{0.1}\text{Fe}_{12}\text{O}_{19}$  (NP)

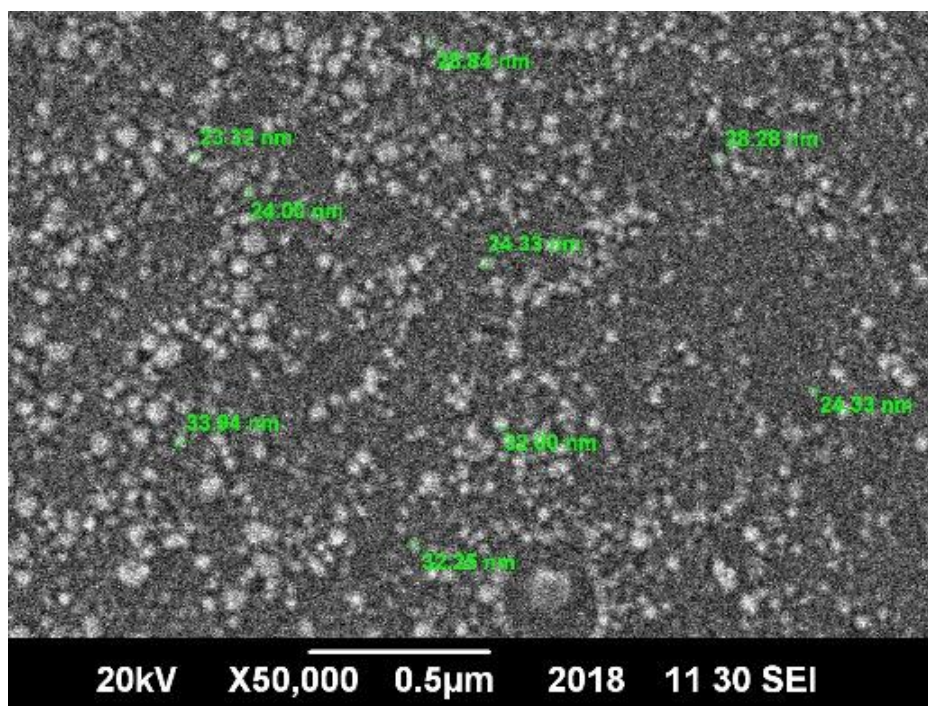


Fig.4.9. SEM image of  $\text{Ba}_{0.65}\text{Zn}_{0.175}\text{Ni}_{0.175}\text{Fe}_{12}\text{O}_{19}$  (NP)

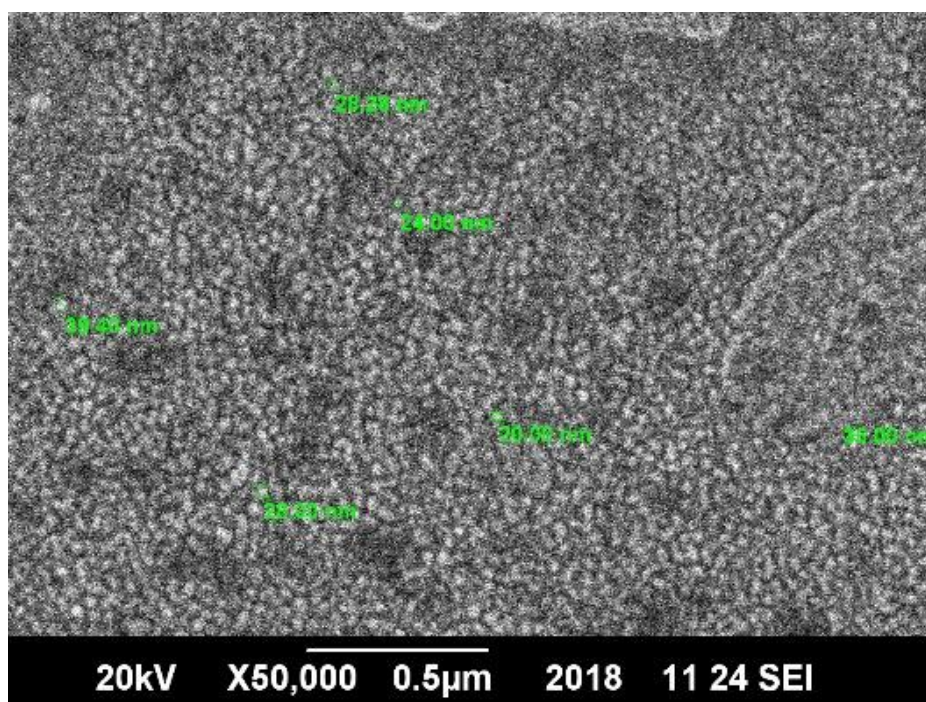


Fig.4.10 SEM image of  $\text{Ba}_{0.6}\text{Zn}_{0.2}\text{Ni}_{0.2}\text{Fe}_{12}\text{O}_{19}$  (NP)

### 4.3. FTIR Analysis

The FTIR spectra of barium hexaferrite powders after calcination at 800 °C obtained by sol gel technique are shown in figures 4.15 and 4.16. All the FTIR spectra show two signature absorption peaks of hexaferrite in the range of 1000 to 400  $\text{cm}^{-1}$  with which the formation of inorganic or ferrite ions is confirmed in crystal lattice.[94]. For standard sample of **BaFe<sub>12</sub>O<sub>19</sub>** the peak at 434.98  $\text{cm}^{-1}$  indicate A<sub>2u</sub> vibration of octahedral Fe (4+)-O bonds and other peak at 592.02  $\text{cm}^{-1}$  indicate vibration of Fe(3+)O<sub>4</sub> tetrahedral [94]. The higher frequency band ( $\nu_1$ ) (676.92 – 558.98  $\text{cm}^{-1}$ ) and lower frequency and ( $\nu_2$ ) (356.16 – 419.20  $\text{cm}^{-1}$ ) are associated to tetrahedral and octahedral sites. [95-96].

It demonstrates that the normal vibrational modes for tetrahedral clusters are higher than the octahedral ones. Longer bond length is possessed by octahedral clusters and short bond length of tetrahedral cluster. IR-spectrum of sample material demonstrates the particular stretching vibration bands at different peaks, for Zn series peaks of lower frequency are observed at 430.74, 432.23 and 433.36 $\text{cm}^{-1}$  while higher frequency peaks are observed at 583.57, 581.99 and 579.20 $\text{cm}^{-1}$ . For Zn and Ni series peaks of lower frequency are observed at 431.89, 431.03 and 438.89 $\text{cm}^{-1}$  while higher frequency peaks are observed at 583.15, 584.29 and 582.99 $\text{cm}^{-1}$ . In both series Metal–oxygen stretching vibrations at tetrahedral sites are observed in high frequency range. On the other hand lower frequency range shows metal–oxygen stretching vibrations in octahedral sites[R]. The characteristic peaks are presented in Fig. 4.15 & 4.16 are found to be observed at different positions for different composition of dopants, because ionic radius of dopant is different than standard sample. That's why bond length varies in all samples [97].

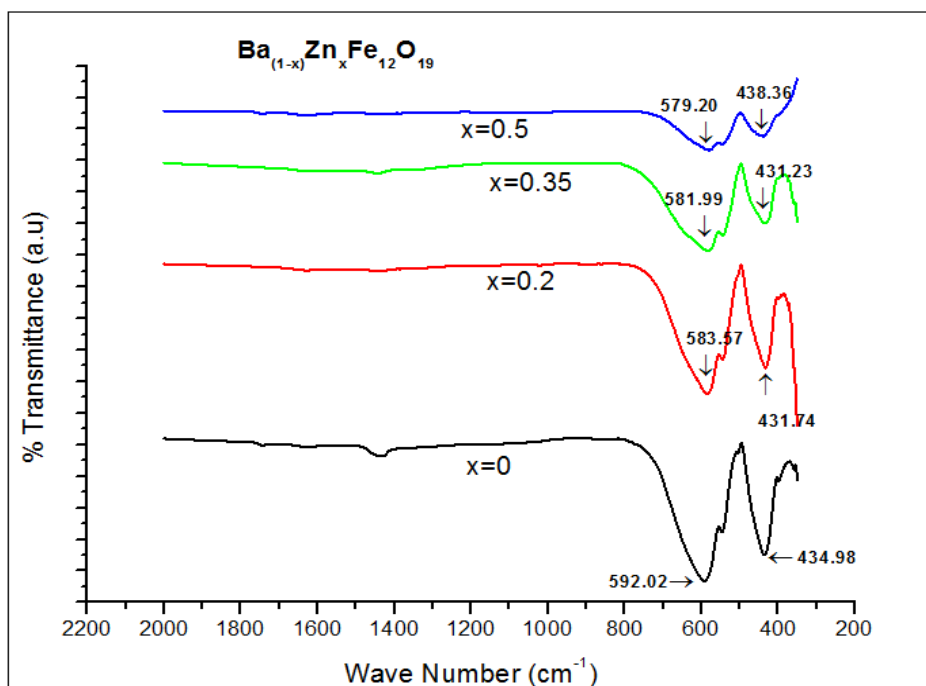


Fig.4.11: FTIR spectroscopy of Ba<sub>1-x</sub>Zn<sub>x</sub>Fe<sub>12</sub>O<sub>19</sub> (NP) (x=0,0.2,0.35 & 0.5)

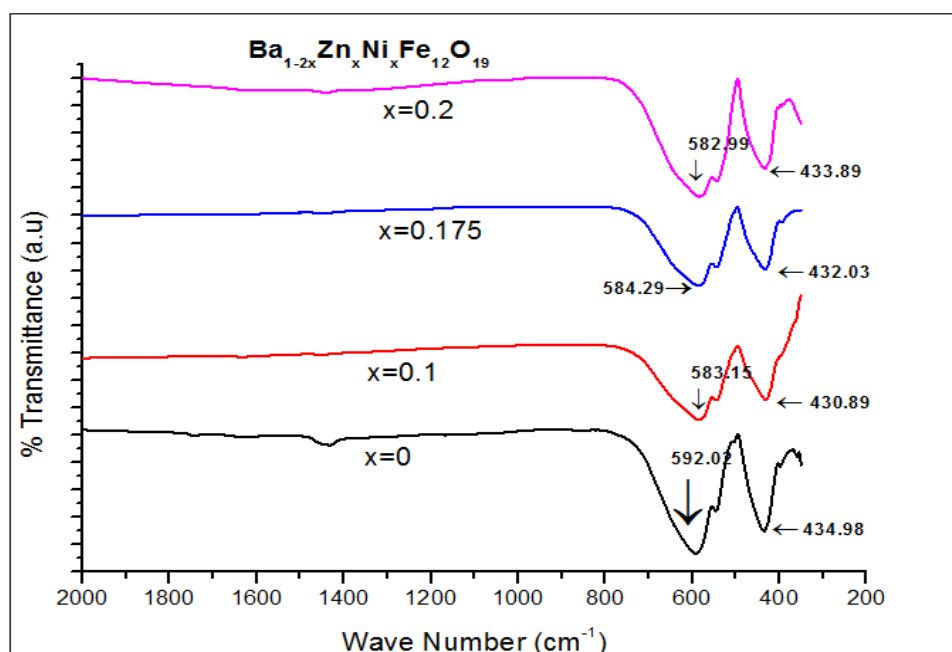


Fig 4.12: FTIR spectroscopy of Ba<sub>1-2x</sub>Zn<sub>x</sub>Ni<sub>x</sub>Fe<sub>12</sub>O<sub>19</sub> (NP) (x=0,0.1,0.175 & 0.2)

## 4.4. Electrical Properties

Various parameters including dielectric constant, AC conductivity, dielectric loss and tangent loss ( $\tan \delta$ ) are estimated from the dielectric measurements carried out for the ferrite samples. Substitution of Zn and Ni in hexaferrite matrix is expected to enhance the dielectric loss of barium hexaferrites. Which is our requirement for improving in its electromagnetic absorbing property.

### 4.4.1. Dielectric properties

The study of dielectric properties provides detailed information about the behavior of electrical charge-carriers.

#### 4.4.1.1. Dielectric constant ( $\epsilon'$ ).

Figures 4.13 and 4.17 show the variation of dielectric constant for Zn and Ni doped barium hexaferrite series with respect to frequency from 100Hz to 500MHz are. Maximum value of 133 is observed on substitution of both Zn and Ni in series of  $\text{Ba}_{1-2x}\text{Zn}_x\text{Ni}_x\text{Fe}_{12}\text{O}_{19}$  (NP) for  $x=0.2$ .

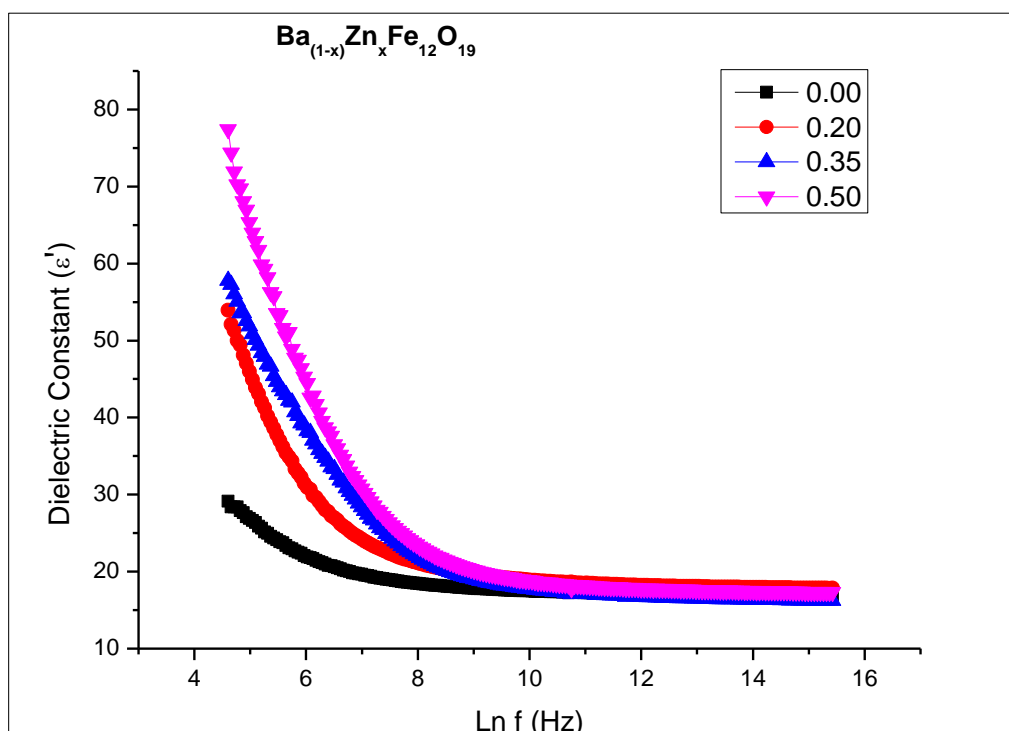


Figure.4.13 Dielectric Constant vs log natural of frequency  $\text{Ba}_{1-x}\text{Zn}_x\text{Fe}_{12}\text{O}_{19}$ (NP)

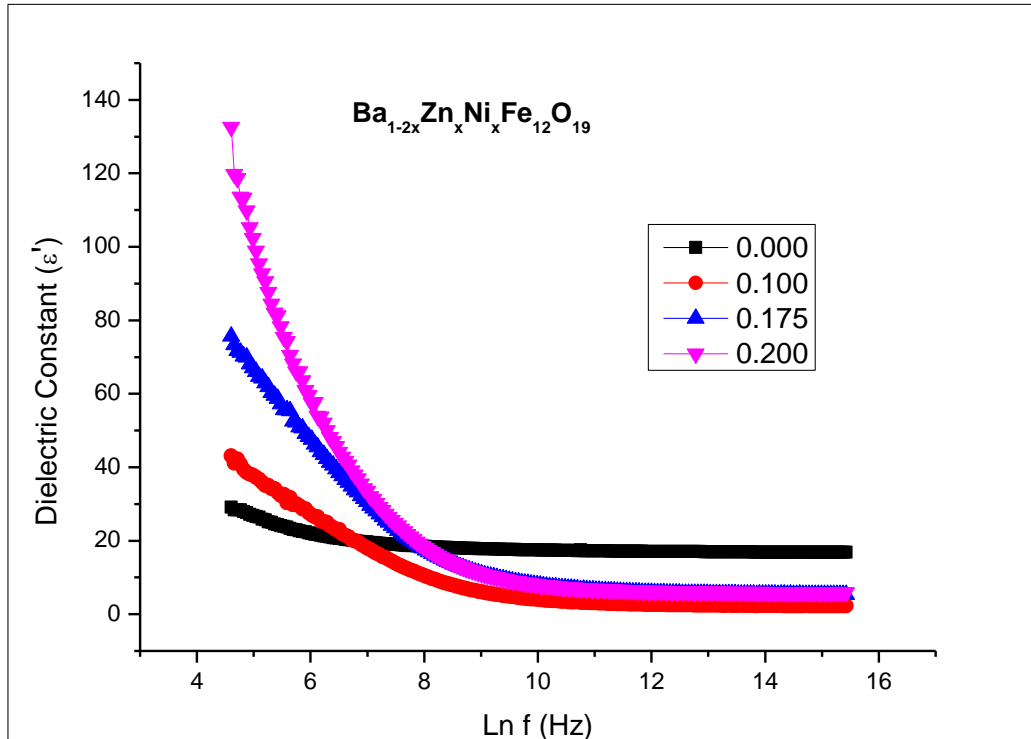


Figure.4.14 : Dielectric Constant vs log natural of frequency  $Ba_{1-2x}Zn_xNi_xFe_{12}O_{19}$  (NP)

#### 4.4.1.2. Dielectric losses

Dielectric loss tangent ( $\tan\delta$ ) actually measures the relative loss of electrical energy faced by electric field over a range of frequency, i.e relative energy loss upon fluctuation of electric field.  $\tan\delta$  also shows the same behavior of decreasing with increasing frequency as shown in Fig 4.15to 4.18.

It has been demonstrated that the un-doped barium hexaferrite has less dielectric parameters ( $\epsilon'$ ,  $\epsilon''$  &  $\tan \delta$ ) values when it is doped, new samples show an increase in these parameters at 100Hz. At higher frequency there is reduction in these parameters. A summary of measured electrical properties are given in table 4.3 and 4.4.

(figures on next page.)



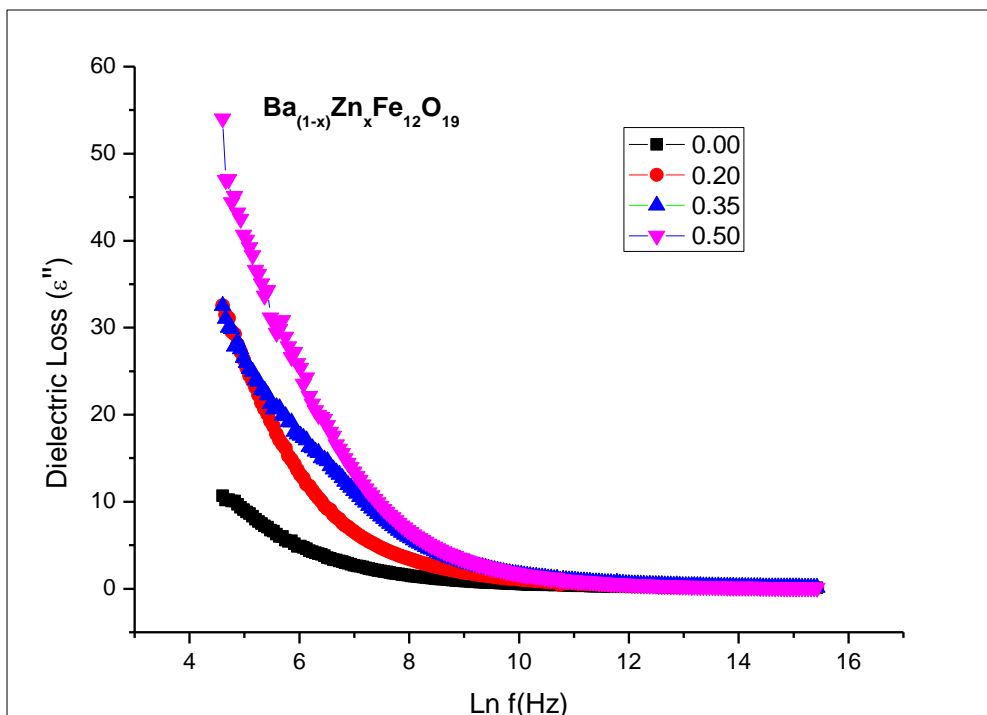


Figure.4.15: Dielectric Loss vs log natural of frequency  $\text{Ba}_{1-x}\text{Zn}_x\text{Fe}_{12}\text{O}_{19}$  (NP)

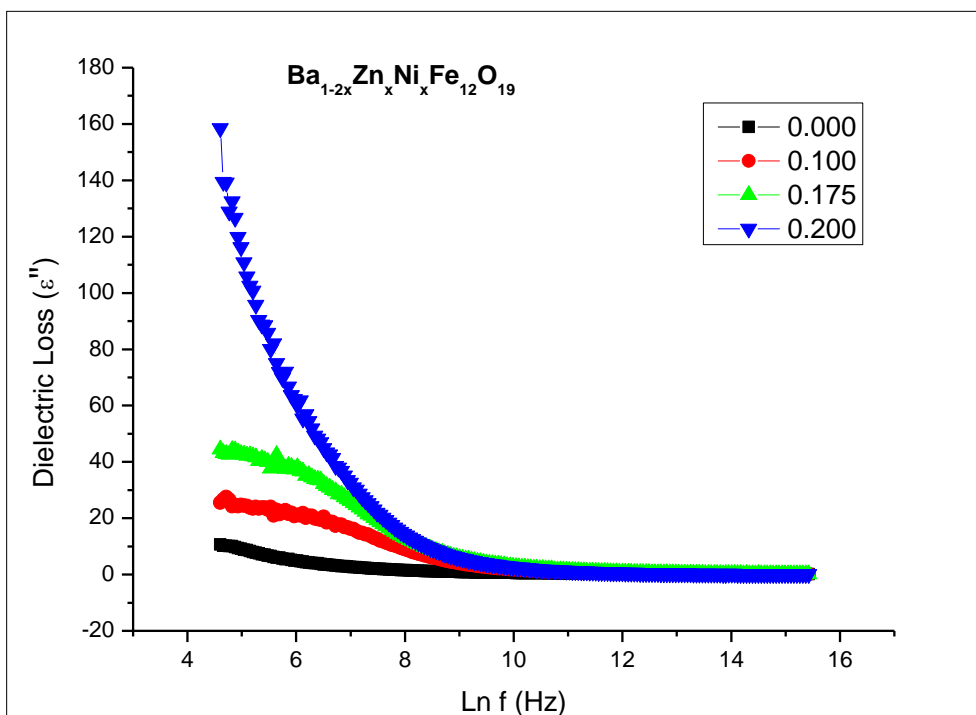


Figure 4.16: Dielectric Loss vs log natural of frequency  $\text{Ba}_{1-2x}\text{Zn}_x\text{Ni}_x\text{Fe}_{12}\text{O}_{19}$  (NP)

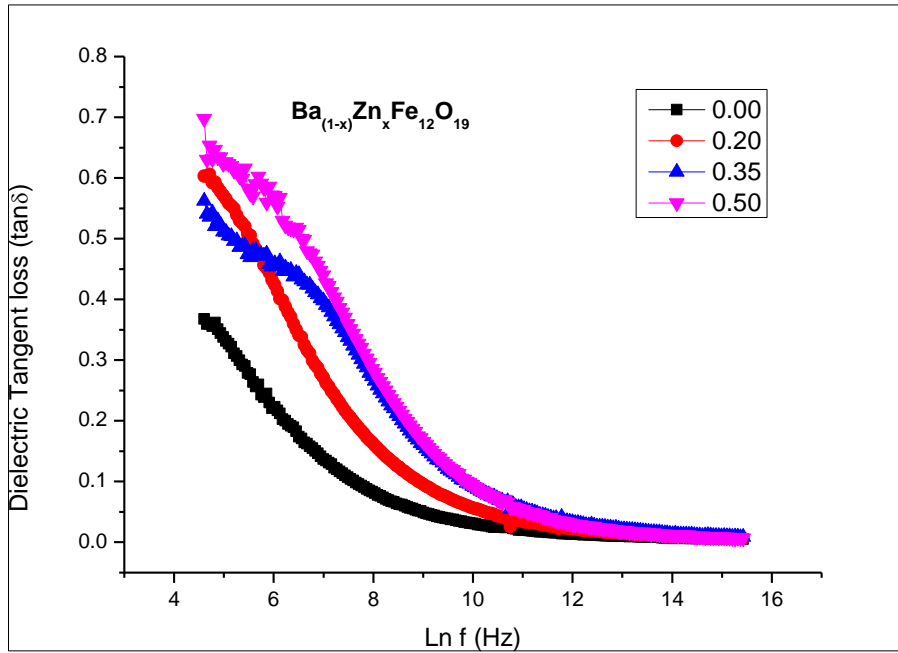


Figure.4.17 : Dielectric Tangent Loss vs log natural of frequency  $Ba_{1-x}Zn_xFe_{12}O_{19}$  (NP)

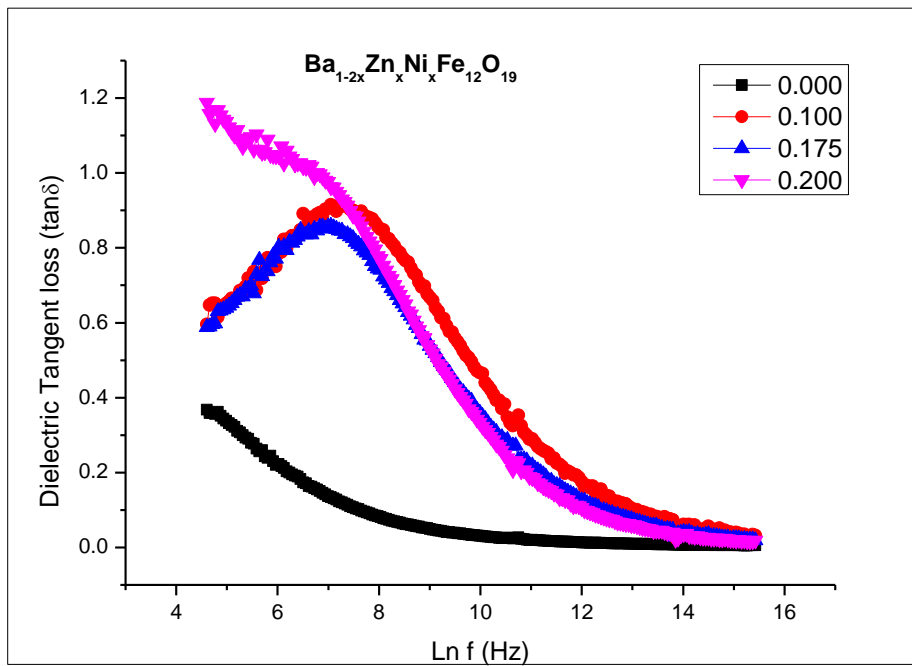


Figure 4.18 : Dielectric Tangent Loss vs log natural of frequency  $Ba_{1-2x}Zn_xNi_xFe_{12}O_{19}$  (NP)

#### 4.4.2. AC Conductivity ‘ $\sigma'$ ’

Figure 4.19 and 4.20 which shows that the AC conductivity  $\sigma'$  is generally increased with an increase in the frequency for all the samples. Exchange of electrons between  $\text{Fe}^{2+}$  and  $\text{Fe}^{3+}$  are responsible for both the phenomena. The exchange of electron between  $\text{Fe}^{2+}$  &  $\text{Fe}^{3+}$  is major cause of conduction which varies with frequency and observed to be high at higher frequency as compared to that at low frequency.

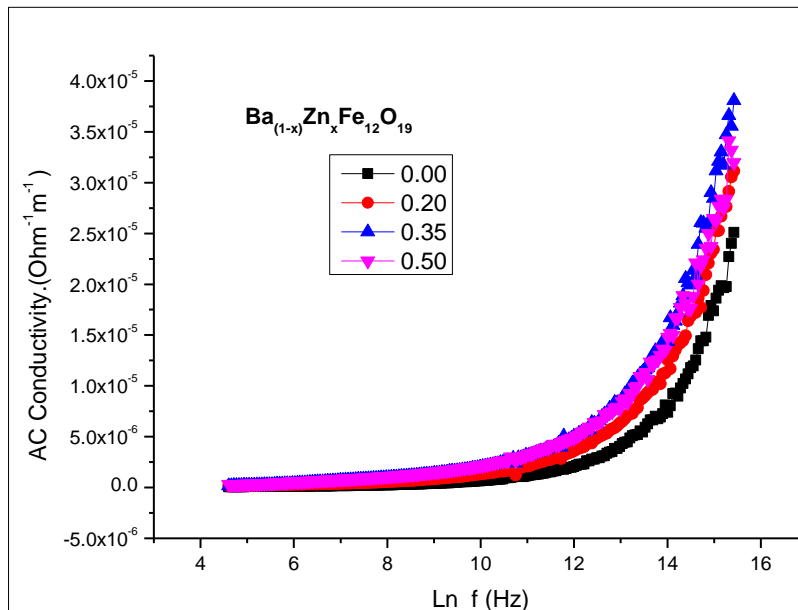


Figure.4.19 : AC Conductivity vs log natural of frequency  $\text{Ba}_{1-x}\text{Zn}_x\text{Fe}_{12}\text{O}_{19}$  (NP)

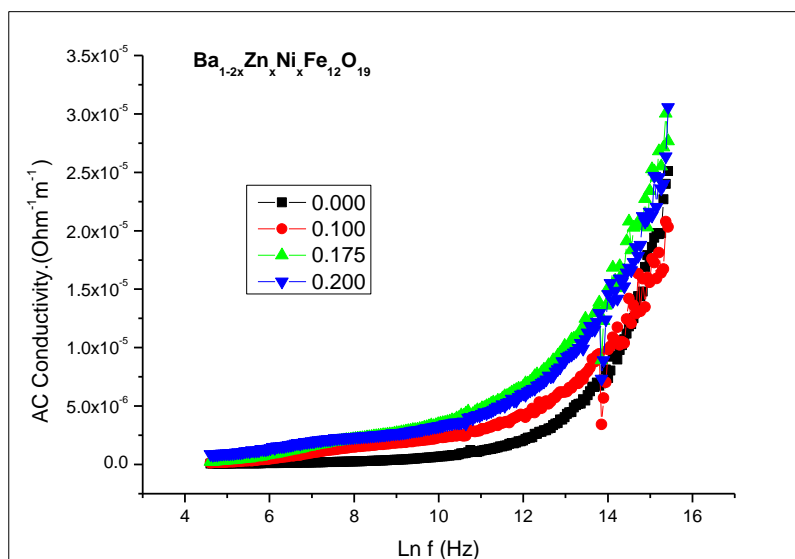


Figure.4.20 : AC Conductivity vs log natural of frequency  $\text{Ba}_{1-2x}\text{Zn}_x\text{Ni}_x\text{Fe}_{12}\text{O}_{19}$  (NP)

**Table 4.3** Dielectric constant & loss, Tangent loss and AC conductivity at 100 Hz

Composition	Dielectric Constant ( $\epsilon'$ ) at 100 Hz	Dielectric Loss ( $\epsilon''$ ) at 100 Hz	Tangent Loss $\tan \delta$ at 100 Hz	AC Conductivity ( $\Omega^{-1}\text{m}^{-1}$ ) at 100 Hz
<b>BaFe<sub>12</sub>O<sub>19</sub></b>	29.1	10.07	0.368	$5.95 \times 10^{-8}$
<b>Ba<sub>0.8</sub>Zn<sub>0.20</sub>Fe<sub>12</sub>O<sub>19</sub></b>	53.9	32.5	0.603	$1.81 \times 10^{-7}$
<b>Ba<sub>0.65</sub>Zn<sub>0.35</sub>Fe<sub>12</sub>O<sub>19</sub></b>	57.8	32.5	0.562	$1.81 \times 10^{-7}$
<b>Ba<sub>0.5</sub>Zn<sub>0.5</sub>Fe<sub>12</sub>O<sub>19</sub></b>	77.4	54.0	0.698	$3.00 \times 10^{-7}$
<b>Ba<sub>0.8</sub>Zn<sub>0.1</sub>Ni<sub>0.1</sub>Fe<sub>12</sub>O<sub>19</sub></b>	43.0	25.6	0.595	$1.42 \times 10^{-7}$
<b>Ba<sub>0.65</sub>Zn<sub>0.175</sub>Ni<sub>0.175</sub>Fe<sub>12</sub>O<sub>19</sub></b>	75.7	44.5	0.588	$2.47 \times 10^{-7}$
<b>Ba<sub>0.6</sub>Zn<sub>0.2</sub>Ni<sub>0.2</sub>Fe<sub>12</sub>O<sub>19</sub></b>	133	158	1.19	$8.78 \times 10^{-7}$

**Table 4.4.** Dielectric constant & loss, Tangent loss and AC conductivity at 5M Hz

Composition	Dielectric Constant ( $\epsilon'$ ) at 5 MHz	Dielectric Loss ( $\epsilon''$ ) at 5 M Hz	Tangent Loss $\tan \delta$ at 5 MHz	AC Conductivity ( $\Omega^{-1}\text{m}^{-1}$ ) at 5 MHz
<b>BaFe<sub>12</sub>O<sub>19</sub></b>	16.8	0.0903	$5.38 \times 10^{-3}$	$2.51 \times 10^{-5}$
<b>Ba<sub>0.8</sub>Zn<sub>0.20</sub>Fe<sub>12</sub>O<sub>19</sub></b>	17.8	0.112	$6.29 \times 10^{-3}$	$3.11 \times 10^{-5}$
<b>Ba<sub>0.65</sub>Zn<sub>0.35</sub>Fe<sub>12</sub>O<sub>19</sub></b>	16.2	0.137	$8.46 \times 10^{-3}$	$3.80 \times 10^{-5}$
<b>Ba<sub>0.5</sub>Zn<sub>0.5</sub>Fe<sub>12</sub>O<sub>19</sub></b>	17.3	0.115	$6.65 \times 10^{-3}$	$3.19 \times 10^{-5}$
<b>Ba<sub>0.8</sub>Zn<sub>0.1</sub>Ni<sub>0.1</sub>Fe<sub>12</sub>O<sub>19</sub></b>	2.3	0.0731	0.0318	$2.03 \times 10^{-5}$
<b>Ba<sub>0.65</sub>Zn<sub>0.175</sub>Ni<sub>0.175</sub>Fe<sub>12</sub>O<sub>19</sub></b>	5.3	0.0996	0.0187	$2.77 \times 10^{-5}$
<b>Ba<sub>0.6</sub>Zn<sub>0.2</sub>Ni<sub>0.2</sub>Fe<sub>12</sub>O<sub>19</sub></b>	5.91	0.11	0.0182	$2.77 \times 10^{-5}$

#### 4.4.3. Comparison graphs of Electrical properties of Samples

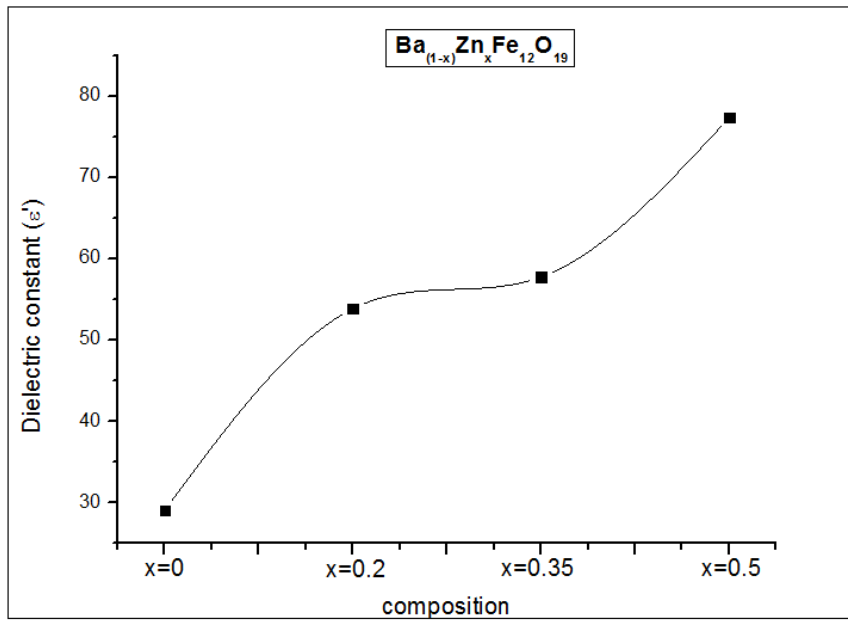


Fig 4.21 : Comparison of **Dielectric Constant at 100Hz** of **Ba<sub>1-x</sub>Zn<sub>x</sub>Fe<sub>12</sub>O<sub>19</sub> (NP)**

(for x=0,0.2,0.35,0.5)

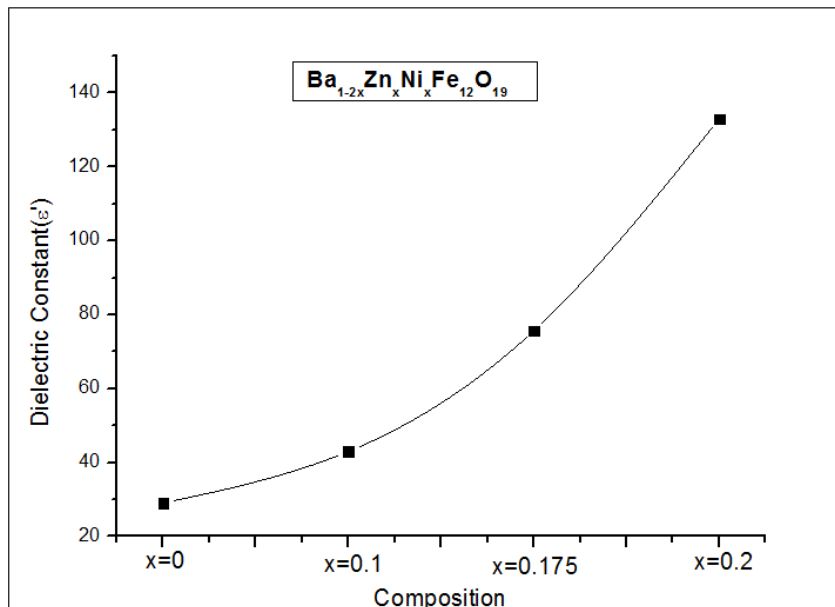


Fig 4.22: Comparison of **Dielectric Constant at 100Hz** of **Ba<sub>1-2x</sub>Zn<sub>x</sub>Ni<sub>x</sub>Fe<sub>12</sub>O<sub>19</sub> (NP)**

(for x=0,0.1,0.175,0.2)

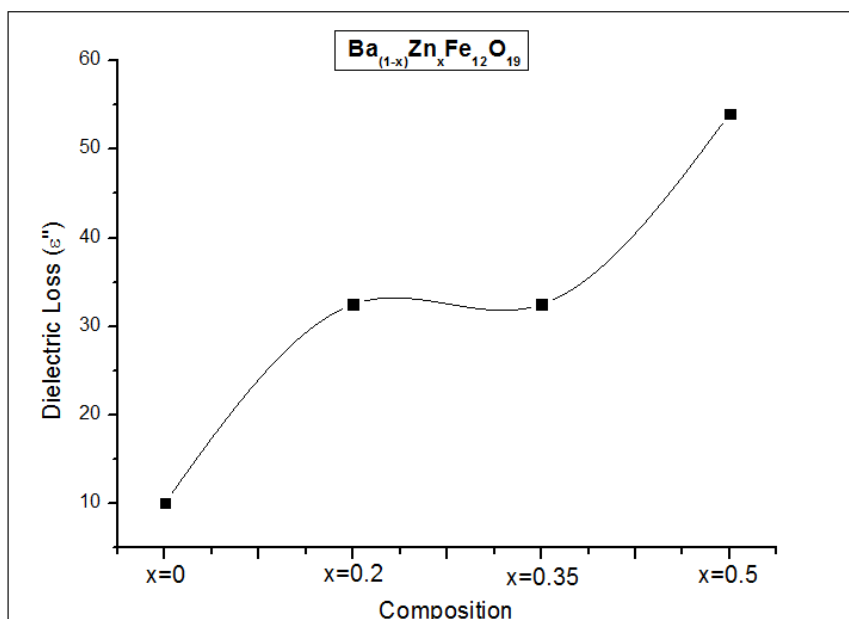


Fig 4.23: Comparison of **Dielectric Loss at 100Hz** of **Ba<sub>1-x</sub>Zn<sub>x</sub>Fe<sub>12</sub>O<sub>19</sub> (NP)**

(for x=0,0.2,0.35,0.5)

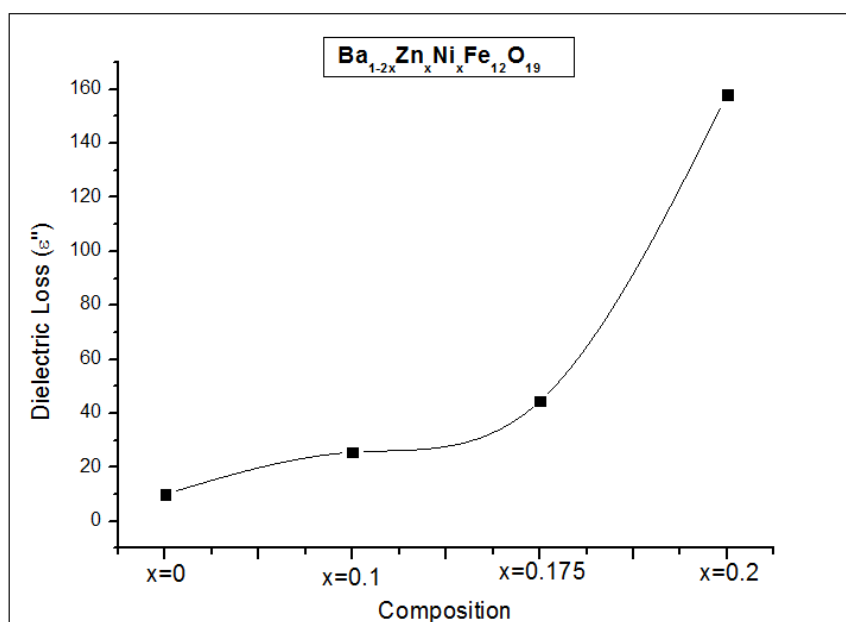


Fig 4.24 : Comparison of **Dielectric Loss at 100Hz** of **Ba<sub>1-2x</sub>Zn<sub>x</sub>Ni<sub>x</sub>Fe<sub>12</sub>O<sub>19</sub> (NP)**

(for x=0,0.1,0.175,0.2)

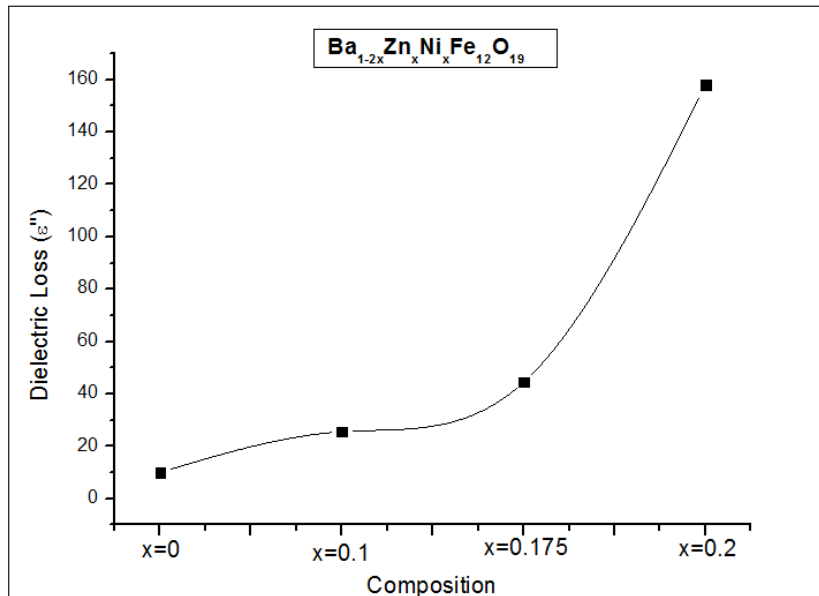


Fig 4.25: Comparison of AC conductivity at 100Hz of  $\text{Ba}_{1-2x}\text{Zn}_x\text{NiFe}_{12}\text{O}_{19}$  (NP)

(for x=0,0.2,0.35,0.5)

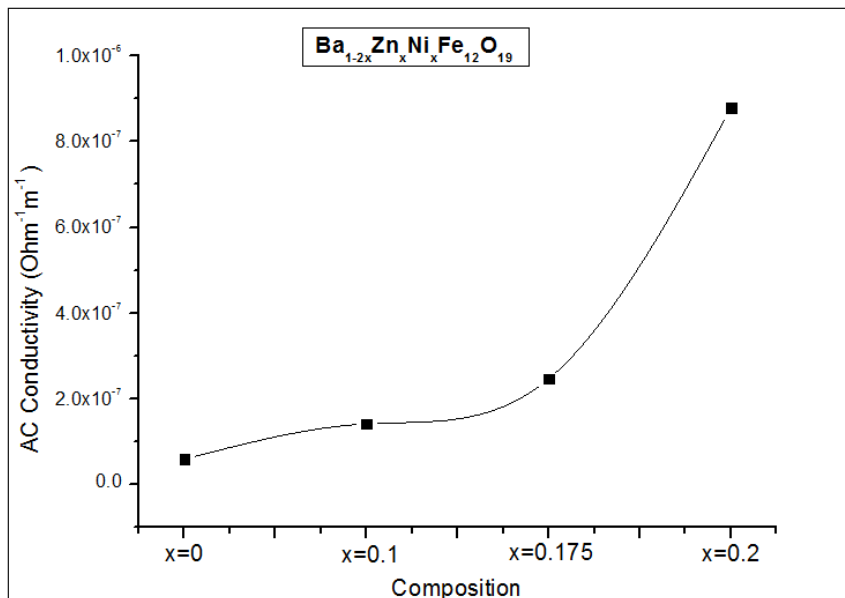


Fig 4.26: Comparison of AC conductivity at 100Hz of  $\text{Ba}_{1-2x}\text{Zn}_x\text{NiFe}_{12}\text{O}_{19}$  (NP)

(for x=0,0.1,0.175,0.2)

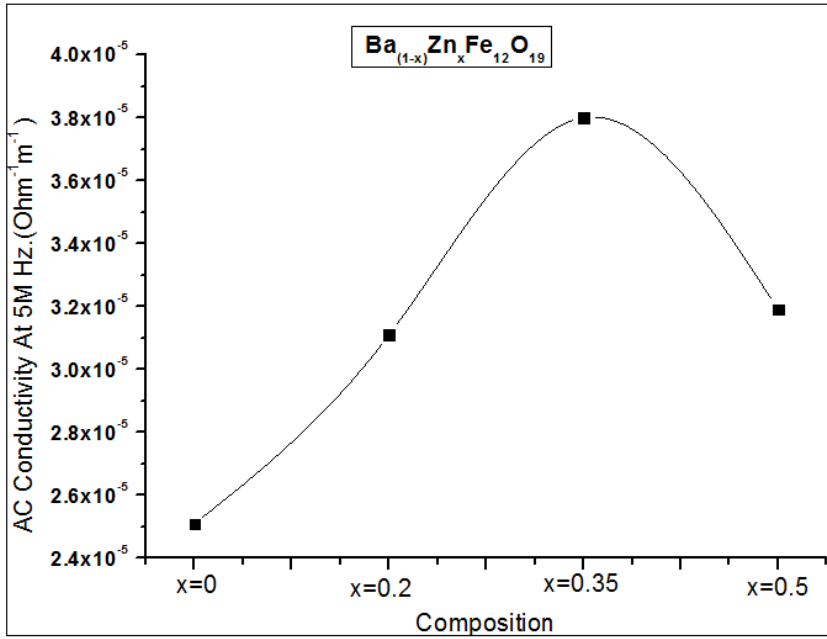


Fig 4.27: Comparison of AC conductivity at 5MHz of Ba<sub>1-x</sub>Zn<sub>x</sub>Fe<sub>12</sub>O<sub>19</sub> (NP)  
(for x=0,0.2,0.35,0.5)

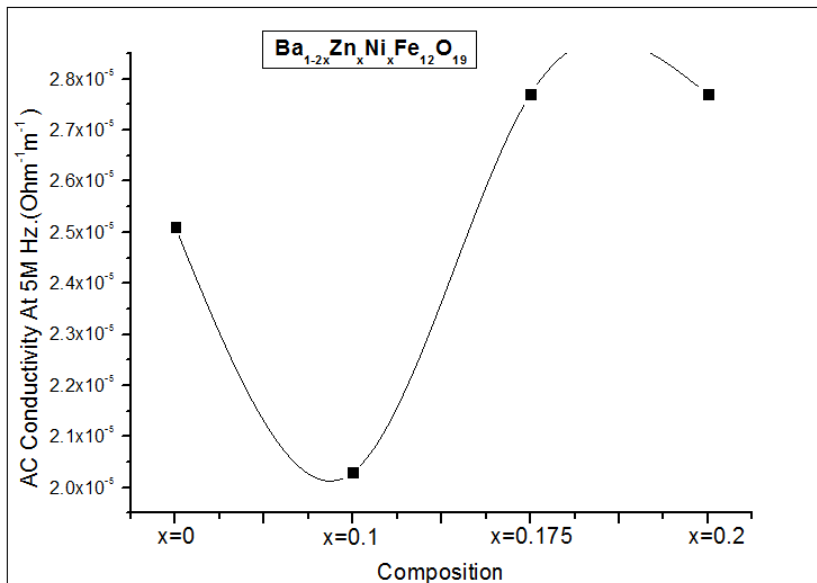


Fig 4.28: Comparison of AC conductivity at 5MHz of Ba<sub>1-2x</sub>Zn<sub>x</sub>Ni<sub>x</sub>Fe<sub>12</sub>O<sub>19</sub> (NP)  
(for x=0,0.1,0.175,0.2)



#### 4.4.4. AC impedance spectroscopy.

The AC impedance (its real and imaginary parts) were plotted against log natural of frequency in fig 4.29 to 4.34 and cole cole plot ( $Z'$  vs  $Z''$ ) are plotted for both the series of samples in fig 4.40 & 4.41. In these plots The plots incomplete semi-circle which shows that resistance is caused by the grain boundaries. Size of semi circle represents the amount of resistance offered by sample, it has been observed that with variation in dopant concentration size of plotted curve also varied.

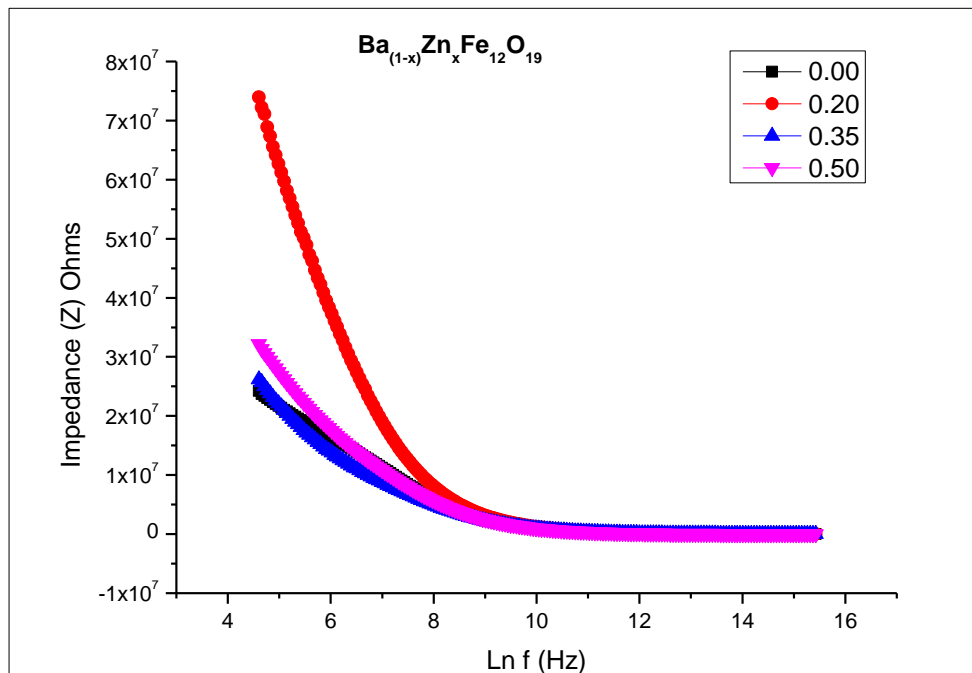


Figure.4.29: Impedance  $Z$  vs  $\ln f$  for  $\text{Ba}_{1-x}\text{Zn}_x\text{Fe}_{12}\text{O}_{19}$  (NP)

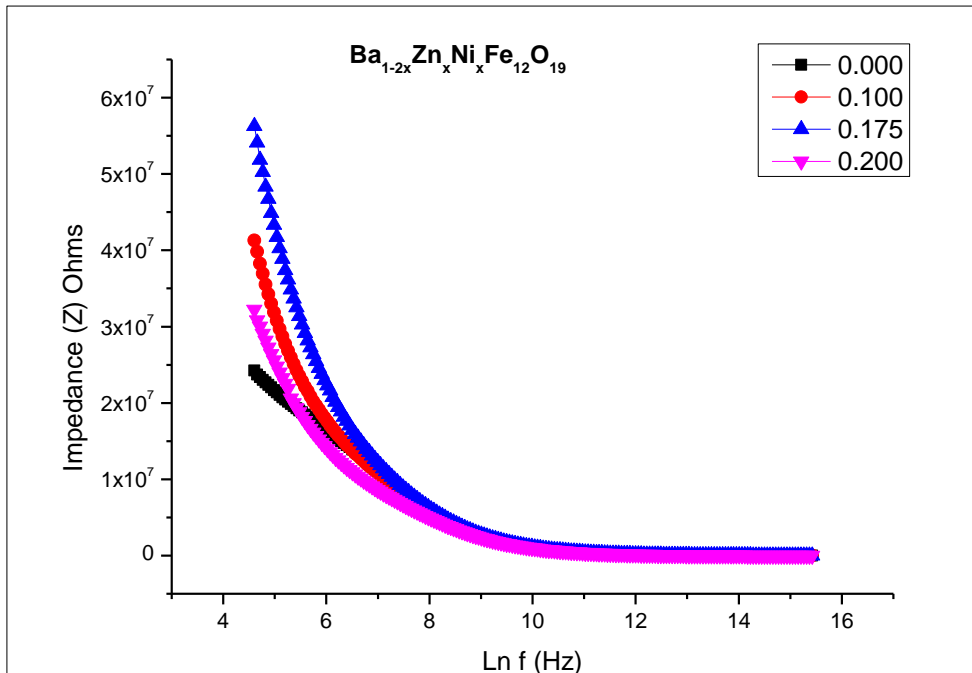


Figure.4.30: Impedance  $Z$  vs  $\ln f$  for  $\text{Ba}_{1-2x}\text{Zn}_x\text{Ni}_x\text{Fe}_{12}\text{O}_{19}$  (NP)

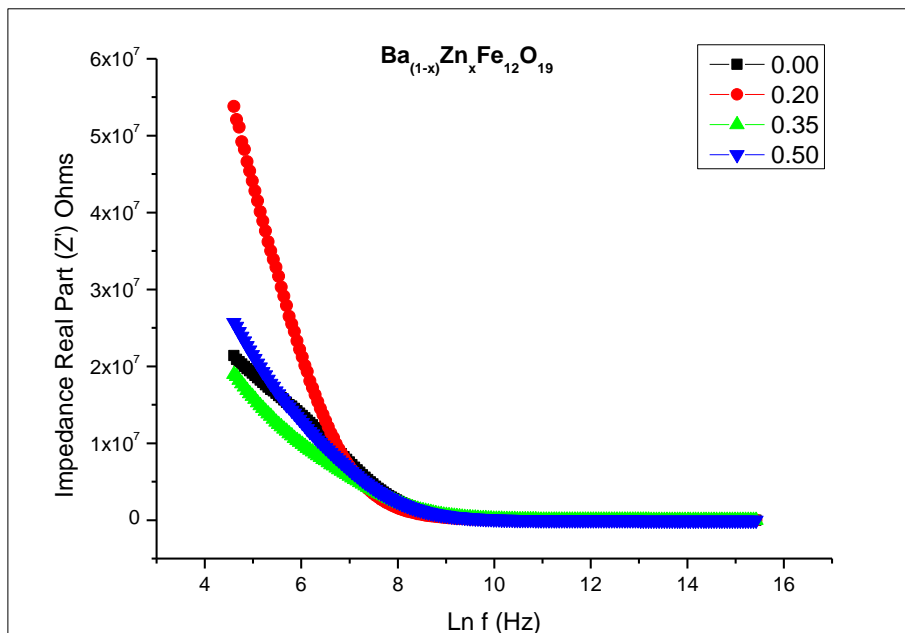


Figure.4.31: Impedance ( $Z'$  Real Part) vs log natural of frequency  $\text{Ba}_{1-x}\text{Zn}_x\text{Fe}_{12}\text{O}_{19}$  (NP)

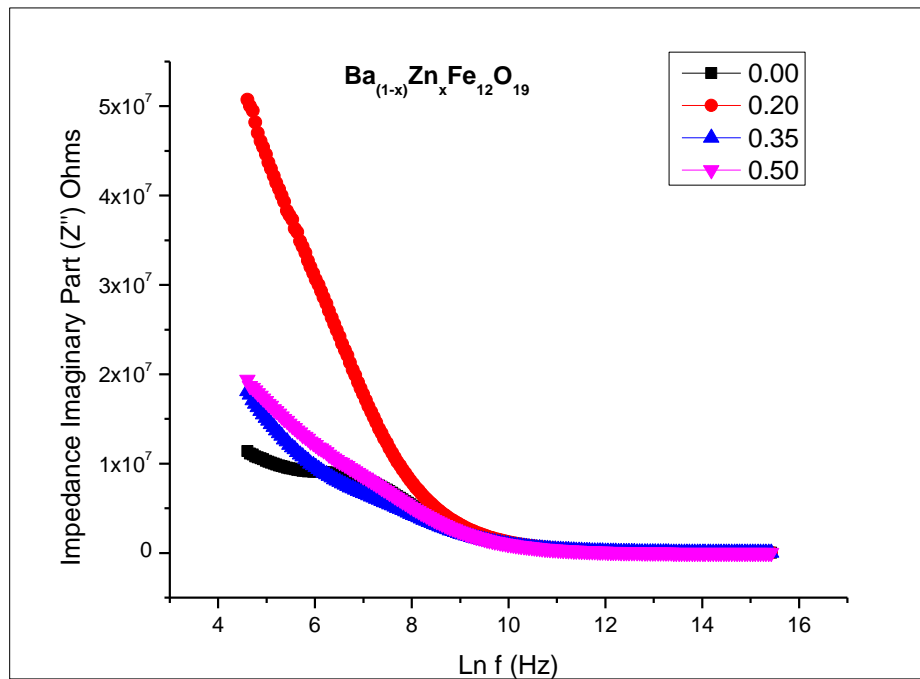


Figure.4.32 : **Impedance** ( $Z''$  Imaginary Part) vs log natural of frequency  $Ba_{1-x}Zn_xFe_{12}O_{19}$  (NP)

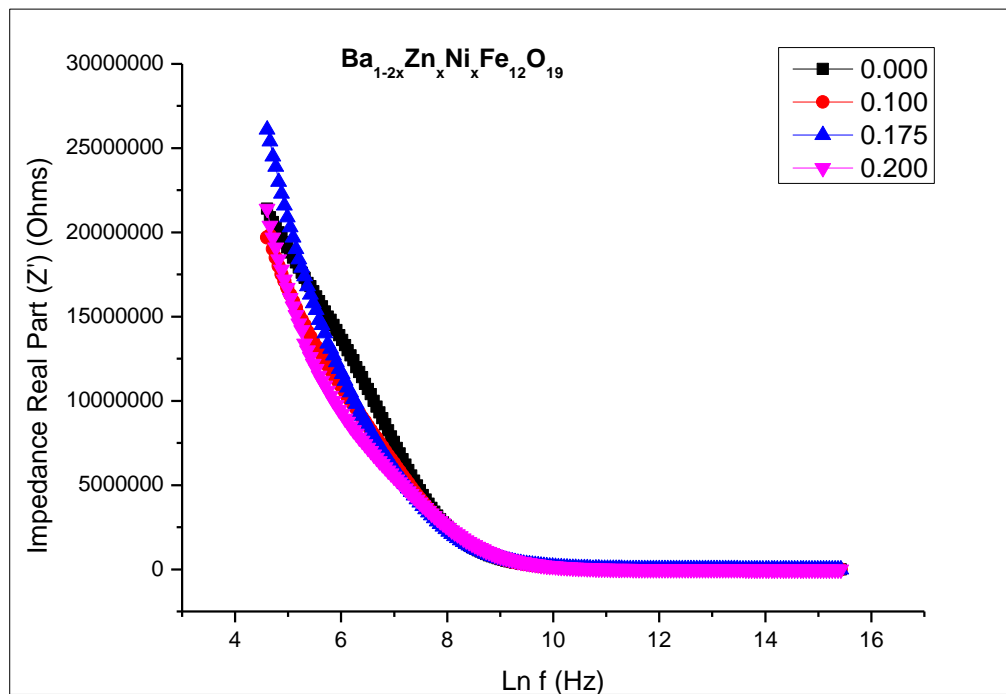


Figure.4.33 : **Impedance** ( $Z'$  Real Part) vs log natural of frequency  $Ba_{1-2x}Zn_xNi_xFe_{12}O_{19}$  (NP)

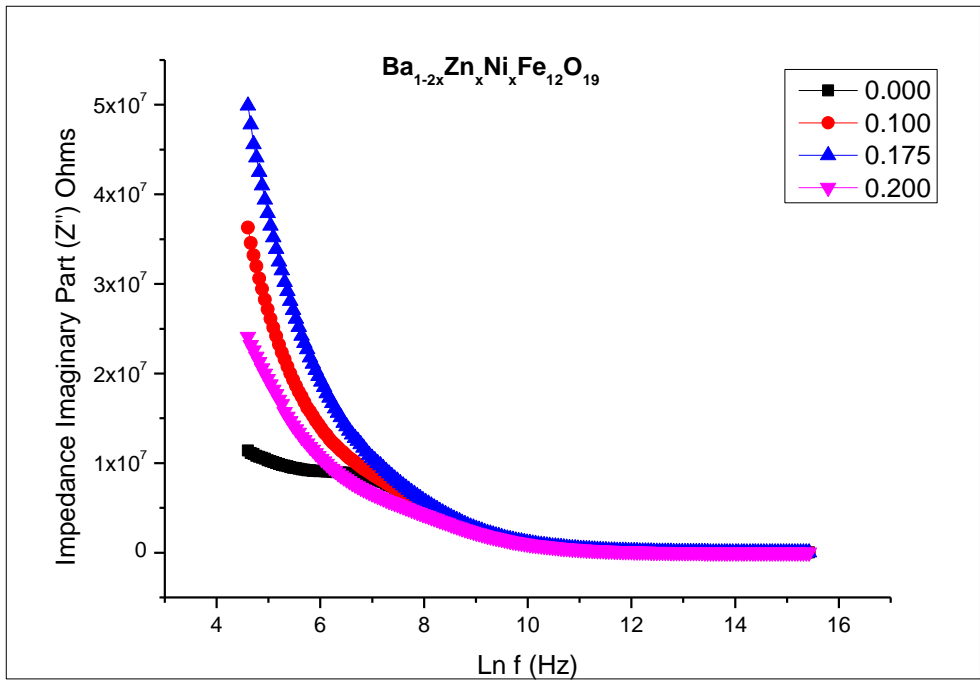


Figure.4.34: **Impedance** ( $Z''$  Imaginary Part) vs log natural of frequency  $Ba_{1-2x}Zn_xNi_xFe_{12}O_{19}$  (NP)

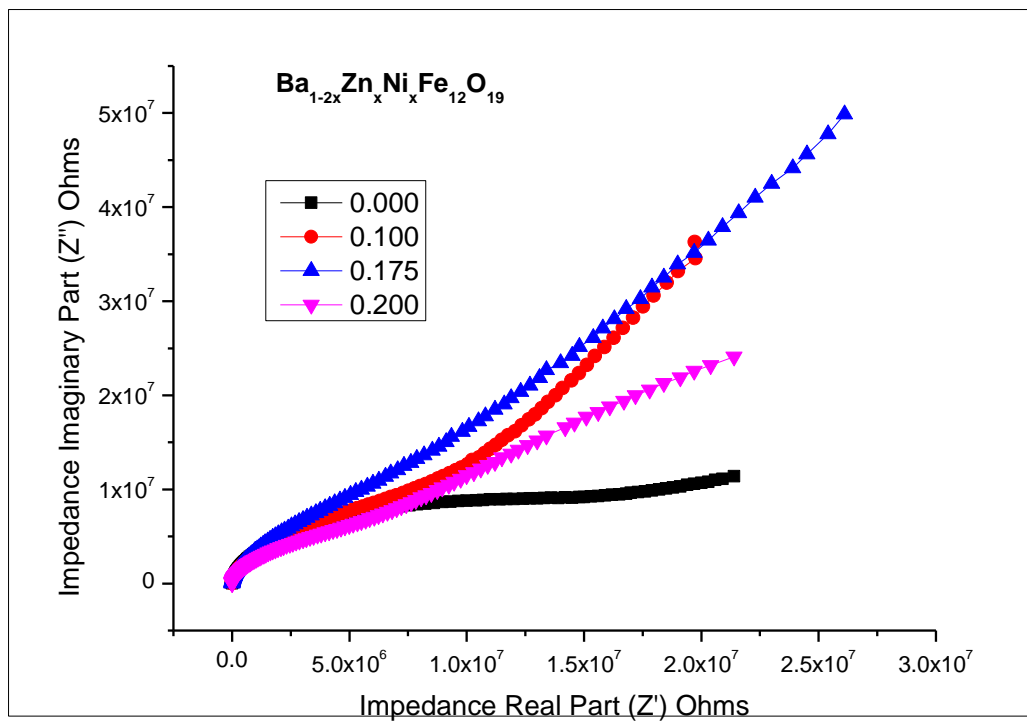


Figure.4.35 :Cole Cole Plot ( $Z'$  vs  $Z''$ )  $Ba_{1-x}Zn_xFe_{12}O_{19}$  (NP)

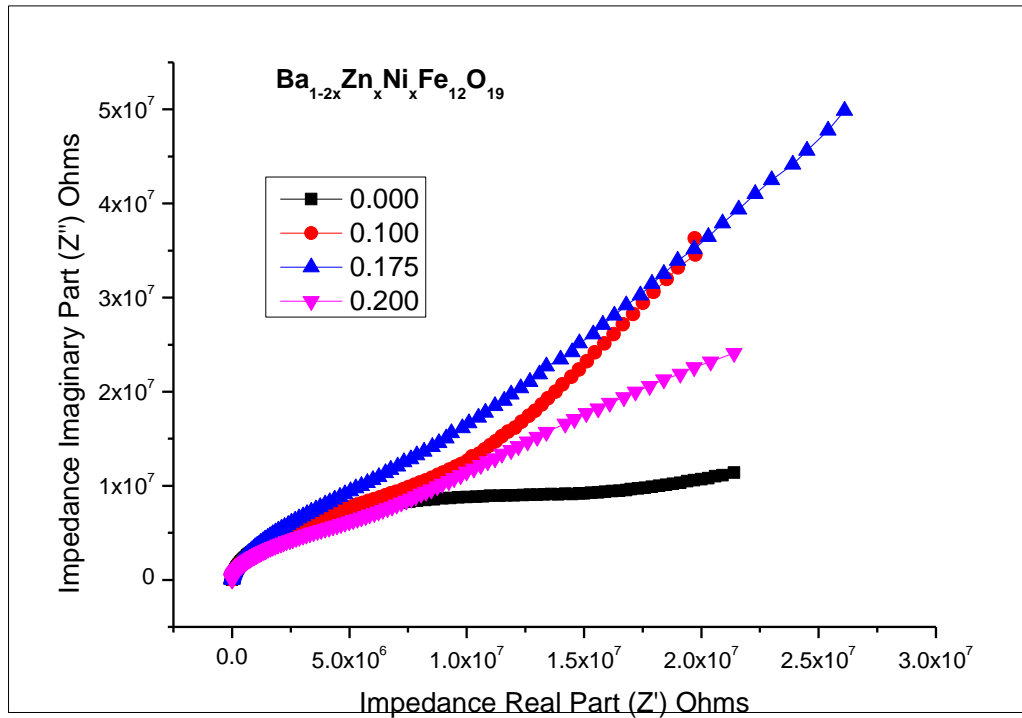


Figure.4.36: Cole Cole Plot ( $Z''$  vs  $Z'$ )  $Ba_{1-2x}Zn_xNi_xFe_{12}O_{19}$  (NP) .

#### 4.4.5. Cole–Cole (or Nyquist) diagram (for Electric Modulus “ M ”) .

Complex impedance spectroscopy is a useful method for studying relaxation process of a material. Grain boundary and grains are studied in this technique. The imaginary part of impedance is use to study conductive and resistive phenomenon. Polarization phenomenon can be studied by Imaginary part of electric modulus  $M''$  and permittivity  $\epsilon''$ . Formulae of Electric Moduli are discussed in chapter 3 [98].

(figures on next page)

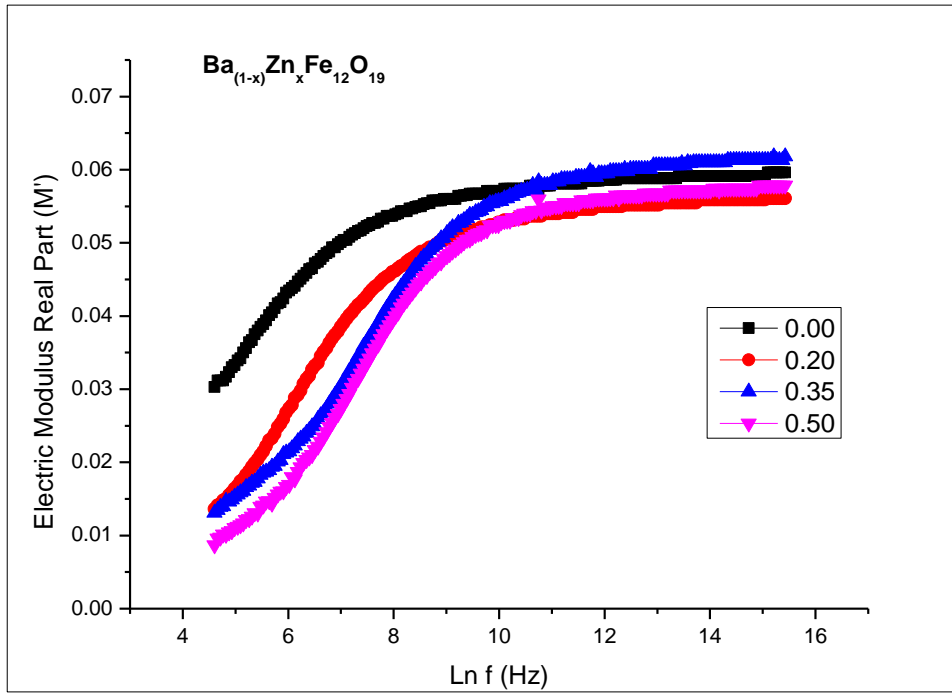


Figure.4.37: Electric Modulus graph (M' (real part) vs ln f) for  $Ba_{1-x}Zn_xFe_{12}O_{19}$  (NP)

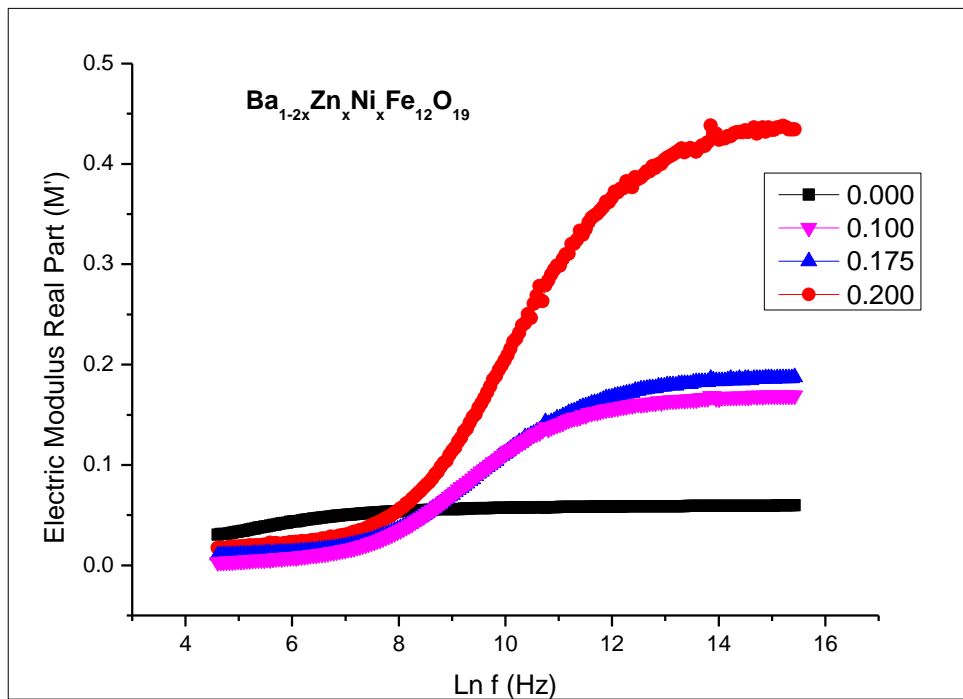


Figure.4.38 : Electric Modulus graph (M' real part vs ln f) for  $Ba_{1-2x}Zn_xNi_xFe_{12}O_{19}$  (NP)

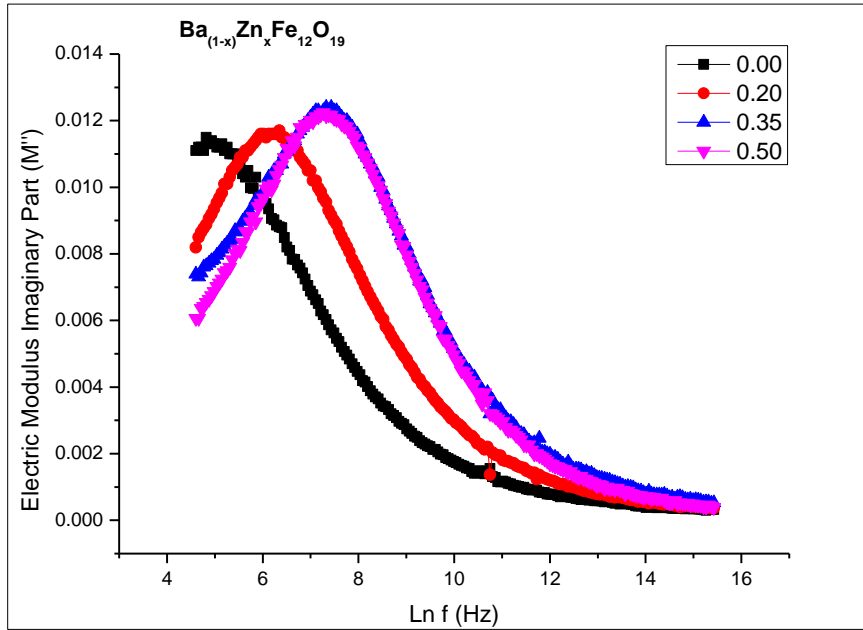


Figure.4.39 : Electric Modulus plot ( $M''$  imaginary part vs  $\ln f$ ) for  $Ba_{1-x}Zn_xFe_{12}O_{19}$  (NP)

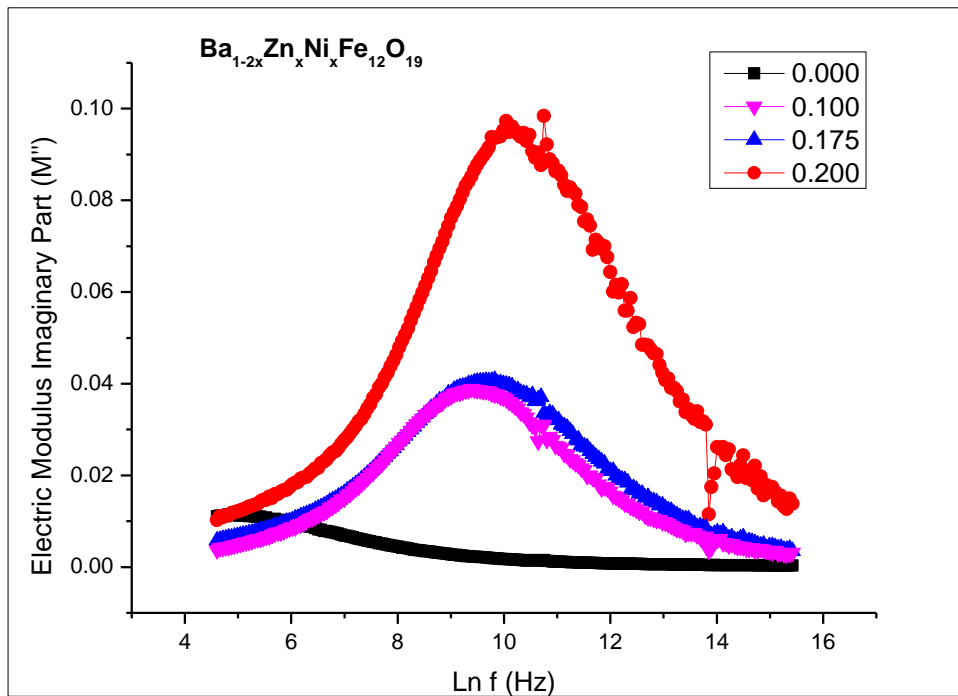


Figure.4.40: Plot ( $M''$  imaginary part vs  $\ln f$ ) for  $Ba_{1-2x}Zn_xNi_xFe_{12}O_{19}$  (NP)

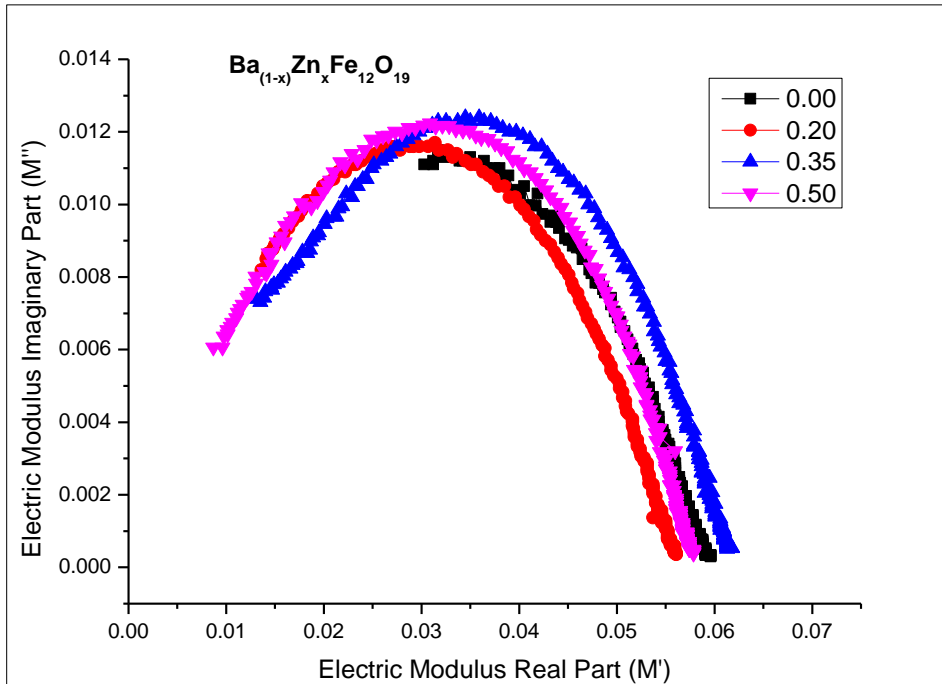


Figure.4.41: Cole Cole Plot ( $M'$  vs  $M''$ )  $Ba_{1-x}Zn_xFe_{12}O_{19}$  (NP)

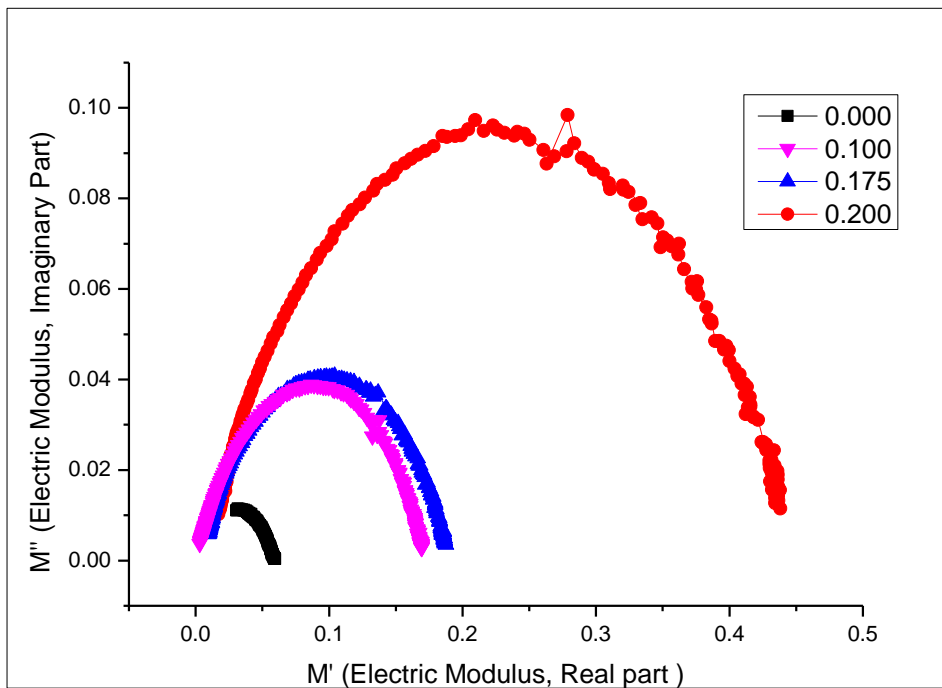


Figure.4.42 :Cole Cole Plot ( $M'$  vs  $M''$ )  $Ba_{1-2x}Zn_xNi_xFe_{12}O_{19}$  (NP)



## 4.5 Conclusion

The use of hexaferrites in technology has been widely cited in literature during the last two decades. Total control of the microstructure is a basic requirement of these technologies that includes control over particle size and desired shape.

Barium hexaferrites having compositional arrangement of  $\text{Ba}_{1-x}\text{Zn}_x\text{Fe}_{12}\text{O}_{19}$  for the range of  $x$  values ( $x = 0.00, 0.20, 0.35, 0.50$ ) and  $\text{Ba}_{1-2x}\text{Zn}_x\text{Ni}_x\text{Fe}_{12}\text{O}_{19}$  with values ( $x = 0.000, 0.100, 0.175, 0.200$ ) were prepared by auto combustion method also known as sol gel method. The samples after synthesis were annealed at  $800\text{ }^\circ\text{C}$  for 8 hours. X-ray diffraction examination shows the presence of single hexagonal phase in 7 prepared samples. Lattice parameters of the crystal system were likewise measured from the information got from the diffraction pattern. It has been observed during experimentation that the lattice constants 'a' and 'c' slightly vary for substitution of Zinc and Nickel samples. Range of crystallite size was measured to be 48-60 nm, with an increasing trend which is also in close agreement from SEM results. Mass density of the materials demonstrated decreasing pattern and x-ray density also reduce which results into slight increase in porosity of the samples series. FT-IR spectra give the characteristic absorption bands for the hexaferrite samples at 592 to 579 and 431 to 438 $\text{cm}^{-1}$  showing the metal-oxygen bond. It has also been observed that dielectric constant reduces sharply with the increase in the value of frequency at the end it becomes independent of frequency at high frequencies. Dielectric relaxation is responsible for diminishing in the dielectric constant with frequency, which is in agreement of Koop's model. The dielectric loss enhance with the addition of Zn and Ni at Ba sites, which is an evidence that electromagnetic absorption property of synthesised samples is improved. [99].

## 4.6 Future Recommendations

The prepared samples can be tested further in the X-band frequency region by preparing the present samples with polymer matrix, PVC/polychloroprene.

Similarly, other rare earth metals combinations with transition metals can be used to further improve the microwave absorbing properties in X and Ku band. These ferrite powders can further be used to prepare polymer sheets of different thickness which can be tested at the entire frequency range of electromagnetic waves.

Properties can be varied and improved by changing the experimental conditions like pH, calcinations temperature, heat treatment duration, changing the ingredients and also by changing the percentage of ingredient metallic ions to give various recipes, suitable to meet the requirements of rapidly growing technologies.

# References

- [1] W. Ervens and H. Wilmesmeier, Ullmann's Encyclopedia of Industrial Chemistry, 5th edition A16 (1990)51.
- [2] C.W. Chen, Magnetism and Metallurgy of Magnetic materials, North Holland Publishing Company, (1997) 42.
- [3] <http://www.britannica.com/EBchecked/topic/357014/magnetic-ceramics>
- [4] C. Kittel, Introduction to Solid State Physics, 7th edition, Wiley(1996)78.
- [5] J. S. Blakemore, "Solid State Physics", 2nd Edition, Cambridge University Press(1985)201.
- [6] S. O. Kasap, "Principles of Electronic Material and Devices" 3rd Edition, McGrawHill(2002)94.
- [7] W.H. Yeadon & A. W. Yeadon, Handbook of small Electric Motors, Mcgraw Hill Company Inc. USA(2001)87.
- [8] S. Hirosawa, A. Hanaki, H. Tomizawa and A.Hamamura, Physica B, 164 (1990) 117.
- [9] J. Beretka and M. Ridge, J. Chemical Society (A) 10 (1968) 2463.
- [10] Y. Goto and K. Takahashi, J. of Jap. Soc. Powder Metallurgy, 17 (1971) 193.
- [11] J. Wang, F. Ren, R. Yi, A. Yan, G. Qiu, X. Liu, Journal of Alloys and Compounds, 479 (2009) 791.
- [12] Materials Science and Engineering: An Introduction, 7th Edition (2003) Chapter 20: Magnetic Properties)356.
- [13] C. Kittel, Rev. Mod. Physics 21 (1949) 541.
- [14] J. F. Nye, "Physical Properties of Crystals: Their Representation by Tensors and Matrices", Oxford University Press, Oxford, (1998)321.
- [15] [http://www.magnets.bham.ac.uk/magnetic\\_materials/type.htm](http://www.magnets.bham.ac.uk/magnetic_materials/type.htm).
- [16] <http://what-when-how.com/materialsparts-and-finishes/magnetic-materials-hard- and soft>
- [17] [http://en.wikipedia.org/wiki/Ferrite\\_\(magnet\)#cite\\_note-Carter\\_2007-1](http://en.wikipedia.org/wiki/Ferrite_(magnet)#cite_note-Carter_2007-1)

- [18] J. Smit and H. P. J. Wijn, "Ferrites: Physical Properties of Ferrimagnetic Oxides in Relation to Their Technical Applications", Philips Technical Library, Eindhoven, Netherlands, (1959) 342.
- [19] W. H. von Aulock (Ed.), A. S. Boxer, J. F. Ollom, and R. F. Rauchmiller, "Handbook of Microwave Ferrite Materials", Academic Press, London, (1965)67.
- [20] T. Mishima, U. S. Patent 2,2027,966; Ohm, 19 (1932) 353.
- [21] S. Geller and M. A. Gilleo, J. Phys. Chem. Solids 3 (1957) 30.
- [22] M. A. Gilleo and S. Geller, Phys. Rev. 110 (1958) 73.
- [23] J. J. Went, G. W. Ratheneau, E. W. Gorter, and G. W. Van Oosterhout, Philips Tech.Rev. 13 (1952) 194.
- [24] H. P. J. Wijn, Nature, 170 (1952) 707.
- [25] P. B. Braun, Nature, 170 (1952) 708.
- [26] Robert C. Pullar , Progress in Material Science, 57 (2012) 1191.
- [27] G. H. Jonker, H. P. Wijn and P. B. Braun, Philips. Tech. Rev. 18 (1956-1957) 145.
- [28] Rajshree B. Jotania, Pratiksha A. Patel / International Journal of Engineering Research and Applications (IJERA) 2 (2012) 494.
- [29] A.E. Van Arkel, E.J.W. Verwey, M.G. Van Bruggen, Rev. Trv. Chim. 55 (1936) 331.
- [30] JJ Went, GW Rathenau, EW Gorter, GW Van Oosterhout., Philos Technol. Rev., 13 (1952)194.
- [31] J.L. Snoek. Philos Technol Rev 8 (1946) 353.
- [32] J. Smit & H.P.J. Wijn Ferrites Philips Technical Library, Eindhoven; 1959.
- [33] International Centre for Diffraction Data, Newton Square, PA, USA PDF No. 84-1531 (SrFe<sub>12</sub>O<sub>19</sub>), 84-757 (BaFe<sub>12</sub>O<sub>19</sub>), 84-2046 (PbFe<sub>12</sub>O<sub>19</sub>).
- [34] Li Z, Gao F. Can J Chem., 89 (2011) 573.
- [35] M.Matsumoto, A. Morisako, S.Takei. J Alloys Compd 326 (2001) 215.
- [36] P.B. Braun. Nature, 170 (1952)234.
- [37] A. G. Smolenski and A. A. Andreev, Bull. Acad. Sci. 25 (1961) 1405.
- [38] ,V.L. Moruzzi and M.W. Shafer, J. Am. Ceram. Soc. 43 (1960) 367.
- [39] A. Deschamps, F. Bertaut, Acad Sci; 244 (1957) 3069.
- [40] AH. Mones, E. Banks, J Phys Chem Solids; 4 (1958) 217.

- [41] UN. Mulay, APB. Sinha. *Indian J Pure Appl Phys.* 8 (1970) 412.
- [42] F.K. Lotgering, *J Phys Chem Solids* 35 (1974) 1633.
- [43] EW. Gorter. *Philos Res Rep*; 9 (1954) 403.
- [44] E. Ogawa, O. Kubo. In: *Ferrites, proc ICF6 Tokyo and Kyoto*(1992)1410.
- [45] SB. Narang, LS. Huidara. *J Ceram Process Res*; 7 (2006) 113.
- [46] M. Drogenik, M. Kristl, A. Znidarsic, D. Hanzel, D. Lisjak, *J Am Ceram Soc.* 90 (2007) 2057.
- [47] Ü. Özgür, Y. Alivov, and H. Morkoç, “Microwave Ferrites, Part 2: Passive components and electrical tuning”, to be published in *J. Mater. Sci.: Materials in Electronics*(2009)98.
- [48] E. Neckenburger, H. Severin, JK. Vogel, G. Z. Winkler, *Angew Phys*;18 (1964) 65.
- [49] MA. Vinnik, *Russ J Inorg Chem*; 10 (1965) 1164.
- [50] SI. Kuznetsova, EP. Naiden, et al. *Inorg Mater*; 24 (1988) 856.
- [51] EP. Naiden, VI. Itin. OG. Terekhova, *Tech Phys Lett*; 29 (2003) 889.
- [52] W. Roos, *J Am Ceram Soc*; 63 (1980) 601.
- [53] K. Haneda, C. Miyakawa, H. Kojima, *J Amer Ceram Soc*; 57 (1974) 354.
- [54] S. Okamoto, *J Am Ceram Soc* (1968) 51.
- [55] G. Litsardakis, AC. Stergiou, J. Giorgiou, S. Sklavounos, et al. *J Magn Magn Mater*; 120 (1993) 58.
- [56] E. Matijevic, *J Colloid Interface Sci*; 117 (1987) 593.
- [57] C. Surig, D. Bonnenberg, KA. Hempel, et al. *J Phys IV*; 7 (1997) 315.
- [58] VKS. Sankaranarayanan, QA. Pankhurst, DPE. Dickson, *J Magn Magn Mater*; 125 (1993) 199.
- [59] M.A.Ahmed, N.Okasha, and R.M.Kershi, *journal Physica B: Condensed Matter* Volume 405,(2010)3223
- [60] Muhammad Javed Iqbal, Razaqat Ali Khan, Shigeru Takeda, Shigemi Mizukami, Terunobu Miyazaki, *journal, Journal of Alloys and Compounds* Volume 509, (2011)7618
- [61] A.Haq and M.Anis-ur-Rehman, *journal Physica B: Condensed Matter* Volume 407(2012)822
- [62] S.M.El-Sayed, T.M.Meaz, M.A.Amer, H.A.El Shersaby, *journal Physica B: Condensed Matter* Volume 426(2013)137

- [63] JieLI, HuaiwuZHANG , QiangLI , YuanxunLI , GuoliangYU , Journal of Rare Earths Volume 31 (2013) 983
- [64] Hasan M.Khan, M.U.Islam, YongbingXu, M.Asif Iqbal and IrshadAli, Journal of Alloys and Compounds Volume 589, (2014) 258.
- [65] O.M.Hemeda, Nasser Y.Mostafa, Omar H.Abd Elkader, D.M.Hemeda, A.Tawfik, M.Mostafa. Journal of Magnetism and Magnetic Materials Volume 394(2015)96.
- [66] S. Ozah, N.S. Bhattacharyya Journal of Magnetism and Magnetic Materials 374 (2014) 516.
- [67] Virender Pratap Singh et al in 2014 Journal of Magnetism and Magnetic Materials 378(2015) 478.
- [68] S.Chakrabarty, M.Pal and A.Dutta ,journal , Materials Chemistry and Physics Volume 153,(2015)221-22.
- [69] Rutvi J.Pandya, U.S.Joshi, O.F.Caltunb journal, Procedia Materials Science Volume 10,(2015)168.
- [70] S. Noushin Ezzati et al journal of Alloys and Compounds 646 (2015) 1157
- [71] Samira Mandizadeha, Faezeh Soofivanda , Masoud Salavati-Niasaria, Samira Bagherib, Journal of Industrial and Engineering Chemistry Volume 26, (2015)167.
- [72] C.Choodamania ,B. Rudraswamy G.T.Chandrappab, journal ,Ceramics International Volume 42,(2016)1056.
- [73] A.Poorbafrani & E.Kiani, Journal of Magnetism and Magnetic Materials Volume 416, (2016)10.
- [74] Preeti Gairola et al Synthetic Metals 221 (2016) 326.
- [75] Alireza Shayan, Majid Abdellahi, Fazlollah Shahmohammadian, Saeid Jabbarzare, Amirsalar Khandan, Hamid Ghayour, Journal of Alloys and Compounds Volume 708,(2017)538.
- [76] Faseeh ur Raheem et al Journal of Alloys and Compounds 708 (2017) 903.
- [77] Anum Zafar et al in 2017 journal of Alloys and Compounds 727 (2017) 683.
- [78] Karamveer Chahal et al in 2017 Journal of Alloys and Compounds 737 (2018) 387.

- [79] M. Ben Ali et al Journal of Magnetism and Magnetic Materials Volume 398, (2016) 20.
- [80] [www.academia.edu/.../X-ray Diffraction\\_Principle\\_Instrument](http://www.academia.edu/.../X-ray_Diffraction_Principle_Instrument)
- [81] T. Damen, S. P. S. Porto, B. Tell, Phys. Rev., 142 (1966) 2.
- [82] P. R. Emtage, J. App. Phys., 48 (1977) 4372.
- [83] M. Inada, J. J. Phys., 17 (1978) 10.
- [84] F. S. Hickerne, J. App. Phys., 44 (1973) 1061.
- [85] S. K. Tiku, C. K. Lau, K. M. Lakin, App. Phys. Lett., 35 (1980) 318-320.
- [86] C. Eberspacher, A. L. Fahrenbruch, R. H. Bube, Thin Solid Films, 136 (1986) 1-10.
- [87] P. F. Carcia, R. S. McLean, M. H. Reily, G. Nunes, Jr. App. Phys. Lett., 82 (2003), 7.
- [88] T. V. Butkhuji et al., J. Crys. Growth, 117 (1992) 366-369.
- [89] D. Vogel, P. Krüger and J. Pollmann, Phys. Rev., 52 (1995) 14316.
- [90] Tammy P. Chou, Qifeng Zhang, Glen E. Fryxell, Guozhong Cao, Adv. Mater., 19 (2007) 2588.
- [91] Seema Rani, Poonam Suri, P. K. Shishodia, R. M. Mehra, 92 (2008) 1639.
- [92] <http://www.microscopemaster.com/nanotechnology.html>
- [93] A. Singh, S. B. Narang et al. Eur. Phys. J. Appl. Phys, 33, (2006) 189.
- [94] C. Jagadish and S. J. Pearton, "Zinc Oxide Bulk, Thin Films and Nanostructures Processing, Properties and Application" Elsevier (2006) 362.
- [95] Z. L. Wang and Z. C. Kang, Plenum press, (1998) 465.
- [96] Z. L. Wang, J. Phys. Condensed Matter, 16 (2004) 829.
- [97] K. H. Hellwege, O. Madelung, A. M. Hellege, 19 (1987) 119.
- [98] Z. L. Wang, J. Phys., Condens. Matter, 16 (2004) 829.
- [99] G. H. Lee, Y. Yamamoto, M. Kourogia, M. Ohtsua, Thin Solid Films, 386 (2001) 117.